THE UNIVERSITY
of EDINBURGH

Ruthenium alkylidene metathesis

Veronica Forcina

A Thesis Submitted for the Degree of Doctor of Philosophy

The University of Edinburgh

2018

Declaration

I declare that the work in this thesis was carried out by me under the supervision of Prof. Guy Lloyd-Jones FRS and Prof. Dieter Vogt and is in accordance with the requirements of the University of Edinburgh. This work is original, except where indicated by special reference in the text, and no part of the dissertation has been previously submitted for any academic award.

Signed…….

Date……..

Abstract

The olefin metathesis of oleochemicals is a promising method to produce valuable compounds from renewable feedstocks. However, several issues hinder the industrial application of this methodology such as low catalyst turn over number (TON), selectivity and substrate conversion. Using the ethenolysis of methyl oleate (MO) as a model reaction, the optimisation of this valuable process was investigated. A range of commercially available metathesis pre-catalysts were examined and evaluated based on several key criteria: conversion of methyl oleate, selectivity towards ethenolysis over self metathesis and TON. After identifying the best performing catalyst (Hoveyda-Grubbs 1st generation pre-catalyst), the remaining reaction conditions (ethylene pressure, catalyst loading, reaction time and temperature) were investigated using design of experiments. The optimised conditions obtained gave excellent conversion of methyl oleate. It is proposed that the remaining issues of selectivity and TON may be improved by applying a membrane separation technique.

The initiation mechanism of Grubbs 3rd generation pre-catalyst (GIII) was also investigated to unravel the difference in selectivity compared to Grubbs 2nd generation pre-catalyst (GII) (12 % and 17 % respectively), as both pre-catalysts should give the same catalytically-active alkylidene species. The model reaction of GIII with ethyl vinyl ether (EVE) was followed by stopped-flowed UV spectroscopy (SF-UV). Due to the extreme sensitivity of the GIII pre-catalyst, substantial optimisation of the instrument set-up was required in order to achieve reproducible kinetic data and anaerobic conditions. The model reaction was studied by SF-UV at different concentrations of EVE and the effect of 3-bromopyridine addition was also investigated. The kinetic data suggests that the initiation of GIII proceeds *via* a combination of associative and dissociative pathways. Accordingly, two different alkylidene active species are able to react with an olefin (MO) when GIII is used as pre-catalyst compared with one alkylidene species when GII is employed as pre-catalyst. This is proposed to be crucial for the difference in selectivity between GII and GIII pre-catalysts in the ethenolysis of MO.

Lay Summary

The interest in producing the chemical building blocks for plastics and cosmetics from renewable resources has increased due to depletion of non-renewable resources. Olefin metathesis is a chemical transformation which allows the production of fine chemical building blocks from plant oils by using a catalyst. A model reaction was used to study this chemical process in order to implement it for industrial application. Firstly, different commercially available catalysts were tested to identify the one which enables the most efficient formation of the desired compounds. In addition, for the best performing catalyst the key parameters that affect the reaction outcome were investigated utilising specialist modelling software. This study resulted in a highly efficient metathesis process. Subsequently, the activation of two of the catalysts tested was investigated to gain detailed insight into how the species involved in the activation process can effect the reaction outcome. The activation process for one of the catalysts was very quick and the catalyst studied decomposes in contact with air. For these reasons a stopped-flow ultra-violet spectrometer was used in the study as this instrument enables quick mixing of reactants and analysis. The data collected was analysed and simulated to allow a suitable reaction mechanism to be proposed. This study suggests the formation of different species in the initiation processes of the two catalysts under investigation, which is thought to be the reason for the different reaction outcome obtained.

Acknowledgements

Firstly, I would like to thank Professor Guy Lloyd-Jones for giving me the possibility to continue my PhD in Edinburgh, for always finding the time to help me with passion and patience. It has been an incredible pleasure to have the opportunity to work for such a talented chemist.

I would like to thank Professor Dieter Vogt to give me the chance to start this PhD in Edinburgh by choosing me among other candidates and following my research during the first years.

I would like to thank the past and current members of the GLJ group for welcoming me as a member of the group from the very first day, you all made the difficult period of changing research group way easier. Thank you for all the help in the lab and for being my emotional support team during this very stressful period. Thanks to Ruth for training me with the SF-NMR, to Eric for the organocatalysis advice and for having always believed in me so much and to Kathrine for the time she spent correcting my presentations. Thanks to Chris for early morning chats, for all the help the thesis (especially the formatting part), to Craig for the chats about Italian culture and for always taking my stuff from the upper shelfs of the GB, to Tom for sharing the SF issues and for all the help during the thesis writing. Thanks to Alex for being always friendly and for the motivational poster, to Hannah for being always smiley and happy even when I bump into her chair for the one millionth time, to Harvey for the chemistry and the life chats, for being always so kind and calm, to Mags for the help with Dynochem, for the chats in the instrument room and for the hugs. Thanks to Eduardo for making me try real Mexican food and for sharing with me the struggle to live in such a cold place, to Ariana for all the help with the NMR and for being always so positive and lovely.

I would like to thank the members of the Vogt group for making my first period in Edinburgh easier and funnier. Thanks to Maria for sharing with me the initial project, to Dani for being so helpful and caring, to Anna for all the help with organic chemistry issues.

Thanks to Lewis and George for showing me everything in the lab when I first started trying to cover their Scottish accent. Thanks to Laura and Eszter for sharing with me the troubles of beginning a PhD and the difficulties of changing research group.

I would like to thank Alisia and Sally for being the best travel team ever during the last three years and hopefully in the future.

I would like to thank the members of the Campopiano group who adopted me with kindness.

Especially Pete and Alexis for the nights with fondue, Champagne and sake, for being always happy to meet me. Thanks to Piera to always be sweet, kind and supportive and to Lindsey for the laugh and the joy she brought.

I would like to thank the Italian crew for the evenings eating homemade pasta and listening to Italian songs from the 90s.

I would like to thank my family for all their support during these years. Thanks to my sister for always believing in me and finding a way to make me laugh even in the worst situations; for being there for me no matter what happens in our lives. Thanks to my dad for making me feel the best and for being always enthusiastic. Thanks to my mum for teaching me to be a hard worker.

I would like to thank a special friend who has been my partner in crime, my best friend and my family in Edinburgh. Thanks to Annabel for surviving with me fire, water and all the possible weather conditions. Thanks for being always there for me even when it was extremely difficult, for understanding me even when I was not talking, for bringing so much joy in my life. These years in Edinburgh would have not been the same without you, I thought I found a flatmate and I found an amazing friend for life.

I would like to thank Chiara for being by my side for almost all my life or at least since I can remember, thank you for putting my feet always on the ground.

Thanks to you all, I would not be able to be where I am without you.

List of abbreviations

Ac	acetyl
BOC	*tert*-butyloxycarbonyl
C	Celsius
Cat. Load.	Catalyst loading
cm	centimetres
CM	cross metathesis
COD	1, 5-cyclooctadiene
Conv.	Conversion
Cy	cyclohexyl
3D	three dimensions
Da	Dalton
DEDAM	diethyl diallyl malonate
DFT	density functional theory
DoE	design of experiments
EVE	ethyl vinyl ether
FEAST	further exploitation of advanced shell technology
FID	flame ionization detector
G	Grubbs
GC	gas chromatography
Gly	glycine
HG	Hoveyda-Grubbs
HMSBO	hydrogenated metathesized soybean oil
HNBR	hydrogenated nitrile butadiene rubber
HPLC	high-performance liquid chromatography
i-Pr	isopropyl
IS	internal standard
µL	microliters
M	molar
Me	methyl
Mes	mesylate
mL	milliliters
MO	methyl oleate
Mol	mole

MS	mass spectroscopy
NBR	nitrile butadiene rubber
NHC	N-heterocyclic carbene
NMR	nuclear magnetic resonance
Obs	observed
OCT	olefin conversion technology
OSN	organic solvent nanofiltration
OVAT	one variable at a time
PDI	polydispersity index
Ph	phenyl
PPEK	polyether ether ketone
Ppm	parts per million
Press.	Pressure
PVC	polyvinyl chloride
RCM	ring closing metathesis
Rf	response factor
ROMP	ring opening metathesis process
s	second
SBO	soybean oil
SF	stopped-flow
SHOP	shell higher olefin process
SIMe	1,3-bis(2,4,6-trimethylphenyl)dihydroimidazole)
SVD	singular value decomposition
T	temperature
TLC	thin-layer chromatography
TMS	tetramethylsilane
TON	turn over number
UV	ultraviolet

Table of Contents

Chapter 1 Introduction: olefin metathesis

Metathesis is a formal bimolecular process involving the exchange of one or more bonds between similar interacting chemical species. The carbon-carbon double bonds are broken and reformed to give a statistical mixture olefins (Scheme 1.1).[1] However when one of the product is volatile, such as ethylene, equilibrium is pushed to the right. Conversely, under high pressure of ethylene, the equilibrium is pushed to the left (Scheme 1.1).

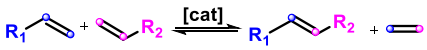

Scheme 1.1 Olefin metathesis general reaction scheme

The first reported metathesis reaction was published in 1960 when Eleuterio and co-workers at Du Pont found that propene (**1**) heated with molybdenum on alumina leaded to ethylene (**2**) and 2-butene (**3**) with 43 % propene conversion.[2] The reaction was later named metathesis by Calderon in 1967.[3]

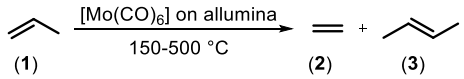

Scheme 1.2 First reported catalysed metathesis reaction

The academic and industrial importance of olefin metathesis reaction was highlighted in 2005 when Yves Chauvin, Richard Schrock and Robert Grubbs were awarded with a Nobel Prize “for the development of the metathesis method in organic synthesis”. In 1971 Yves Chauvin unravelled the mechanism of metal catalysed metathesis, opening the path to pre-catalyst development and logical improvement of the reaction class.

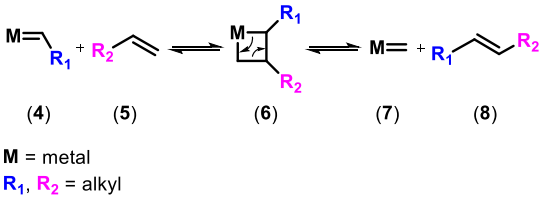

Scheme 1.3 Schematic of Chauvin mechanism

The first commercial metathesis pre-catalyst was synthesised by Richard Schrock in 1990 (Figure 1.1).[4] This pre-catalyst (Figure 1.1) was found to be unstable under air and intolerant

to some functionalities, such as aldehydes and protic functionalities (RCO_2H, RSH, ROH). Two years later Robert Grubbs developed a further improved pre-catalyst (Figure 1.1), which was stable toward water, oxygen and minor impurities and compatible with a wider range of functional groups than the Schrock pre-catalyst.[5] However, the molybdenum based Schrock pre-catalyst was far more active than Grubbs ruthenium based 1st generation pre-catalyst.[6]

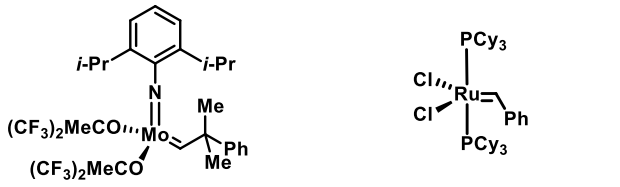

(**9**) (**10**)

Schrock catalyst **Grubbs 1st generation catalyst**

Figure 1.1 Schrock and Grubbs 1st generation pre-catalysts
Me = methyl, Ph = phenyl, Cy = cyclohexyl, *i*-Pr = isopropyl

Since the 1990s a vast quantity of research has been directed into the development of more efficient catalysts and the optimization of reaction conditions for industrial applications.[7] Indeed the use of olefin metathesis as a carbon-carbon bond-forming tool guarantees high reaction efficiency (few reaction steps involved leading to less waste) as the process is catalytic, requiring typically 1-5 mol% of catalyst; it requires relatively short reaction times and mild conditions to give good yields and it can tolerate a wide range of functional groups. Cross metathesis has already found some industrial applications in processes such as the Shell Higher Olefin Process (SHOP) (Scheme 1.4a)[8] and the Further Exploitation of Advanced Shell Technology (FEAST) Process (Scheme 1.4b).[9]

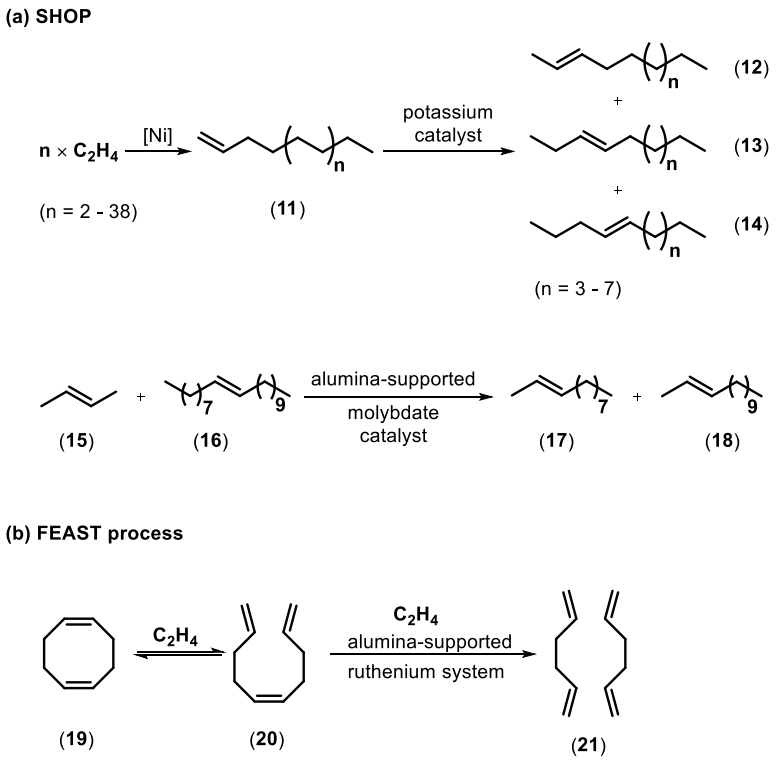

Scheme 1.4 Examples of the main industrial uses of cross metathesis

In the SHOP process C12-C18 olefins are produced *via* nickel catalysed oligomerization of ethylene (Scheme 1.4a), followed by double bond isomerization over a solid potassium metal catalyst to obtain the desired C10-C14 fraction (**12**, **13**, **14**, Scheme 1.4a). The latter isomerised mixture is then passed over alumina-supported molybdate catalyst yielding 10-15 wt% of the desired C11-C13 products (**17**, **18**, Scheme 1.4a) per pass. The obtained olefin products are further converted in fatty alcohols used as precursors for detergents. The FEAST process consists of the production of 1,5-hexadiene (**21**, Scheme 1.4b), a precursor of a variety of compounds, from 1,5-cyclooctadiene (COD, **19**, Scheme 1.4b). The 1,5,9-decatriene (**20**, Scheme 1.4b), obtained by reaction of COD (**19**) with ethylene, undergoes an ethenolysis reaction over alumina-supported ruthenium systems to give the desired product (**21**).

There are three main types of olefin metathesis: ring-opening metathesis polymerisation (ROMP) (Scheme 1.5a), ring-closing metathesis (RCM) (Scheme 1.5b) and cross metathesis (CM) (Scheme 1.5c). ROMP has been intensively used in polymerization chemistry as the reaction is thermodynamically favoured for ring-strain release (Scheme 1.5a), whereas RCM (Scheme 1.5b) has taken longer to become of common use due to development of more functional group tolerant catalysts. Finally cross metathesis (Scheme 1.5) has been widely

investigated in order to improve the reaction selectivity avoiding the formation of self metathesis products and improving regioselectivity (*cis* and *trans* products mixture formed).[1]

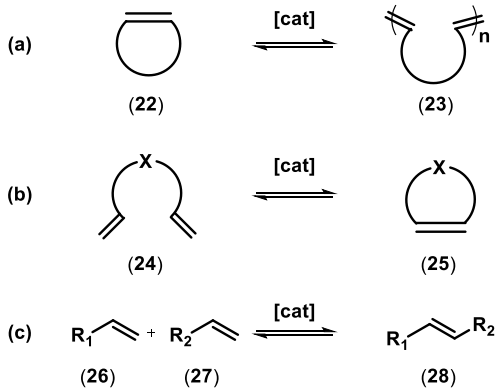

Scheme 1.5 Main types of olefin metathesis reactions

The mechanism involved in both cyclic and acyclic olefin metathesis is widely accepted to go *via* a series of carbenes and metallocyclobutane complexes as described by Chauvin.[10] Despite the fact that reaction conditions, catalyst composition and olefin substitutions can affect the relative stability of the carbenes and metallocyclobutanes, the olefin metathesis mechanism has been proven to follow the Chauvin model for all catalysts.

1.1 Metathesis pre-catalyst development

The pioneering work by Chauvin showed that metathesis pre-catalysts should either contain an alkylidene or be readily converted into one under the reaction conditions. The early olefin metathesis pre-catalysts were developed by Schrock (**29**, Figure 1.2) and they were mainly based on molybdenum. Despite the high reactivity of these pre-catalysts, they had critical drawbacks related with the low functional group tolerance, high sensitivity to moisture and solvent impurities.[4]

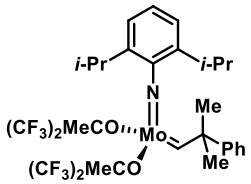

(**29**)

Schrock catalyst

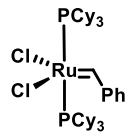

(**30**)

Grubbs 1st generation

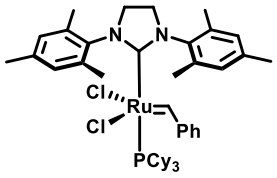

(**31**)

Grubbs 2nd generation

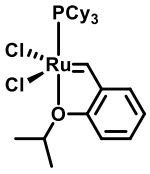

(**32**)

Hoveyda-Grubbs 1st generation

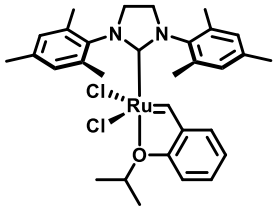

(**33**)

Hoveyda-Grubbs 2nd generation

Figure 1.2 Schrock and ruthenium-based metathesis pre-catalysts

The more recent ruthenium-alkylidene based Grubbs pre-catalysts have more organic functional group tolerance than the Schrock pre-catalyst. The catalytic activity of the former is also less affected by moisture and impurities in the solvents than the latter.[7b] However Grubbs 1st generation pre-catalyst (**30**, GI) was still less reactive than the Schrock pre-catalyst. The replacement of one of the phosphine (PCy_3) ligands in GI with a more electron-donating N-heterocyclic carbene (NHC) ligand, led to Grubbs 2nd generation pre-catalyst (**31**, GII) with

more efficient catalytic performance.[15] Indeed, Grubbs 2nd generation pre-catalysts showed higher reactivity then GI and longer catalyst life time. The NHC ligands help to stabilize the 14-electron intermediate (**65**, Scheme 1.15) during the metathesis catalytic cycle. This is due to strong σ-donation and poor π-acceptor properties of these ligands (NHC) together with their bulkiness and non-labile nature.

The bulkiness of the NHC ligand avoids the formation of bimolecular catalyst complexes, which are known to lead to catalyst decomposition for 1st generation pre-catalysts. Grubbs 2nd generation pre-catalyst is more stable to air and water and it tolerates different functional groups. Cross metathesis of previously inaccessible functionalities were successfully performed with GII, as shown for the unprotected benzaldehyde (**34**, Scheme 1.6) with ethyl acrylate (**35**).

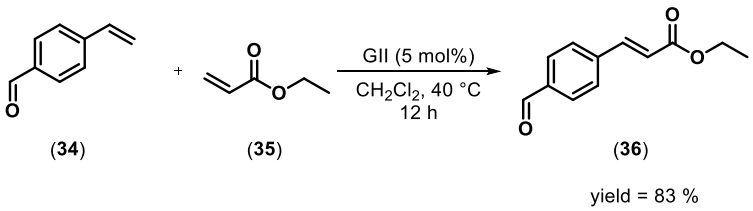

Scheme 1.6 Cross metathesis of 4-vinyl-benzaldehyde (**34**) with ethyl acrylate (**35**)
Yield calculated by ^{1}H-NMR

The loss of catalytic activity of GI in ROMP in the presence of an excess of 2-isopropoxy styrene (**37**, Scheme 1.7) drove Hoveyda and co-workers to investigate the possibility of a coordination of the ether functionality to the ruthenium metal centre.[7d]

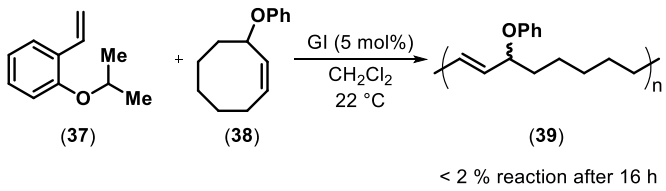

Scheme 1.7 ROMP reaction in presence of an excess of 2-isopropoxy styrene (**39**)
GI = Grubbs 1st generation pre-catalyst, Ph = phenyl

This was the starting point for the synthesis of an internal metal-oxygen chelated pre-catalyst named Hoveyda-Grubbs 1st generation pre-catalyst (**32**, HGI). This pre-catalyst (**32**) showed very good stability to air and moisture. A series of different RCM were successfully catalysed by HGI (**32**) forming the desired products in high yields (Scheme 1.8). The RCM showed good performances with six-membered heterocycles, such as **41** (Scheme 1.8a), as well as the

more challenging seven- (**43**, Scheme 1.8b) and eight- (**45**, Scheme 1.8c) membered heterocycles.

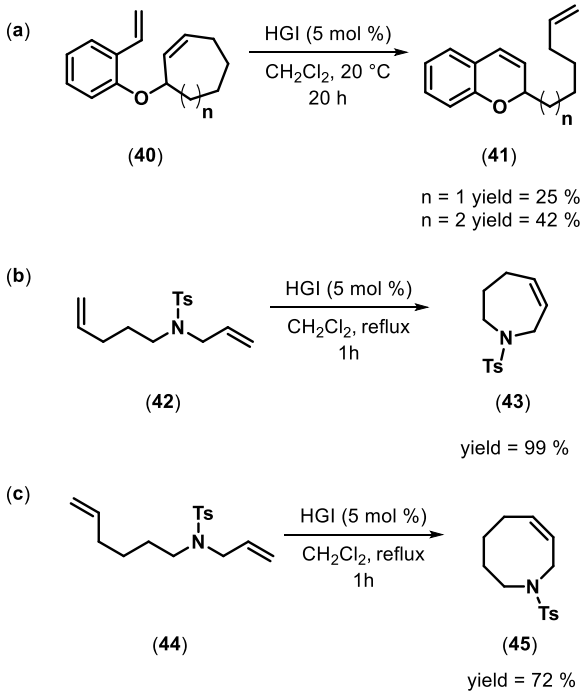

Scheme 1.8 Examples of HGI catalysed ring-closing metathesis of acyclic dienes
Ts = tosyl

In 2000 the Hoveyda Grubbs 2nd generation[16] (**33**, Figure 1.2) pre-catalyst synthesis and metathesis application was published. This pre-catalyst is phosphine free and it has improved thermal stability and moisture tolerance when compared with GII. The HGII allowed the RCM of dienes at ambient temperature and can tolerate the incorporation of free (**46**, Scheme 1.9a) and protected alcohol substrates (**48**, Scheme 1.9b) with excellent levels of conversion at ambient temperature.[16]

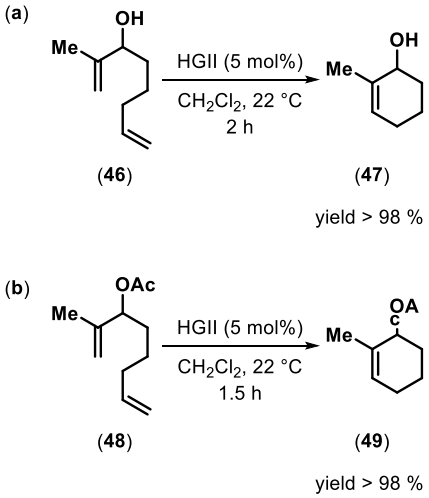

Scheme 1.9 Examples of dienes RCM catalysed by HGII

During the investigation of possible pre-catalysts for the CM of acrylonitrile (**51**, Scheme 1.10), Grubbs 3rd generation pre-catalyst (GIII, **53**) was developed.[7a] This pre-catalyst (**53**) was found to successfully catalyse the CM of acrylonitrile with allyl benzene (Scheme 1.10). Grubbs 3rd generation pre-catalyst gave a significantly higher yield than GII (67 % versus 27 %) and a similar yield to HGIII (67 % versus 68 %) in the reaction under study (Scheme 1.10).

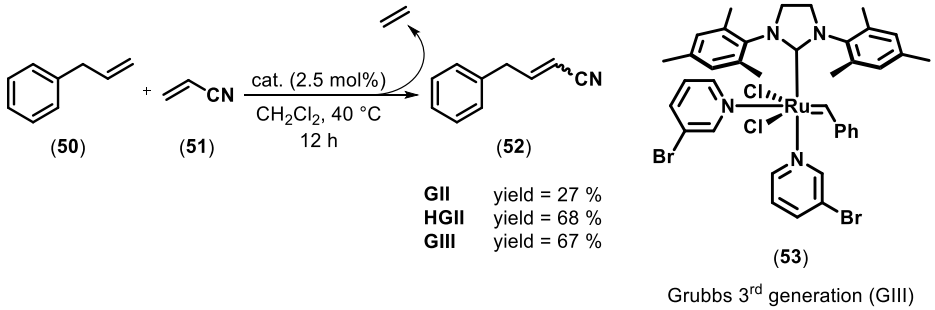

Scheme 1.10 Acrylonitrile cross metathesis with allyl benzene
GII = Grubbs 2nd generation pre-catalyst, HGII = Hoveyda-Grubbs 2nd generation pre-catalyst, GIII = Grubbs 3rd generation pre-catalyst, cat. = catalyst

Grubbs 3rd generation pre-catalyst has also been shown to be an excellent pre-catalyst for ROMP. For example, in 2002 Grubbs and co-workers reported the ROMP of COD (1, 5-cyclooctadiene, **54**) with GIII (**53**, Scheme 1.11) to give the polymer (**55**) in excellent yield and with short reaction times.[7a]

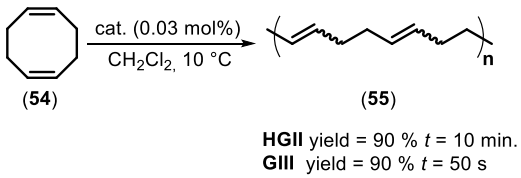

Scheme 1.11 ROMP of COD catalysed by HGI and GIII
HGI = Hoveyda-Grubbs 1st generation pre-catalyst, GIII = Grubbs 3rd generation pre-catalyst, yields calculated by ^{1}H-NMR, t = reaction time, s = seconds, min. = minutes

This initial report opened the path for application of GIII in polymerisation ROMP reactions. Indeed GIII combines fast polymerization rates and good functional group tolerance with narrow polydispersity index (PDI) as shown in the ROMP of norbornene (**56**, Scheme 1.12).[17] The breadth of molecular weight distribution in a polymer is measured by PDI, the higher the PDI value, the broader the molecular weight distribution, which is generally undesired.[18] The same reaction (Scheme 1.12) gave poor PDI when catalysed by GII.

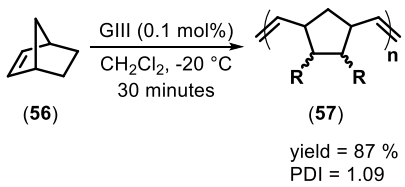

Scheme 1.12 ROMP of norbornene catalysed by GIII
PDI = polydispersity index

The high performace of GIII in the ROMP reaction is related to the very fast initiation step of the pre-catalyst so that chain termination and transfer reactions are absent during the turnover.[17]

Despite the intense pre-catalyst development that has been conducted since the first metathesis pre-catalyst was synthesised,[2] there are still many challenges to be tackled in order to exploit olefin metathesis to its maximum potential in both academic laboratories and in industrial settings.

1.2 Mechanism of olefin metathesis

Since the first metathesis reaction was published[2] its mechanism has been the focus of many studies[10-11] as the reaction appeared as a four-centre process which is forbidden by Woodward-Hoffmann rules. The absence of free cyclobutane in the metathesis mechanism was firstly highlighted by Pettit[11] and co-workers who noticed that free cyclobutane was not converted to ethylene under the same reaction conditions which allow ethylene degenerate metathesis.[11] The early mechanistic proposal for olefin metathesis involved 'pairwise' mechanisms.[11-12] The formation of a 'quasi-cyclobutane' intermediate complex (**60**,Scheme 1.3) was proposed to be generated from a bis-alkene complex (**59**) giving a direct interconversion of the alkenes. The molecular orbital description of the intermediate (**60**) was not widely accepted even if the quasi-cyclobutane mechanism accounted for the metathesis products at equilibrium (**62**, Scheme 1.3). Grubbs and co-workers suggested the cyclometallation of the reactants (**58**) leading to a metallocyclopentane intermediate (**63**, **64**, Scheme 1.3), which forms the product (**61**) by sigmatropic rearrangement followed by retrocyclometallation.[12]

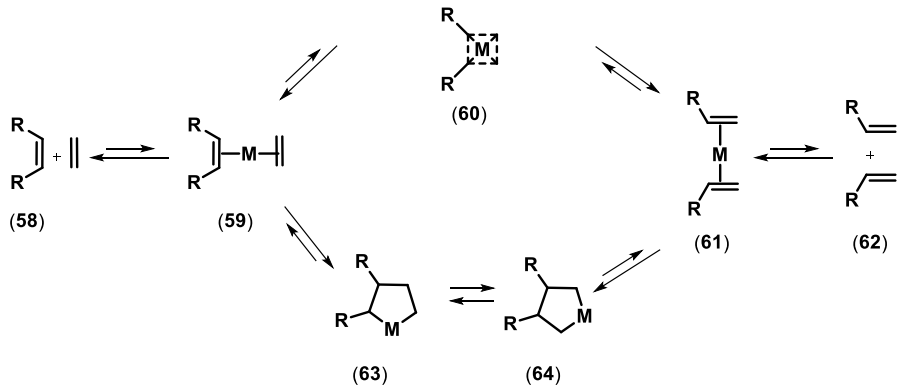

Scheme 1.13 Proposed metathesis pathways
'quasi-cyclobutane' (upper); metallocyclopentane (lower)

The breakthrough for the metathesis mechanism came in 1970 when Chauvin and Hérisson disproved the pairwise mechanism and proposed a sequential mechanism to be operative,[13] by studying the co-reaction of cyclic and acyclic olefins in the presence of $WOCl_4/Al(C_2H_5)_2Cl$ and $WOCl_4/Sn(C_4H_9)_4$ catalyst systems.

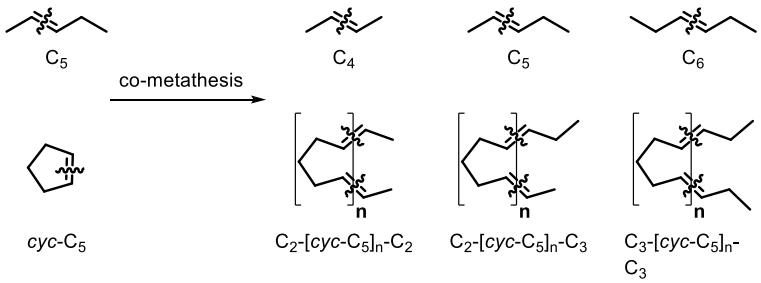

Scheme 1.14 Pent-2-ene (C_5) and cyclopentene (*cyc*-C_5) co-metathesis
Mono acyclic olefin products (upper), high molecular weight telomers and polymers (lower)

The products of pent-2-ene (C_5) and cyclopentene (*cyc*-C_5) co-metathesis (Scheme 1.14) were analysed in a fully equilibrated mixture of acyclic mono olefins (C_4:C_5:C_6 = 1:2:1) and taking into account that the rate of pent-2-ene homo-metathesis is comparable with the telomerisation reaction. At the early stage of the reaction the products were found to be C_2-$(C_5)_n$-C_2 and C_3-$(C_5)_n$-C_3 telomers produced in parallel with the C_4 and C_6 olefins and with a constant statistical telomer ratio of 1:2:1 (Scheme 1.14). The product distribution is inconsistent with a pairwise mechanism(Scheme 1.3) which would have given pure C_2-$(C_5)_n$-C_3 telomer products at the beginning of the reaction and then increasing concentrations of C_2-$(C_5)_n$-C_2 C_3-$(C_5)_n$-C_3 telomers as the reaction progresses. The results suggested that the two extremities of the telomer arise from two different olefin units. A chain reaction mechanism (Scheme 1.15) was proposed where the catalyst is an alkylidene complex (**65**, Scheme 1.15) and the carrier for one half of the olefin and sequential reactions of one olefin with two other olefins.

The Chauvin mechanism (Scheme 1.15) consists of a [2+2] cycloaddition of one of the olefin with the metal alkylidene species catalyst to form a four membered ring intermediate (**67**) which will open by retro [2+2] cycloaddition to generate one olefin product and a metal alkylidene bearing the olefin reactant (**69**). The latter can react with the other olefin reactant as previously to lead to the cross metathesis product (**72**) and the metal alkylidene species (**36**) to continue the catalytic cycle.

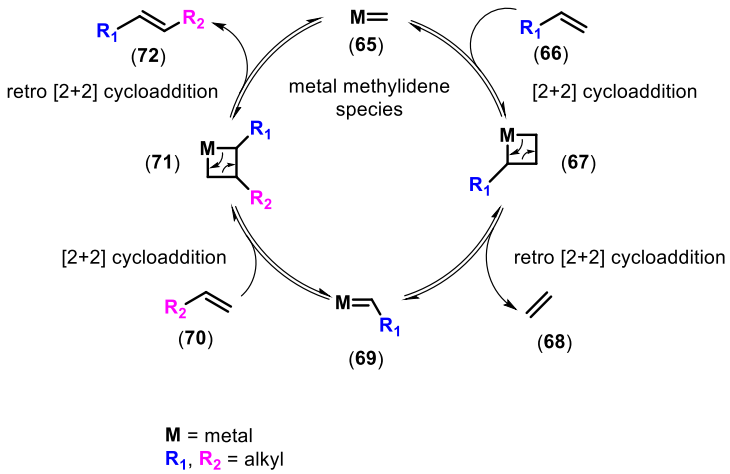

Scheme 1.15 Chauvin catalytic cycle
Shown for terminal alkene cross metathesis

The Chauvin mechanism involves the formation of a metal alkylidene active species (**65**, Scheme 1.15) from the pre-catalyst *via* a first catalyst turnover (Scheme 1.16) before the propagation takes place.

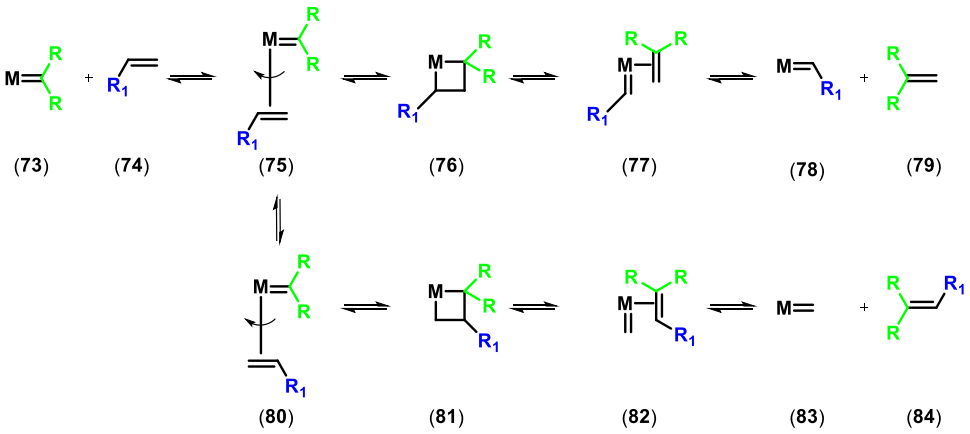

Scheme 1.16 Chauvin mechanism for olefin metathesis (initiation)

Both alkylidenes (**78**, **83**, Scheme 1.16) formed in the initiation process can undergo propagation (Scheme 1.17). After the formation of the metallocyclobutane intermediate (**93**, **100**, Scheme 1.17) the new coordinated olefin undergoes topologically identical shift in a perpendicular direction to the initial olefin shift (**94**, **101**, Scheme 1.17), leading to a metal alkylidene with the new olefin coordinated (**95**, **102**, Scheme 1.17). A new olefin is liberated from this alkylidene species (ethylene) which contains a carbene from the catalyst and a carbene from the starting olefin (**95**, **102**, Scheme 1.17). The metal alkylidene species

generated in this step has one of the two carbene of the starting olefin (**95**, **102**, Scheme 1.17) and it can re-enter a cycle of the same type. More in detail, two different metallocyclobutene can be formed in the new catalytic cycle depending on the orientation of the coordinated olefin (**87** and **92**, **99** and **104**, Scheme 1.17): one leading to the symmetrical olefin which will give productive metathesis (**92**, **99**, Scheme 1.17) and one the starting olefin giving a degenerate metathesis cycle (**87**, **104**, Scheme 1.17).

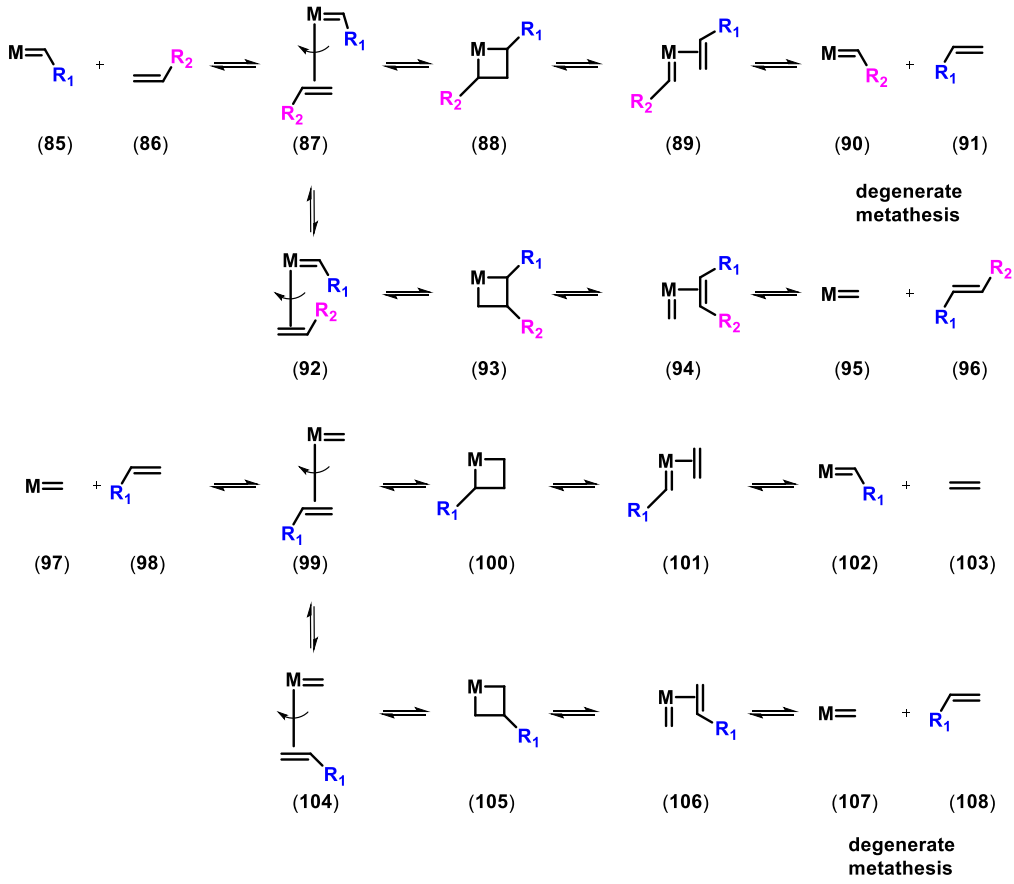

Scheme 1.17 Chauvin mechanism for olefin metathesis (propagation)

Further studies by Katz[14] and Grubbs[7c] confirmed the Chauvin mechanism to fit well for ruthenium, molybdenum and tungsten based pre-catalysts for olefin metathesis. This opened the path to the development of new efficient pre-catalysts based on isolable alkylidene complexes as precursors.

1.3 Challenges in cross metathesis

Cross metathesis is a very powerful tool to synthesise carbon-carbon bonds, however some issues in achieving high efficiency and selectivity remain. Cross metathesis reactions are often affected by side-reactions, such as self metathesis (**112**, **113**, Scheme 1.18). In addition, catalyst decomposition is a critical issue to overcome in order to allow the use of low catalyst loading.

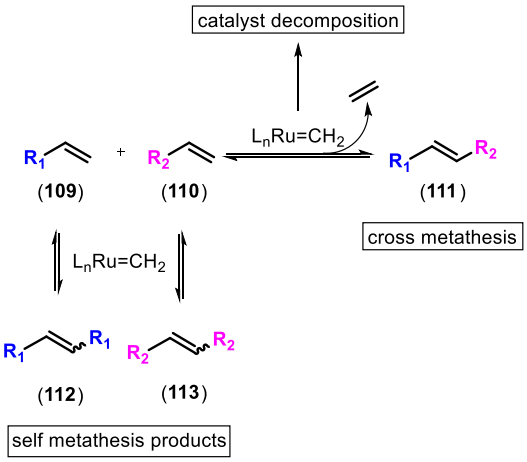

Scheme 1.18 Schematic example of the main challenges in cross metathesis

To achieve selective cross metathesis different approaches have been proposed. The use of a solid support for one of the olefin substrate was published for the reaction of terminal olefins with allyldimethylsilyl polystyrene (**114**) in the presence of GI as a pre-catalyst (Scheme 1.19).[19]

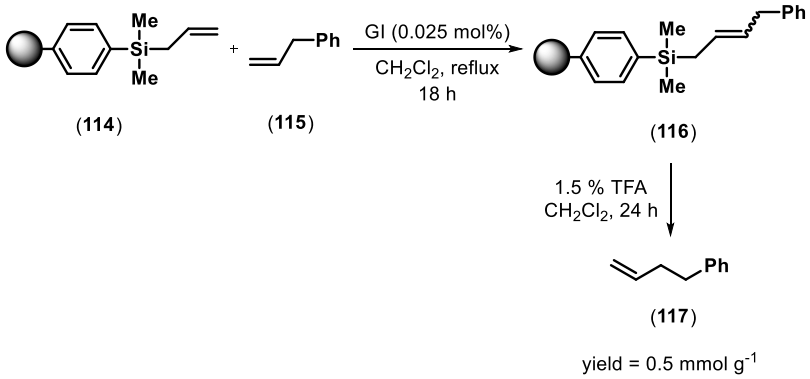

Scheme 1.19 Cross metathesis on allyldimethtlsilyl polystyrene (**114**)
Ph = phenyl, Me = methyl, GI = Grubbs 1st generation pre-catalyst, isolated yield calculated per gram of (**114**)

A two-step procedure was reported by Grubbs and co-workers as a method to avoid self metathesis products (Scheme 1.1).[20] The method consists of carrying out the self metathesis of a terminal olefin (**118**) first and then reacting an excess of product (**119**) with a second terminal olefin (**121**) to give the desired cross metathesis product (**120**).

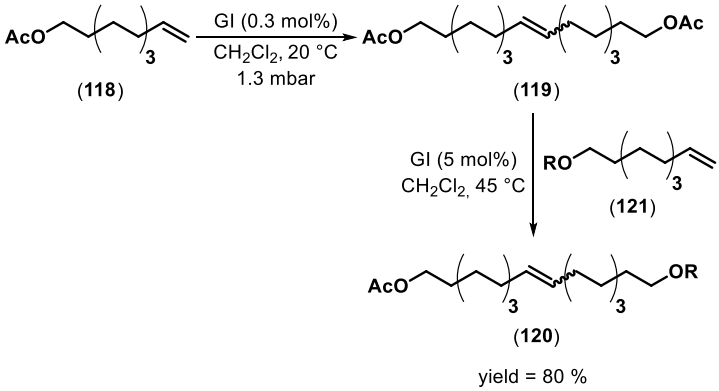

Scheme 1.20 Example of two-step selective cross metathesis
R = N-BOC-Gly, BOC = *tert*-butyloxycarbonyl, Gly = glycine, Ac = acetyl

The cross metathesis product can also be favoured by using an excess of one of the olefins. An example being the ethenolysis reaction, cross metathesis with ethylene as one of the reactant, performed at high ethylene pressures.[21] An example being the ethenolysis of ethyl crotonate (**122**, Scheme 1.21) to give ethyl acrylate (**123**) and propylene (**124**) with TONs which increase from 124 to 266 by increasing the ethylene pressure from 10 psi to 40 psi.[21]

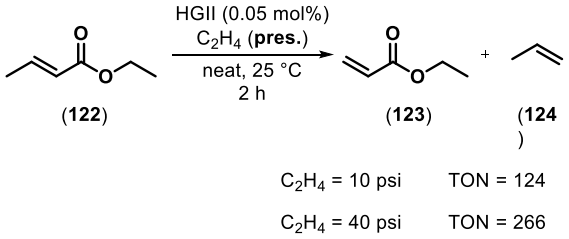

Scheme 1.21 Ethenolysis of ethyl crotonate (**122**)
TON = turnover number, HGII = Hoveyda-Grubbs 2nd generation pre-catalyst, pres. = pressure, psi = pounds per square inch

However, ethylene favours the decomposition of the ruthenium catalyst by increasing the concentration of the methylidene species (**125**, Scheme 1.22).[22] This species (**125**) is unstable and it reacts with free phosphine (PCy_3) when the ruthenium pre-catalyst used is phosphine based (**30**, **31**, GI, GII) leading to catalyst decomposition (Scheme 1.22).[23]

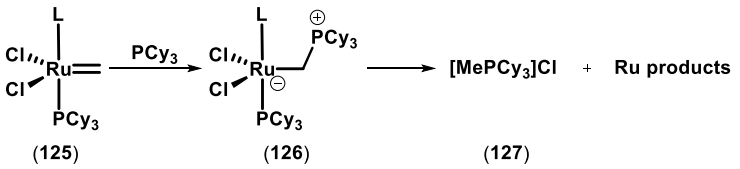

L = PCy_3 (GI), SIMes (GII), *o-iso*propoxyphenylmethylene (HGI)

Scheme 1.22 Decomposition pathway for phosphine based pre-catalysts (GI, GII)
GI = Grubbs 1st generation pre-catalyst, GII = Grubbs 2nd generation pre-catalyst,
PCy_3 = tricycloehexylphosphine, SIMe = 1,3-bis(2,4,6-trimethylphenyl)dihydroimidazole

Phosphine free pre-catalysts like Hoveyda-Grubbs 2nd generation have been previously proposed to decompose predominantly *via* β-hydride elimination of the metallocyclobutane (**128**, Scheme 1.23) leading to the allyl hydride (**129**), which then undergoes reductive elimination, generating propene (**130**).[24]

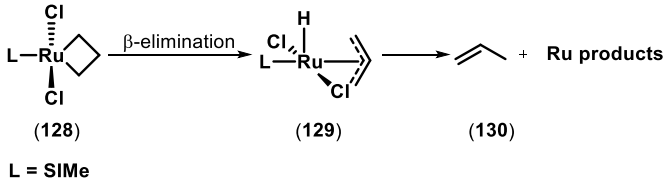

Scheme 1.23 Decomposition pathway for Hoveyda-Grubbs 2nd generation pre-catalyst (HGII)
SIMe = 1,3-bis(2,4,6-trimethylphenyl)dihydroimidazole

Recent detailed studies by Fogg and co-workers revealed that the predominant decomposition pathway occurs *via* formation of a bimolecular ruthenium complex (Figure 1.3) for HGII and GIII (**33**, **53**).[25]

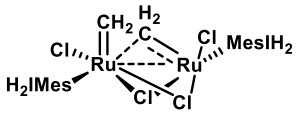

Figure 1.3 Bimolecular decomposition product
SIMe = 1,3-bis(2,4,6-trimethylphenyl) dihydroimidazole

With bimolecular coupling having a significant contribution on the decomposition of GIII, the efforts to synthesise high initiation efficient pre-catalysts needs to be balanced against acceleration in catalyst decomposition.

Despite the challenges related with an efficient and successful olefin cross metathesis reaction, many applications in synthesis and industrial processes have been reported.

1.4 Metathesis applications: from fine chemicals to oleochemicals

The improvements of metathesis pre-catalysts have made them user friendly, compatible with a wide range of functional groups and commercially available. These advances have allowed metathesis to be routinely used in the synthesis of pharmaceuticals,[26] polymers[17] and oleo chemicals.[27]

RCM has found wide use in pharmaceutical industry for the synthesis of large macrocycles (8 and 11 membered rings), which are usually difficult to synthesise due to the intramolecular entropic barrier encountered.[28] An example is the synthesis of tricyclic triazole (**134**), used in cancer treatment, by RCM of **132**. Subsequent hydrogenation and deprotection of the methoxy groups gives the desired product in 74 % yield (Scheme 1.24).[26a]

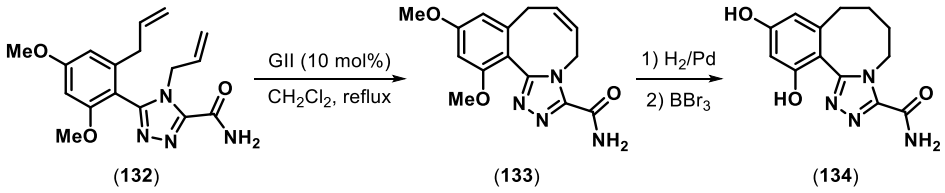

(**132**) (**133**) (**134**)

yield = 66 % yield = 74 %

Scheme 1.24 Example of RCM of 8-membered ring in the synthesis of tricyclic triazoles
GII = Grubbs 2nd generation pre-catalyst, Me = methyl

Cross metathesis is typically less utilised within the field of pharmaceutical synthesis compared with RCM. However, cross metathesis is still a key tool in the formation of carbon-carbon bonds. For example, the synthesis of Voxilaprevil, part of a three-drug cocktail for the re-treatment of hepatitis C, has been achieved by cross metathesis of cyclopropyl fragment **135** and difluoroallylic unit **136** in the presence of Ru-based pre-catalyst **139**. Subsequent macro-lactamisation and hydrogenation gave **138** in 59% yield over three steps (Scheme 1.25).[26b]

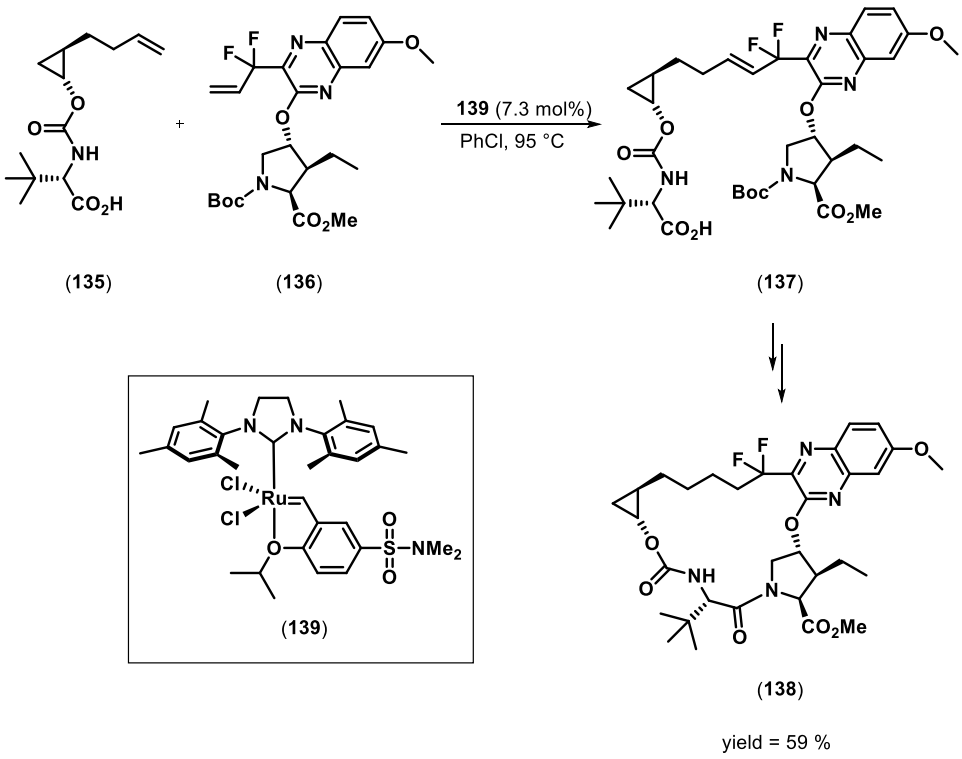

Scheme 1.25 Synthesis of the Voxilaprevir core: cross metathesis step
Me = methyl, Boc = *tert*-butyloxycarbonyl

Cross metathesis has also found major application in speciality chemical manufacturing,[29] the production of high-performance grade hydrogenated nitrile butadiene rubber (HNBR) being one example.[30] Partial metathesis depolymerisation of unsaturated nitrile butadiene rubber (**140**, NBR, Scheme 1.26), followed by hydrogenation gives HNBR (**143**) with improved degradation and chemical resistance.[30]

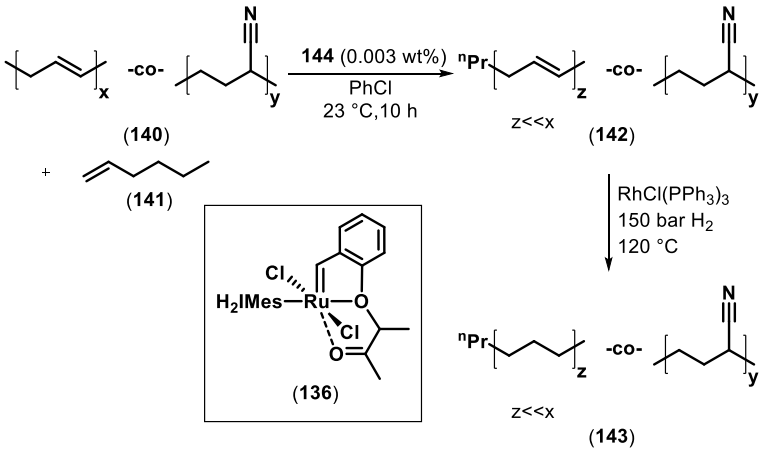

Scheme 1.26 Synthesis of HNBR

Moreover, the preparation of block copolymers with narrow molecular weight distribution has been made more accessible through the development of fast initiating Grubbs 3rd generation pre-catalyst (GIII).[17, 31] The rapid initiation and the high activity of GIII are beneficial to perform controlled living ROMP to make block polymers. In addition the reactions can be carried out at low temperatures (−20 °C) to avoid undesired chain transfer.[17]

Metathesis of unsaturated plant oils has gained increasing interest as a promising route for the production of olefin building blocks starting from renewable resources.[27, 32] Self metathesis of soybean oil (**145**, SBO)[33] is currently employed to convert 8.3 tonnes of purified oil into the hydrogenated metathesized soybean oil (**147**, HMSBO), which is a silicon-free emollient used in personal care products.[33]

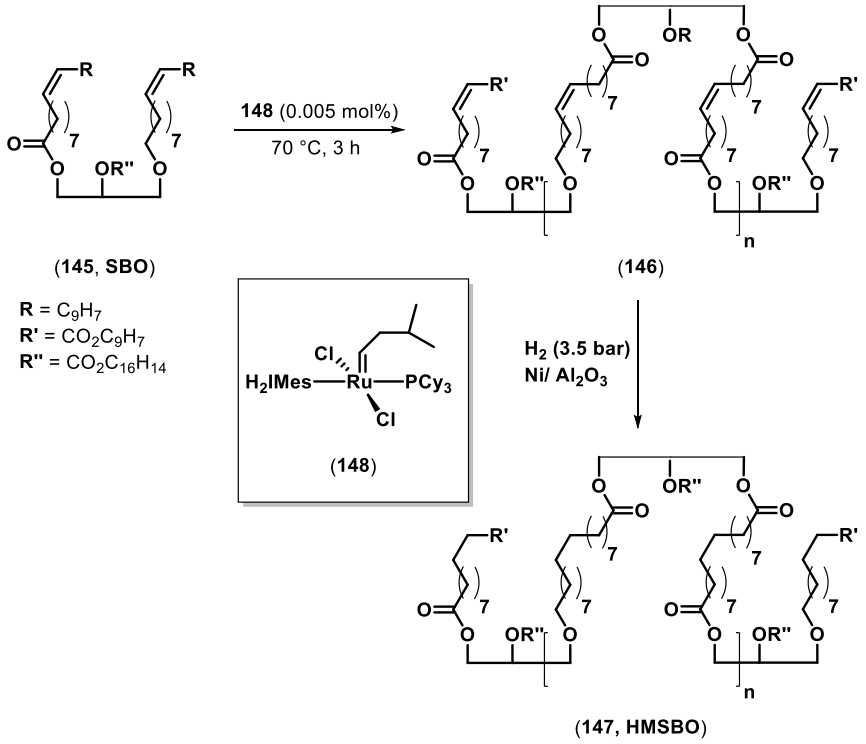

Scheme 1.27 preparation of HMSBO from purified soybean (SBO)
Simplified triglyceride shown

Various chain length products can also be obtained by cross metathesis of oleo chemicals with short chained olefins. Ethenolysis, the cross metathesis with ethylene as one of the substrates, is the most significant example leading to terminal olefins, which are important synthetic building blocks.[34] Indeed, the ethenolysis of methyl erucate (**149**) catalysed by

Neolyst pre-catalyst (**152**)[35] gave the desired terminal olefin product methyl 13-tetradecenoate (**150**) in 72 % yield.[34]

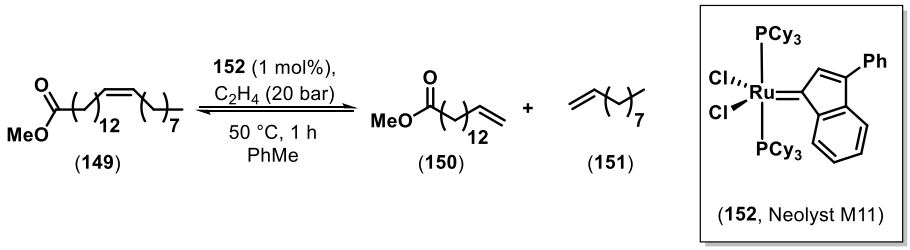

Scheme 1.28 Ethenolysis of methyl erucate (**149**)

The ethenolysis of fatty acid esters has great potential for the production of valuable chemicals from oil-based feedstock and the state of the art for this process is further discussed in chapter 2.

Olefin metathesis has been extensively studied in the last two decades to gain more insight into the reaction mechanism[10,14,36] and to improve the pre-catalyst performances (user friendly, wider substrate scope, lower catalyst loading).[7a-c,16] Although olefin metathesis is currently widely used in different chemistry fields (pharmaceuticals,[26b] polymers,[37] bio refinery[38]), there are still challenges to be addressed.

The ethenolysis of fatty acid esters, for instance, is not an industrially applicable process yet and the mechanism of initiation of some ruthenium pre-catalysts, such as GIII is still unknown.

1.5 References

1. Grubbs, R. H.; Chang, S., *Tetrahedron* **1998**, *54,* 4413-4450.
2. Eleuterio, H. S., german patent, 1072811, **1960**.
3. Calderon, N.; Chen, H. Y.; Scott, K. W., *Tetrahedron Lett.* **1967**, *8,* 3327-3329.
4. Schrock, R. R.; Murdzek, J. S.; Bazan, G. C.; Robbins, J.; DiMare, M.; O'Regan, M., *J. Am. Chem. Soc.* **1990**, *112,* 3875-3886.
5. Nguyen, S. T.; Johnson, L. K.; Grubbs, R. H.; Ziller, J. W., *J. Am. Chem. Soc.* **1992**, *114,* 3974-3975.
6. Connon, S. J.; Blechert, S., *Angew. Chem. Int. Ed.* **2003**, *42,* 1900-1923.
7. (a) Love, J. A.; Morgan, P. J.; Trnka, M. T.; Grubbs, H. R., *Angew. Chem. Int. Ed.* **2002**, *41,* 4035-4037; (b) Schwab, P.; Grubbs, R. H.; Ziller, J. W., *J. Am. Chem. Soc.* **1996**, *118,* 100-110; (c) Dias, E. L.; Nguyen, S. T.; Grubbs, R. H., *J. Am. Chem. Soc.* **1997**, *119,* 3887-3897; (d) Kingsbury, J. S.; Harrity, J. P. A.; Bonitatebus, P. J.; Hoveyda, A. H., *J. Am. Chem. Soc.* **1999**, *121,* 791-799.
8. Camara Greiner, E. O.; Y. Inoguchi, Y.; *Chemical Economics Handbook, Linear alpha-olefins*,IHS Chemical Ed., 2010.
9. Chaumont, P.; John, C. S., *J. Mol. Catal.,* **1988**, *46,* 317-328.
10. Chauvin, Y., *Angew. Chem. Int. Ed.* **2006**, *45,* 3740-3747.
11. S. Lewandos, G.; Pettit, R., *Tetrahedron Lett.* **1971**, *12,* 789-793.
12. Grubbs, R. H.; Brunck, T. K., *J. Am. Chem. Soc.* **1972**, *94,* 2538-2540.
13. Par, J. L. H.; Yves, C., *Die Makromolekulare Chemie* **1971**, *141,* 161-176.
14. Katz, T. J.; McGinnis, J., *J. Am. Chem. Soc.* **1977**, *99,* 1903-1912.
15. Scholl, M.; Trnka, T. M.; Morgan, J. P.; Grubbs, R. H., *Tetrahedron Lett.* **1999**, *40,* 2247-2250.
16. Garber, S. B.; Kingsbury, J. S.; Gray, B. L.; Hoveyda, A. H., *J. Am. Chem. Soc.* **2000**, *122,* 8168-8179.
17. Choi, T.-L.; Grubbs, R. H., *Angew. Chem. Int. Ed.* **2003**, *42,* 1743-1746.
18. Rane, S. S.; Choi, P., *Chem. Mater.* **2005**, *17,* 926-926.
19. Schuster, M.; Lucas, N.; Blechert, S., *Chem. Commun.* **1997**, 823-824.
20. O'Leary, D. J.; Blackwell, H. E.; Washenfelder, R. A.; Grubbs, R. H., *Tetrahedron Lett.* **1998**, *39,* 7427-7430.
21. Schweitzer, D.; Snell, K. D., *Org. Process Res. Dev.* **2015**, *19,* 715-720.
22. Hong, S. H.; Wenzel, A. G.; Salguero, T. T.; Day, M. W.; Grubbs, R. H., *J. Am. Chem. Soc.* **2007**, *129,* 7961-7968.
23. Hong, S. H.; Day, M. W.; Grubbs, R. H., *J. Am. Chem. Soc.* **2004**, *126,* 7414-7415.
24. Romero, P. E.; Piers, W. E., *J. Am. Chem. Soc.* **2005**, *127,* 5032-5033.
25. Bailey, G. A.; Foscato, M.; Higman, C. S.; Day, C. S.; Jensen, V. R.; Fogg, D. E., *J. Am. Chem. Soc.* **2018**, *140,* 6931-6944.
26. (a) J. A. Burlison, W. Ying. 2016/0009724, 2016; (b) A. Cagulada, J. C., L. Chan, D. A. Colby, K. K. Karki, Kato D., Keaton K., Kondapally S., Levins C., Littke A., Martinez, R.; Pcion, D.; Reynolds, T.; Ross, B.; Sangi, M.; Schrier, A.; J.; Seng, P. S., D.; Shapiro, N.; Tang, D.; Taylor, J. G.; Tripp, J.; Waltman, A. W. 9-440-991,2016.
27. Chikkali, S.; Mecking, S., *Angew. Chem. Int. Ed.* **2012**, *51,* 5802-5808.
28. Hughes, D.; Wheeler, P.; Ene, D., *Org. Process Res. Dev.* **2017**, *21,* 1938-1962.
29. Higman, C. S.; Lummiss, J. A. M.; Fogg, D. E., *Angew. Chem. Int. Ed.,* **2016**, *55,* 3552-3565.
30. Ong, C; Mueller, J. M.;Lanxess, WO023674A1, 2011.
31. Leitgeb, A.; Wappel, J.; Slugovc, C., *Polymer* **2010**, *51,* 2927-2946.

32. Biermann, U.; Bornscheuer, U.; Meier, M. A. R.; Metzger, J. O.; Schäfer, H. J., *Angew. Chem. Int. Ed.,* **2011**, *50,* 3854-3871.
33. T. A. Murphy, M. A. T., T.W. Abraham, A. Shafer, Cargill, US20090217568 A1, **2009**.
34. Seidensticker, T.; Vorholt, A. J.; Behr, A., *Eur. J. Lipid Sci Tech* **2016**, *118,* 3-25.
35. Dierker, L. J. G. O. US 20140046081A1, **2011**.
36. Grubbs, R. H.; Hoppin, C. R., *J. Am. Chem. Soc.* **1979**, *101,* 1499-1508.
37. Walsh, D. J.; Lau, S. H.; Hyatt, M. G.; Guironnet, D., *J. Am. Chem. Soc.* **2017**, *139,* 13644-13647.
38. Mol, J. C.; Buffon, R., *J. Brazil. Chem. Soc.* **1998**, *9,* 1-11.

Chapter 2 Ethenolysis of fatty acid esters

2.1 Summary

The ethenolysis of unsaturated oleochemicals is an attractive method for the production of high value chemical products from renewable, cheap, and widely available feedstocks.[1] In particular, the ethenolysis of methyl oleate (**153**, MO, Scheme 2.1) has been extensively reported,[2] as the resulting chemical products, 1-decene (**155**, Scheme 2.1) and methyl-9-decenoate (**154**, Scheme 2.1), are widely employed in the production of lubricants, polyesters,[3] and cosmetics.[4]

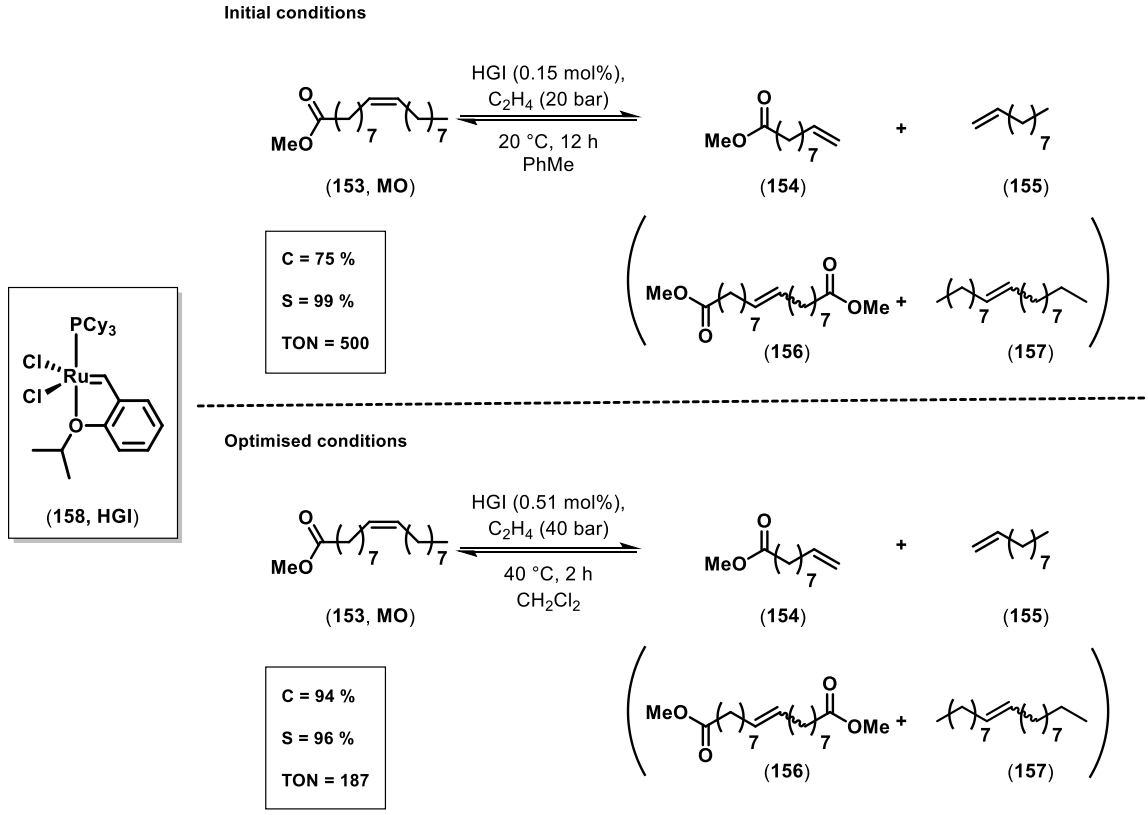

Scheme 2.1 Ethenolysis of methyl oleate: initial and optimised reaction conditions.
C = conversion, S = selectivity, TON = turnover number, HGI = Hoveyda-Grubbs 1st generation pre-catalyst, constant pressure of ethylene

In order to increase the performance of the methyl oleate ethenolysis with respect to selectivity and substrate conversion, the identification of active and stable catalysts is crucial. An evaluation of a range of commercially available metathesis pre-catalysts showed that the Hoveyda-Grubbs 1st generation pre-catalyst (HGI, **158**) afforded the highest conversion and selectivity with the reaction conditions used in this study.

2.2 Introduction

Ethenolysis is a cross metathesis reaction involving ethylene and an internal olefin, to give two terminal olefins in the presence of an olefin metathesis catalyst (Scheme 2.2).[5] Under ideal conditions, involving the complete displacement of the equilibrium towards the reaction products, ethenolysis is an atom-economical reaction which leads to final products having all the starting materials incorporated.[5]

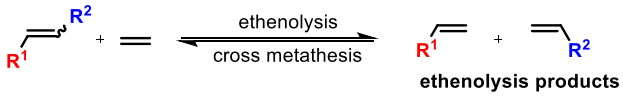

Scheme 2.2 Ethenolysis reaction

In 1967 Bradshaw, Howman and Turner from the British Petroleum Research Centre reported the first example of ethenolysis. They observed propene formation (**160**, Scheme 2.3) with high selectivity towards the ethenolysis products (over 90 %) by passing 2-butene (**159**, Scheme 2.3) and ethylene over an heterogeneous $CoO/MoO_3/Al_2O_3$ catalyst at 180 °C.[6]

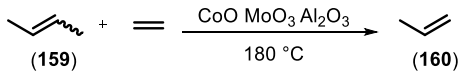

Scheme 2.3 First example of ethenolysis reaction[6]

Since then, various applications of the ethenolysis reaction have been demonstrated, including the synthesis of dienes from cyclic alkenes (Scheme 2.4a) and the formation of shorter terminal olefins from the scission of long chain unsaturated molecules (Scheme 2.4b) and polymers.[5]

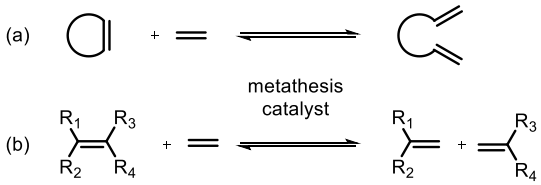

Scheme 2.4 Examples of the application of ethenolysis reactions

Ethenolysis reactions are thought to follow the general Chauvin mechanism for olefin metathesis catalysed by a metal alkylidene as described in chapter 1 (Scheme 2.5).[7] Indeed,

an excess of ethylene favours on one hand the equilibrium to be shifted towards the ethenolysis products (Scheme 2.2) and on the other hand the formation of metal methylidene species which contributes to non-productive metathesis processes (**161**, Scheme 2.5).

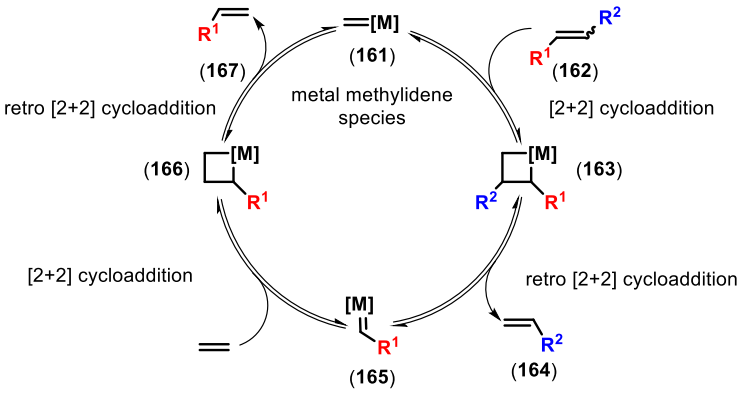

Scheme 2.5 Chauvin mechanism applied to ethenolysis[7]

Moreover, the metathesis catalyst catalyses both ethenolysis and substrate self metathesis and secondary metathesis of the ethenolysis products (Scheme 2.6). An excess of ethylene favours the formation of ethenolysis products over the by-products.

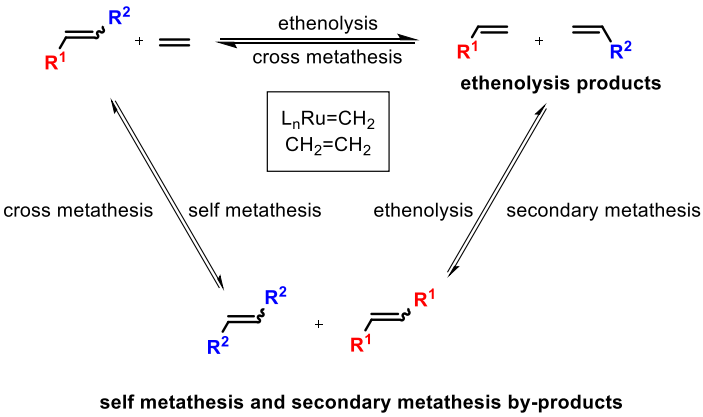

Scheme 2.6 Ethenolysis reaction and side reactions

In addition, ethenolysis reactions are affected by the same limitations previously discussed for cross metathesis reactions such as products isomerization and catalyst decomposition.[5] Despite some reaction limitations, ethenolysis has found extensive application in fine chemistry and industry.[5] Diene formation by opening of strained bicyclic olefins being one

example. Ethenolysis of cyclooctadiene (**168**, COD) catalysed by $MoCl_5/SiO_2$-$SnMe_4$ to give 1,5,9-decatriene (**169**) in 68 % yield and 80 % substrate conversion (Scheme 2.7) has been reported.[8] The product obtained (**169**) was further used for the two-step synthesis of the main sex pheromone component of *Musca Domestica* (**171**).[8]

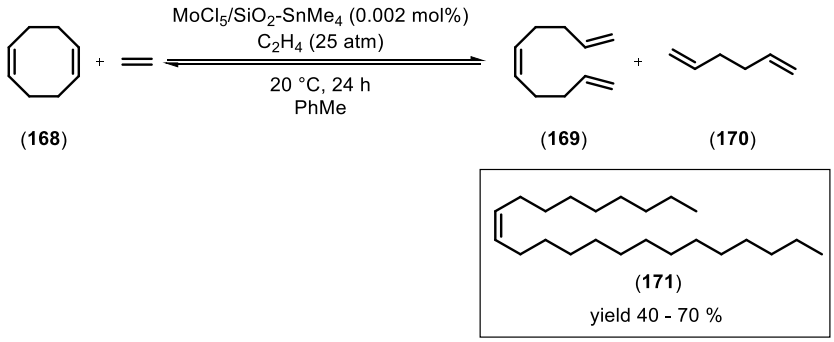

Scheme 2.7 Ethenolysis of COD to form 1,5,9-decatriene as the main product *Z*-9-tricosene (**171**): main sex pheromone component of *Musca Domestica*[8]

At the end of the 1960s Phillips Petroleum developed an industrial scale production using the Phillips Triolefin Process based on the isomerisation of 1-butene to 2-butene over MgO catalyst followed by ethenolysis over WO_3/SiO_2. At temperatures higher than 260 °C and a pressure range of 30-35 bar, a conversion of 2-butene above 60 % and a selectivity for propene higher than 90 % (Scheme 2.8) was achieved.[9] The process was used from 1966 to 1972 to convert propene into ethylene and butene and it is currently employed by ABB Lummus Global as olefin conversion technology (OCT) for the production of propene (Scheme 2.8).[9]

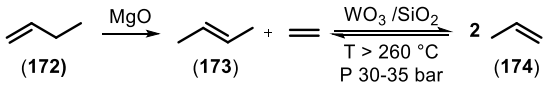

Scheme 2.8 OCT (olefins conversion technology) for propene production

Ethenolysis of fatty acid esters provides a promising way to convert biomass for the production of valuable chemicals.[10] The replacement of fossil feedstocks with bio-based resources - vegetable and seed-based oils- has become of great interest to the society to try and solve issues of renewability.[1] The quality of the substrates is an ongoing challenge for the industrial application of ethenolysis of biomass-derived feedstocks as the presence of low concentration of catalyst poisons, such as water and peroxides,[11] has a detrimental

effect on catalyst productivity.[12] Biomass purification methods - over active supports such as alumina[13]and Magnesol®[14] - have been reported in various patent; however, the industrial application of ethenolysis of biomass has not found industrial application yet. Examples of ruthenium-catalysed ethenolysis of bio-sourced feedstocks have been reported, such as use of methyl ricinoleate (**175**, from ricinoate oil) to obtain methyl-dec-9-enoate (**177**, 85 %) and decenol (**176**, 92 %) with the 2nd generation indenylidene complex (**178**, Scheme 2.9) inducing up to 96 % conversion.[15]

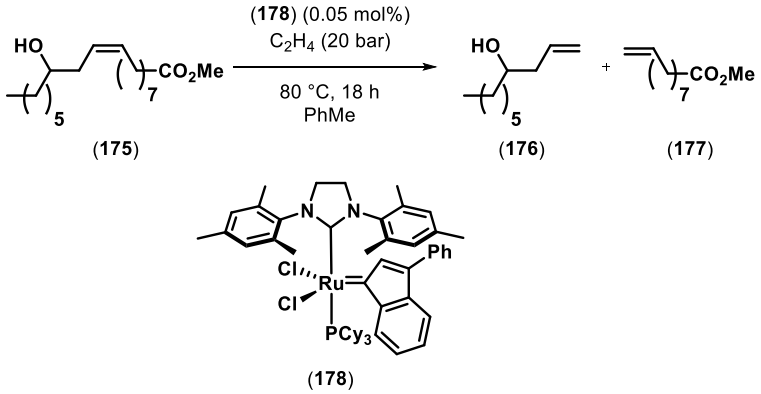

Scheme 2.9 Ethenolysis of methyl ricinoleate

Ethenolysis of methyl oleate (**179**, MO)is a reaction of particular industrial interest, as the products of this process -methyl dec-9-enoate (**180**, Scheme 2.10) and 1-decene (**181**, Scheme 2.10)- are widely valued for the production of lubricants, polyesters and cosmetics.[4],[3]

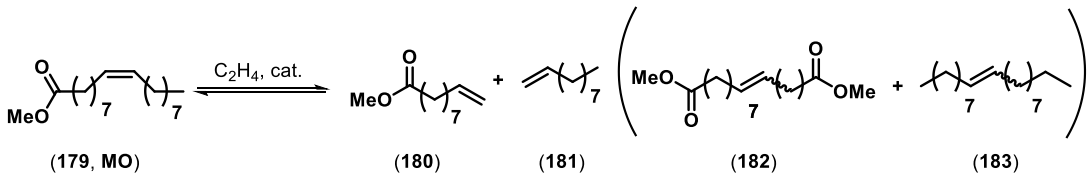

Scheme 2.10 Ethenolysis of methyl oleate

In 1981 the first ethenolysis of MO (**179**) was reported by utilising tungsten and rhenium catalysts using 50 bar of ethylene pressure to convert 60 % to 70 % of the starting material to the co metathesis products (**180**, **181**) in 40 % to 70 % selectivity.[16]

Significant progress has been made since then, especially in respect of catalyst compatibility. Ruthenium-based homogeneous catalysts, which tolerate a broad range of functional groups, have been shown to perform better than tungsten- and molybdenum- based

catalysts.[17] The reaction has been shown to be limited by the interactions between the carbonyl groups in the substrate and the molybdenum catalyst precursors.[18], [19]

The metathesis catalyst promotes not only the ethenolysis process but also the competing self metathesis (**187**, **188**) of the starting material and the secondary cross metathesis of the terminal olefins formed by ethenolysis of MO (**184**, Scheme 2.11).[5]

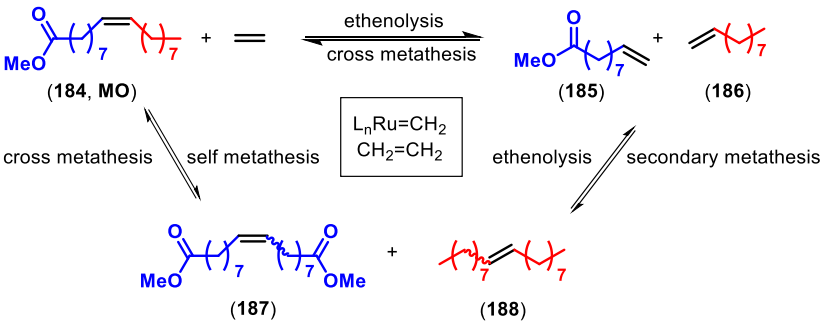

Scheme 2.11 Ethenolysis of methyl oleate and competing reactions

An excess of ethylene favours the formation of ethenolysis products over the side-products. The equilibrium of the reaction is dependent on the concentration of ethylene in solution, which is in turn dictated by the initial pressure and the solubility in the reaction solvent.[5]

In order to achieve an industrially employable ethenolysis process the turnover number (TON) must be higher than 50000, as stated by The Dow Chemical Company, due to the cost and the sustainability of many transition metal homogeneous pre-catalysts, such as ruthenium.[10]

Previous reports on ethenolysis of MO (Scheme 2.12) showed that 1st generation Grubbs pre-catalysts favour the formation of ethenolysis products as the major products,[20] whereas 2nd generation Grubbs pre-catalysts give lower selectivity (Scheme 2.12).[21] Second generation Hoveyda-Grubbs pre-catalysts afford lower selectivity towards self metathesis products over ethenolysis products (Scheme 2.12).[2] The best performing process reported so far has shown a conversion of 99 %, a TON of 99 and a selectivity of 95 % for the ethenolysis product by catalysing the reaction with Grubbs 1st generation pre-catalyst (1 mol%) for 3.5 hours at 1 bar ethylene pressure in toluene (Scheme 2.12).[22] Good conversion (91 %) and selectivity (99 %) has been achieved with Hoveyda-Grubbs 1st generation pre-catalyst (2.5 mol%) and 1 bar ethylene pressure; however, a low TON of 36 was reported.[3]

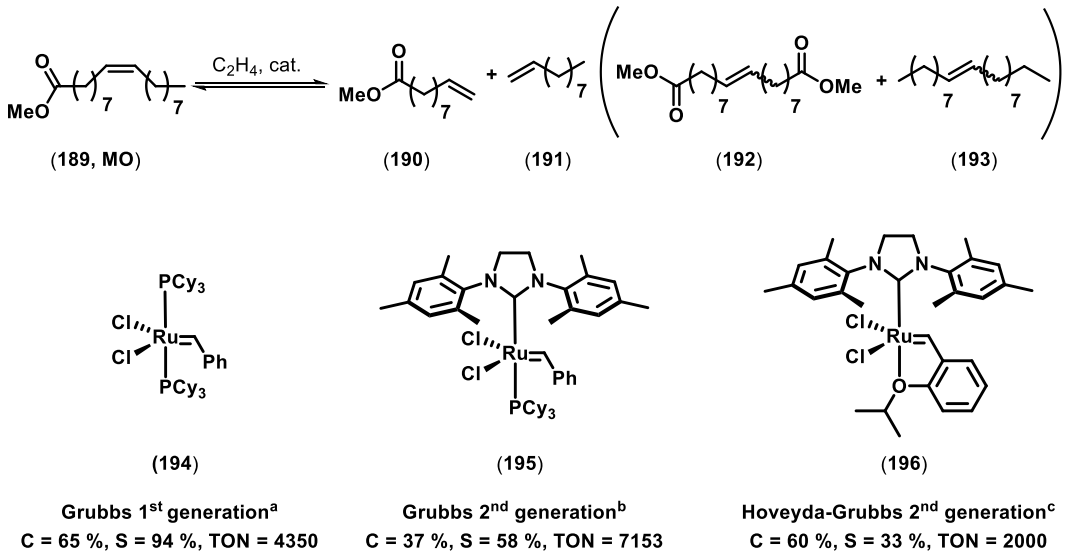

Scheme 2.12 General pre-catalysts trend for ethenolysis of MO
C = conversion, S = selectivity towards 1 and 2, TON = turnover number
[a] C_2H_4 (4 bar), cat. load. (0.014 mol%), 30 °C, 10 h, PhMe;[20]
[b] C_2H_4 (10 bar), cat. load. (0.003 mol%), 60 °C, 2 h, neat;[21]
[c] C_2H_4 (10 bar), cat. load. (0.01 mol%), 40 °C, 0.5 h, neat[2]

The ethenolysis of MO has still not reached the TON required for industrial application in the presence of commercially available pre-catalysts. However, the significant improvements that have been achieved in the last 30 years make this process a promising catalytic reaction for further investigations.

2.3 Membrane Separation in Cross Metathesis

Despite their high activity and selectivity in metathesis reactions, the industrial employment of Grubbs-type pre-catalysts remains challenging. The high cost, toxicity and difficult separation of these pre-catalysts from the reaction mixture have hampered their industrial applications.[23] The complete removal of residual ruthenium species is especially important for applications in the pharmaceutical industry as residual metal content in drug substances is 5 ppm for oral dosage and 0.5 ppm for parenteral administration.[24] The development of methods to separate the catalysts and reuse them in an active form from post-reaction mixtures has gained significant importance. Different methods have been tested to recycle the catalyst: heterogenisation (using polymer supports), biphasic extraction, and membrane separation. The latter has been found to be the most promising method as both the heterogenisation and the biphasic extraction gave lower activity and selectivity than the use of homogeneous catalysts.[23]

Membrane separation techniques can be used to separate the catalyst from the reaction components, avoiding their deactivation (Figure 2.1). In addition, the incorporation of this technique into flow reactors allows catalyst recycling, a process of great importance for sustainable chemical manufacturing. Organic solvent nanofiltration (OSN) is a technique that consists of a pressure driven filtration process capable of separating larger (homogeneous) molecules in the molecular weight range of 200-1000 Da from smaller molecules and having excellent organic solvent compatibility.[24]

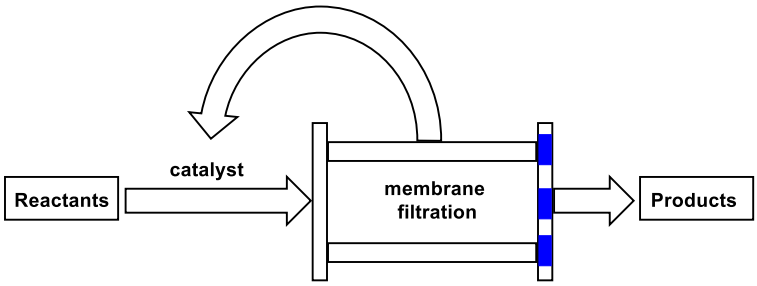

Figure 2.1 Schematic example of membrane separation technique

The vast majority of applications of OSN uses molecular weight enlarged pre-catalysts to achieve a facile filtration, however, the industrial application of these pre-catalysts is hampered from their lack of commercialisation. The goal for industry would be to employ

commercially available pre-catalysts while mantaining high partition of the catalyst from reaction products.

The membrane performances are generally based on the solute rejection and the permeate flux where the solute rejection across the membrane is defined as a measure of its partitioning: the higher the rejection, the better the partitioning, and the easier the separation. The permeate flux of various solvent and solute mixtures is defined as the permeate volume measured per unit of time and effective membrane area.

The application of OSN to metathesis reactions has been reported[23] for the self metathesis of 1-octene (**197**) with Grubbs 1st and 2nd generation and Hoveyda-Grubbs 1st generation pre-catalysts (**199**, **200**) with STARMEM™ as a membrane (Scheme 2.13). In the system under study the rejection of the catalyst (catalyst concentration in the retentate) was greater than 99 %; however, no significant catalytic activity was shown in the coupled reaction-separation and recycling process after the first separation step.

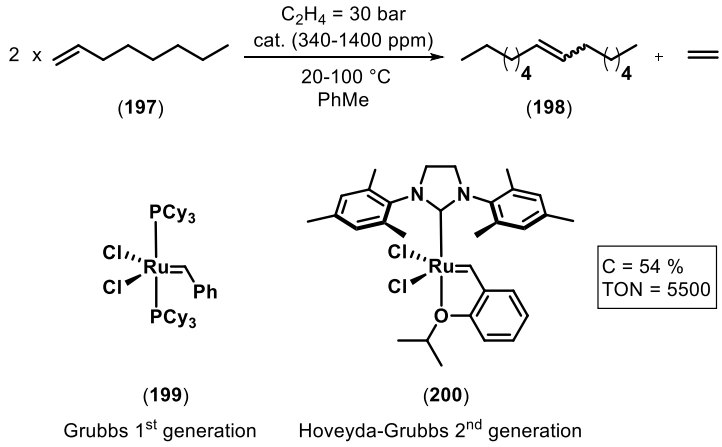

Scheme 2.13 Self metathesis of 1-octene to 7-tetradecene and ethylene
C = conversion (maximum value obtained),
TON = turnover number (overall on 4 cycles of consecutive reaction-separation)

The ring-closing metathesis of *N*-tosyldiallylamine (**201**, Scheme 2.14) has been successfully catalysed by Hoveyda-Grubbs 2nd generation pre-catalyst (**203**) using a continous-flow reactor which employs an in-line separation of the catalyst from the reaction product *via* a membrane.[24] Using systematic, automated (variable flow reactor involved) and oxygen free work-up procedures, the system has been run for 50 hours (70 recycle experiments) using 0.75 mol% of catalyst reaching a total turnover number (TON) of 935 with a ruthenium contamination in the products lower than 1 ppm.

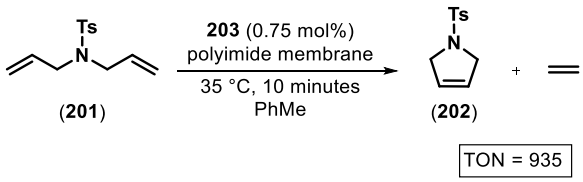

Scheme 2.14 Ring-closing metathesis of *N*-tosyldiallylamine with Hoveyda-Grubbs 2nd generation pre-catalyst (**203**)

The results achieved so far by applying OSN to metathesis reactions are promising and it would be very interesting to expand the scope of the membrane separation technique to other industrially relevant metathesis reactions, such as the ethenolysis of fatty acid esters.

2.4 Project objective

The aim of this project was to improve the performance of the ethenolysis of fatty acid esters (Scheme 2.15) towards high TONs, conversion and selectivity. The chosen model reaction, ethenolysis of methyl oleate, has been investigated by testing commercially available pre-catalysts and by employing Design of Experiments (DoE) to optimise the reaction conditions.

The optimisation process has been focused on improving the conversion because the selectivity and the TONs were planned to be improved using membrane separation techniques to enable catalyst recycling and product separation.

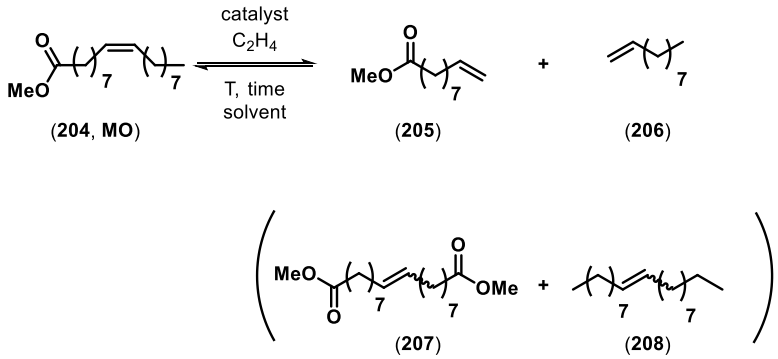

Scheme 2.15 Ethenolysis of methyl oleate

2.5 Catalyst screening

Catalyst screening was performed to identify pre-catalysts with high activity for the ethenolysis of MO, in order to carry out the reaction with low catalyst loadings.

Firstly, an analytical method to analyse the reaction mixture was investigated. The by-products (**207**, **208**, Scheme 2.15) were isolated from the catalytic reaction mixture and identified by comparison with reported ^{1}H-NMR and ^{13}C {^{1}H} NMR spectra.[25] Methyl 9-decenoate (**210**) was synthesised following a reported procedure (Scheme 2.16) [26] whereas 1-decene (**206**) was commercially available.

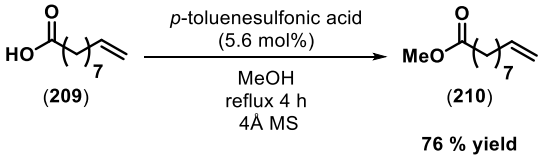

Scheme 2.16 Synthesis of methyl 9-decenoate

The isolated products (**212**, **213**, **214**, and **215**) were analysed by GC-MS to identify the mass spectra and the respective retention times of each compound. A calibration curve for the methyl oleate was performed using *n*-nonane as an internal standard (IS) and the response factor (rf) was obtained from the gradient of the plot obtained (Figure 2.2).

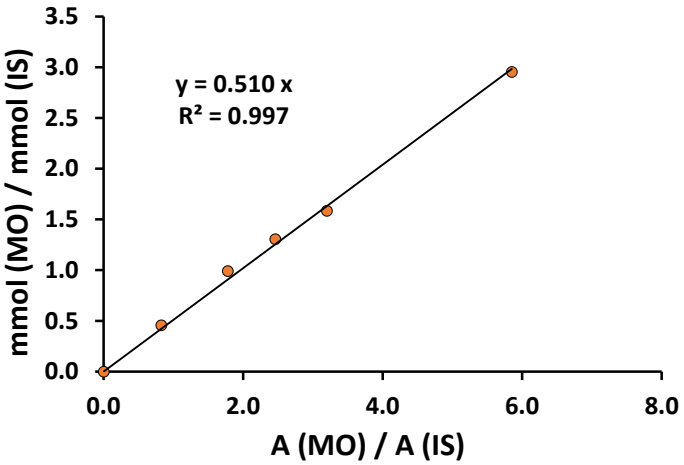

Figure 2.2 GC calibration curve for methyl oleate
ratio between chromatogram peak area of MO and IS on the x-axis,
ratio between MO and IS mmol on the y-axis

The latter result was used to calculate the amount (mmol) of substrate at the beginning and at the end of the reaction (Equation 2.1).

$$mmol\,(MO) = rf * \frac{Area\,(MO)}{Area\,(IS)} * mmol\,(IS)$$

Equation 2.1 Methyl oleate mmol calculation from calibration curve

After the method for analysing the reaction mixture was finalised, preliminary experiments were carried out to identify appropriate conditions for catalyst screening.

Initially, the effect of ethylene pressure and reaction time was studied, starting from a reported benchmark reaction.[27] High constant pressures of ethylene were found to be beneficial to the process (Scheme 2.17) and the conversion reached a maximum value of 79 % after 15 hours.

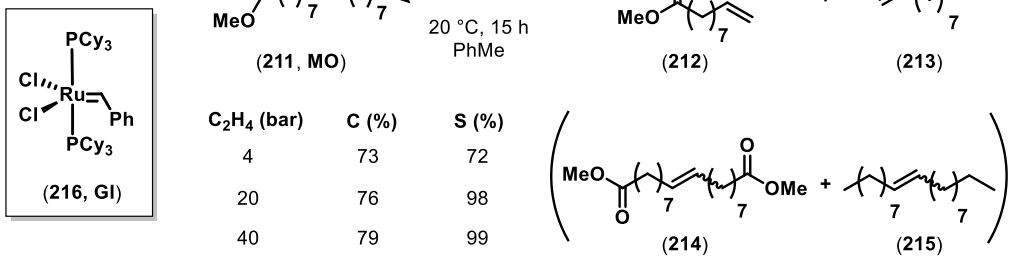

C_2H_4 (bar)	C (%)	S (%)
4	73	72
20	76	98
40	79	99

Scheme 2.17 Ethenolysis of methyl oleate and ethylene pressure screening
C = conversion, S = selectivity, GI = Grubbs 1st generation pre-catalyst
Reaction mixture analysed by GC-FID.
Selectivity = normalised areas (**212** + **213**) / normalised areas (**212** + **213** + **214** + **215**).
Conversion = [1−(mmol MO (initial) /mmol MO (final)]*100

In order to make the catalyst screening both time and cost effective, the catalyst loading was lowered from 1 mol% to 0.15 mol% and the reaction time was shortened to give a benchmark reaction (Scheme 2.18) with a conversion of 60 %, which is convenient for comparison of performance among a range of pre-catalysts.

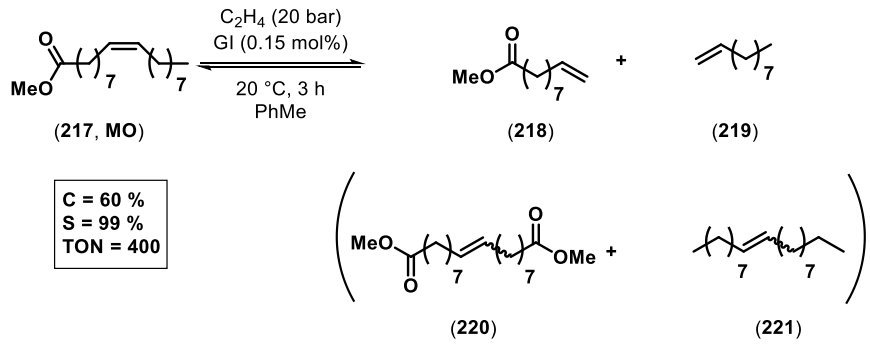

Scheme 2.18 Catalyst screening benchmark reaction
C = conversion, S = selectivity, TON = turnover number, GI = Grubbs 1st generation pre-catalyst
TON = conversion / catalyst loading

A series of commercially available metathesis pre-catalysts were tested and conversion and selectivity towards the ethenolysis products were calculated by GC-FID. The pre-catalysts used in the screening were stored in the glove-box freezer and the reactions were performed utilising pre-catalysts from the same batch.

Low values for selectivity were found for Ru pre-catalysts bearing NHC ligands and a phosphine (Table 2.1, **227**, **228**, **229**). Whereas higher selectivity was obtained when the phosphine ligands were replaced with a chelating *ortho*-isopropoxybenzylidene ligand (Table 2.1, **231**, **232**). High selectivity values and good conversion were reached with Grubbs 1st generation and Hoveyda-Grubbs 1st generation pre-catalysts (Table 2.1, **230**, **233**). The CatMETium® pre-catalysts (Table 2.1, **234**, **235**) led to good conversions, but very low selectivity towards the ethenolysis products. The fast initiating pre-catalyst (**236**, GIII) gave good conversion and low selectivity towards the ethenolysis products (Table 2.1).[28]

The overall trend of results showed high selectivity for the 1st generation pre-catalysts (Table 2.1, **230**, **233**), whereas the 2nd generation pre-catalysts gave poor selectivity (Table 2.1, **227**, **231**) in agreement with previously reported studies.[20], [2], [27]

From the evaluation of a range of commercially available metathesis pre-catalysts Hoveyda-Grubbs 1st generation pre-catalyst was found to be optimal for the ethenolysis of MO (Table 2.1, **233**).

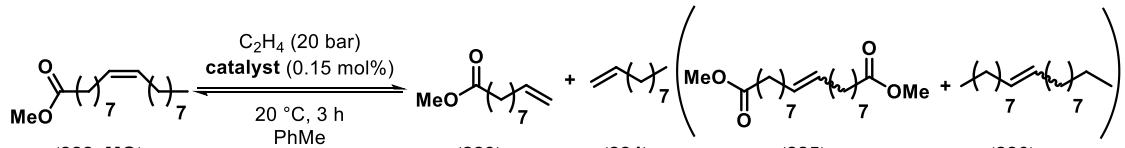

(**222**, **MO**) (**223**) (**224**) (**225**) (**226**)

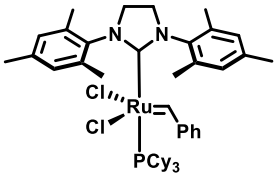

(**227**)

Grubbs 2nd generation
C = 64 %, S = 17 %,
TON = 406

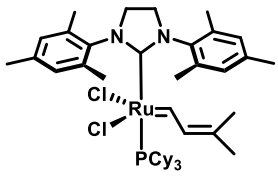

(**228**)

Grubbs C827
C = 60 %, S = 2 %,
TON = 400

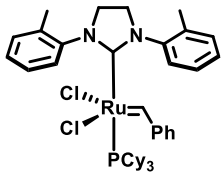

(**229**)

o-Tolyl Grubbs
C = 54 %, S = 20 %,
TON = 36

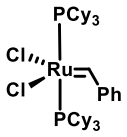

(**230**)

Grubbs 1st generation
C = 60 %, S = 99 %,
TON = 400

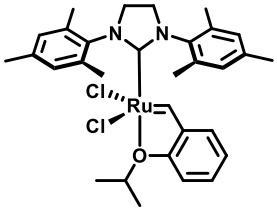

(**231**)

Hoveyda-Grubbs 2nd generation
C = 72 %, S = 60 %,
TON = 480

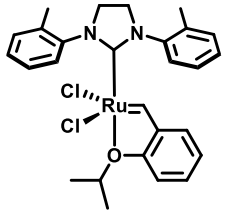

(**232**)

Steward-Grubbs
C = 60 %, S = 26 %,
TON = 400

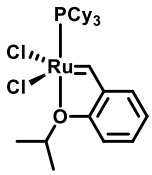

(**233**)

Hoveyda-Grubbs 1st generation
C = 75 %, S = 99 %,
TON = 500

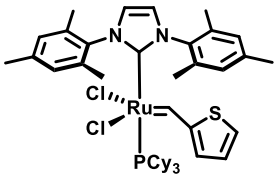

(**234**)

CatMETiumRF2®
C = 68 %, S = 7 %,
TON = 453

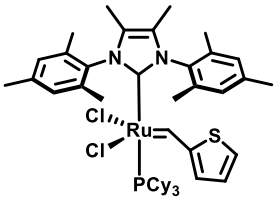

(**235**)

CatMETiumRF3®
C = 66 %, S = 1 %,
TON = 440

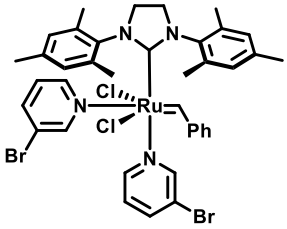

(**236**)

Grubbs 3rd generation
C = 63 %, S = 12 %,
TON = 420

Reaction mixture analysed by GC-FID. Every pre-catalyst was tested in duplicate.
Selectivity = normalised areas (**223** + **224**) / normalised areas (**223** + **224** + **225** + **226**).
Conversion = [1-(mmol MO (initial) /mmol MO (final)]*100. TON = conversion / catalyst loading

Table 2.1 Catalysts screening

2.6 Design of Experiments

Design of experiments (DoE) was employed to further optimise the reaction parameters for the ethenolysis of MO using the Hoveyda-Grubbs 1st generation pre-catalyst, which was found in the preliminary screening (Table 2.1) to be the optimal pre-catalyst in terms of selectivity and activity.

DoE refers to a process of planning, designing and analysing an experiment to gain valid and objective conclusions effectively and efficiently.[29] The use of DoE allows the optimum conditions to be found by choosing points throughout the entire space within the maximum and minimum values given to the variables, whereas the commonly used one variable at a time (OVAT) approach reaches optimum conditions dependent on the starting point. In addition DoE relies on smaller number of experiments than the OVAT approach, therefore the former is a quicker method to reach optimal conditions.

The process under study in a DoE is called a system and the variables that have an influence on the system are labelled as factors. The possible values of the factors used in the design are called levels, while the consequence induced by the factor to the system is the output or response (measurable outcomes of the process) (Figure 2.3). The aim of a DoE is to establish a relationship between the factors and the responses. The change in response when the factor changes from low to high level (effect) is analysed. In addition, the response of a factor depending on the level of other factors (interaction) is evaluated. Following a systematic work flow the full potential of a DoE can be exploited.[30]

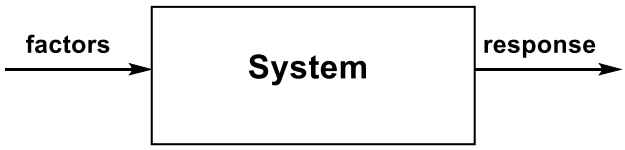

Figure 2.3 Schematic model for DoE
system: process under study; factors: variables that effect the system; response: measurable effect induced by the factors to the system

First, the DoE objective has to be defined to start the process. Then factors have to be identified and their ranges determined, taking into account knowledge of the system under study in order to get values which are relevant and practically achievable. When the factor values have been set, the responses need to be identified. In the same DoE, more than one response can be analysed without creating more experiments. Taking into account the objective of the DoE, the number of factors under study and the resources available, the

experimental design to employ can be chosen. The most common choice is screening designs that help to find the significant factors that affect the responses under investigation from a list of many potential ones. DoE software (e. g. Minitab 17) will generate a series of reactions to perform based on factors, factor levels and type of design. The order of reactions will be randomised by the software to mitigate any bias or error. From the screening design, results, and analysis the most significant factors which affect the responses can be identified. Two-level screening designs are the most frequently used screening designs because they are simple, economical and give most of the information needed in a subsequent response surface design. The simplest two-level screening design is the full factorial which takes into account all possible combinations (L^f) between different factors (f) and their levels (L) with L = 2 for two-level design (Figure 2.4).

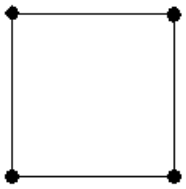

Figure 2.4 Two-level factorial design for 2 factors (L = 2, f = 2)
the points are coded to be factor's lowest levels and factor's highest levels

The interaction effects between the factors are estimated and the number of experiments to perform increases exponentially with the number of factors (2^f). When the number of factors is too high to make the full factorial design convenient, a fractional factorial (FF) design can be chosen. In a FF design only a fraction of the full factorial design is performed, which leads to a loss of information. Indeed from a FF design all the main and interaction effects cannot be estimated individually but the factors are confounded with a 3-factor interaction (e.g. in a system with factors A, B, C, D the factor A will be confounded with BCD, B with ACD and C with ABD). Placket-Burman designs are the main alternative to the saturated fractional factorial designs,[31] these type of designs lead to estimation of only main effects as two factors and higher order interactions are confounded with the main effects. After a screening design, the most important factors that affect the process quality are identified and the system can be further optimised *via* response surface designs.

A surface response model is usually used to refine the design in order to identify the factor settings that optimise the desired responses. The surface response equation differs from a factorial design equation by the addition of a square quadratic term which gives 3D surface

model. This allows a region of a response surface to be mapped and to find the levels of variables which optimise a response.

The two main surface designs are the Box-Wilson central composite design (commonly called "central composite designs") and Box-Behnken design.[31]

The central composite designs contain embedded factorial or fractional factorial design (blue points, Figure 2.5) with centre points augmented with a group of axial points (red points, Figure 2.5), which leads to the curvature estimation of the response. The response variable is modelled with a 3D surface by adding central and axial points to a previous factorial design, so it is especially useful in sequential experiments.

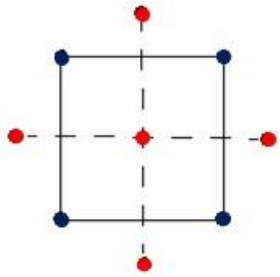

Figure 2.5 Central composite design for two factors
the factorial design (blue points) is improved with center and star points (red points)
to allow estimation of the curvature

The Box-Behnken designs are based on treatment combinations at the midpoints of the edges of the experimental space (Figure 2.6). They have fewer design points than the central composite designs, which makes them less expensive to run with the same number of factors. However, the Box-Behnken designs do not have an embedded factorial design and are not suitable for sequential experiments. They are most useful when the safe operating zone for the process is known because no axial points are generated and all the design points fall within a safe operating zone.

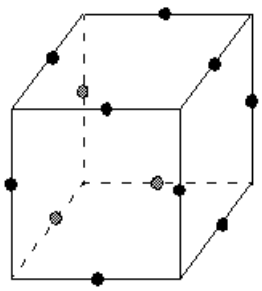

Figure 2.6 Box-Behnken design for 3 factors, the factors levels are at the midpoints of the edges

After response surface design results have been analysed, the optimised conditions suggested by the DoE must be experimentally tested.

2.6.1 Two-level Full Factorial Design

A two-level full factorial design was utilised to identify the parameters that have the greatest effect on the ethenolysis of MO. This method is used to find the significant factors that affect the process output out of a large group of potential factors. The parameters to investigate were selected and a minimum and a maximum value for each of them was chosen, according to experimental restrictions and previous work done (Table 2.2).

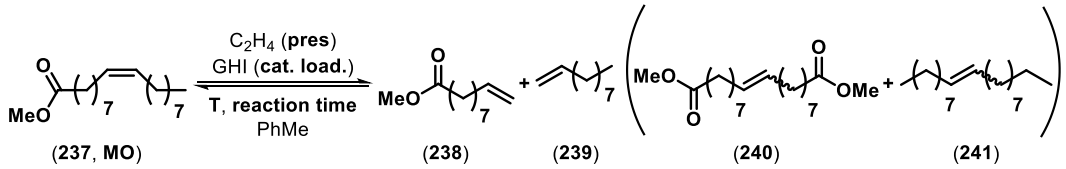

(**237**, **MO**) (**238**) (**239**) (**240**) (**241**)

Factor	Min level	Max level
Temperature (°C)	20	50
Ethylene pressure (bar)	20	40
Reaction time (min)	15	30
Catalyst loading (mol %)	0.15	0.40

Table 2.2 Input factors for two-level full factorial design

The experiments produced by the two-level full factorial design were carried out and the results were analysed, focusing on conversion as a response, as membrane separation was planned to be implemented with the system. The membrane separation technique was proposed to improve TON and selectivity by recycling the catalyst and separating the products.

A normal plot of effects was generated to assess how closely the data followed a normal distribution (Figure 2.7). This graph was obtained by plotting the estimated effects for the main factors and available interactions versus the rank-ordered parameters. From the four factors under investigation (temperature, reaction time, catalyst loading and ethylene pressure) the software identified four single effects and nine interaction effects (15 points total), taking into account the experimental results. The normal plot of effects shows the

significant negative effects on the left side and the positive on the right (Figure 2.7). The fitted line indicates where the points would be expected to fall if the effects were zero. This shows that reaction time and catalyst loading were the parameters with the greatest effect on the reaction conversion (red squares, Figure 2.7).

Figure 2.7 Normal plot of effects for the two-level full factorial design factors: temperature (T = A), reaction time (time = B), catalyst loading (catLoad = C), C_2H_4 pressure (pres = D); response = conversion (conv.); α = level of statistical significance (0.05 means good level of significance); effects not affecting the reaction conversion (blue dots), effects affecting the reaction conversion (red squares)

In addition, a main effects plot (Figure 2.8) was used to examine the differences between mean values of the conversion for the parameters under study. It shows the response mean for each parameter value connected by a line; there is a main effect when the different values of a parameter affect the response differently (steep line). The major effect of the catalyst loading and the reaction time was corroborated by the main effect plot (Figure 2.8).

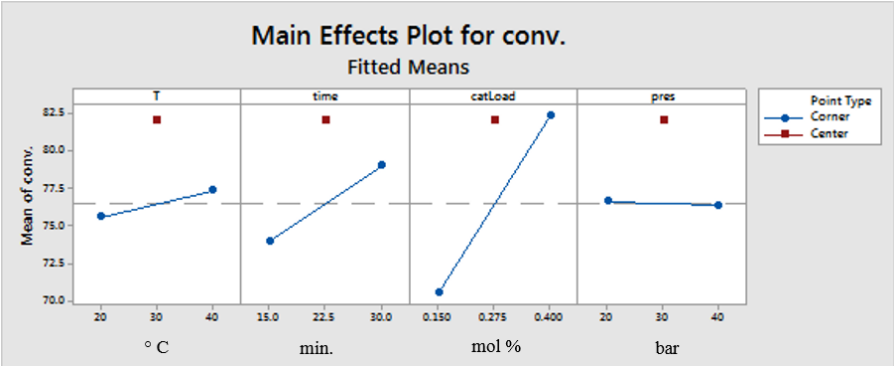

Figure 2.8 Main effects plot for the two-level full factorial design
factors: temperature (T), reaction time (time), catalyst loading (catLoad), C_2H_4 pressure (pres);
response = conversion (conv.);
corner type points (blue dots)= minimum and maximum level for each factor
center type points (red squares) = measure process stability and variability

The parameters that were found to have a smaller effect on the conversion were kept at their optimal values (ethylene pressure at 40 bar and temperature at 40 °C). The ethylene pressure was kept at 40 bar even if the main effect plot shows the conversion to be slightly better at 20 bar by taking into account previous experiments. The parameters that showed a significant effect on the conversion have been further optimised by a central composite response surface design.

2.6.2 Surface Response Design

A central composite design has been used as a surface response design to refine the outputs after the important factors have been determined by factorial design.[31] Maximum and minimum values for catalyst loading and reaction time were chosen (Table 2.3).

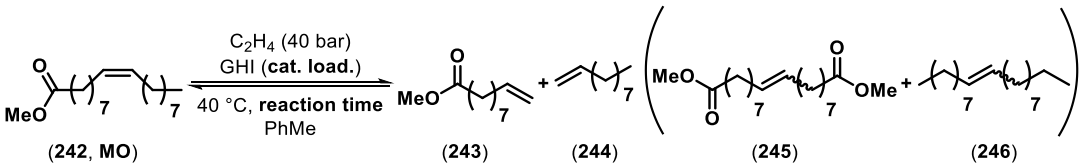

Factor	Minimum level	Maximum level
Reaction time (min)	15	240
Catalyst loading (mol %)	0.01	1

Table 2.3 Input factors central composite design

The experiments generated by the DoE software were performed and the results were elaborated with the aim of identifying the predicted best values for the investigated parameters to lead to the maximum conversion. A contour plot was created in order to explore the potential relationship between three variables as it displays the predictor variables on the x and y axes and the response values in contour (Figure 2.9).

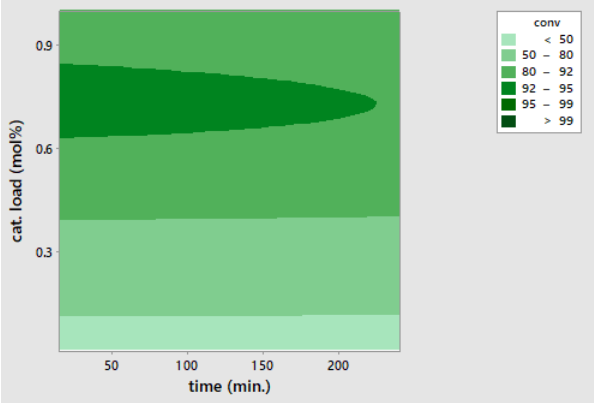

Figure 2.9 Contour plot of conversion vs catalyst loading, time
reaction time (time), catalyst loading (cat. load), response = conversion (conv.);
x-axis = predictor variable for reaction time, y-axes = predictor variable for catalyst loading;
z-axis = response values for the conversion

The response surface results were also elaborated to create a 3D surface plot where the predictor variables are displayed on the x and y axes and the response variable is represented by a smooth surface (Figure 2.10).

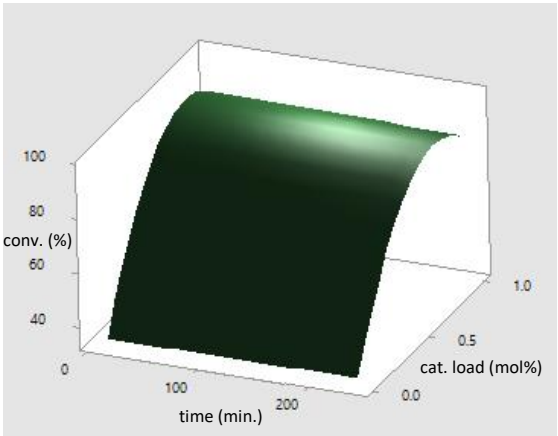

Figure 2.10 Surface plot of conversion
reaction time (time), catalyst loading (cat. load), response = conversion (conv.);
x-axes = predictor variable for reaction time, y-axes = predictor variable for catalyst loading;
z-axis = response variable (conversion)

Both a contour plot (Figure 2.9) and a response surface graph (Figure 2.10) established that the predicted optimum conditions were a catalyst loading of 0.7 mol% and a reaction time of 20 minutes (Table 2.4, entry 2).

The optimum conditions predicted by the DoE were experimentally tested and although the results showed that conversion (Table 2.4, entry 2) was not significantly improved in comparison with the initial conditions of 0.51 mol% of catalyst loading (Table 2.4, entry 1), this was achieved in a much shorter time (20 minutes instead of 2 hours).

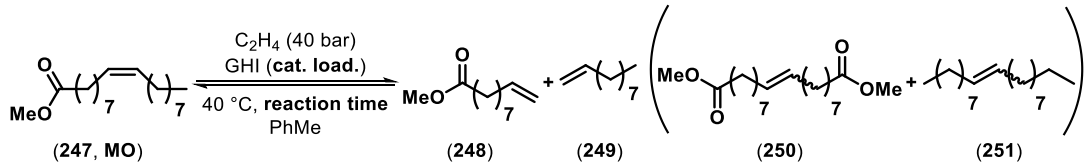

Entry	Time (min)	Cat. load. (mol%)	Conversion (%)	Selectivity (%)	TON
1	120	0.51	87	98	172
2	20	0.70	88	99	126

Conditions: methyl oleate 2.36 mmol, I.S (*n*-nonane) 2.24 mmol, ethylene 40 bar, 2 mL toluene, 40 °C, reaction time. Reaction mixture analysed by GC-FID.

Table 2.4 Reaction performance in the best conditions

The reaction conditions were kept at 0.51 mol% catalyst loading, because the pre-catalyst is the most valuable reactant and the reaction was carried out both neat and in dichloromethane, with the best conversion given in the latter (Table 2.5, entry 2).

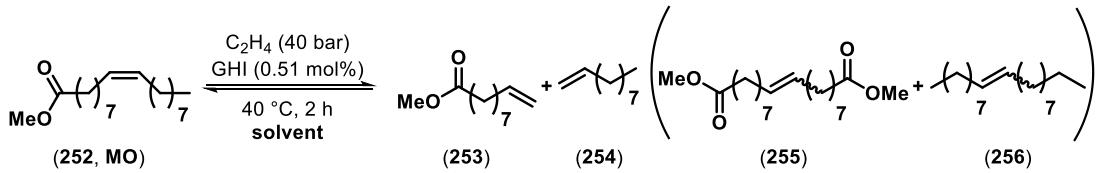

Entry	Solvent	Conversion (%)	Selectivity (%)	TON
1	toluene	87	98	172
2	dichloromethane	94	96	187
3	neat	75	98	148

Conditions: methyl oleate 2.36 mmol, catalyst loading 0.51 mol%, I.S (*n*-nonane) 2.24 mmol, ethylene 40 bar, 2 mL solvent, 40°C, 128 minutes. Reaction mixture analysed by GC-FID.

Table 2.5 Solvent test in the best reaction conditions

2.7 Conclusion and Future Work

The ethenolysis of methyl oleate was studied with the aim of achieving higher conversions, as a membrane separation technique was planned to be used to increase TON and selectivity towards ethenolysis products.

The Hoveyda-Grubbs 1st generation pre-catalyst was found to be the best performing pre-catalyst in the conditions under study after a catalyst screening of the most commonly-employed commercially available metathesis pre-catalysts. The reaction conditions with Hoveyda-Grubbs 1st generation pre-catalyst have been improved *via* DoE (carrying out 33 experiments instead of 81 OVAT). The starting conditions setting gave a conversion of 75 %. The set of conditions given from the DoE showed improved conversion both in dichloromethane (Scheme 2.19a) and in toluene (Scheme 2.19b).

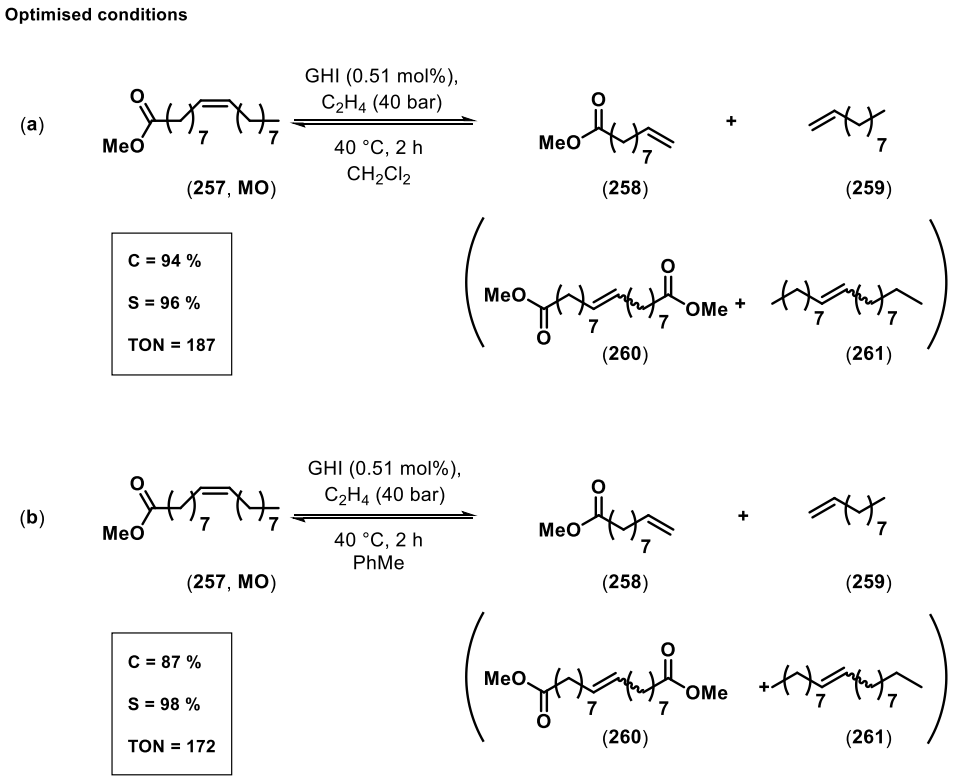

Scheme 2.19 Optimised reaction conditions for the ethenolysis of methyl oleate
C = conversion, S = selectivity, TON = turnover number, HGI = Hoveyda-Grubbs 1st generation pre-catalyst, constant pressure of ethylene

This study opens the path for further improvements of the ethenolysis of methyl oleate towards achieving the TON required for industrial applications (TON = 50000). Indeed, the employment of a flow reactor to perform continuous metathesis coupled with membrane

separation of the catalyst will allow catalyst recycling and products separation leading to higher TON and selectivity.

2.8 References

1. Biermann, U.; Bornscheuer, U.; Meier, M. A.; Metzger, J. O.; Schafer, H. J., *Angew. Chem. Int. Ed.,* **2011**, *50,* 3854-71.
2. Schrodi, Y.; Ung, T.; Vargas, A.; Mkrtumyan, G.; Lee, C. W.; Champagne, T. M.; Pederson, R. L.; Hong, S. H., *CLEAN - Soil, Air, Water* **2008**, *36,* 669-673.
3. Thurier, C.; Fischmeister, C.; Bruneau, C.; Olivier-Bourbigou, H.; Dixneuf, P. H., *Chem. Sus. Chem.,* **2008**, *1,* 118-122.
4. Thomas, R. M.; Keitz, B. K.; Champagne, T. M.; Grubbs, R. H., *J. Am. Chem. Soc.,* **2011**, *133,* 7490-7496.
5. Bidange, J.; Fischmeister, C.; Bruneau, C., *Chem. Eur. J.,* **2016**, *22,* 12226-12244.
6. Bradshaw, C. P. C.; Howman, E. J.; Turner, L., *J. Catal.,* **1967**, *7,* 269-276.
7. Par, J. L. H.; Yves, C., *Macromol. Chem. Physic.,* **1971**, *141,* 161-176.
8. Bykov, V. I.; Butenko, T. A.; Petrova, E. B.; Finkelshtein, E. S., *Tetrahedron,* **1999**, *55,* 8249-8252.
9. Mol, J. C., *J. Mol. Catal. A: Chem.* **2004**, *213,* 39-45.
10. Spekreijse, J.; Sanders, J. P.; Bitter, J. H.; Scott, E. L., *Chem. Sus. Chem.,* **2017**, *10,* 470-482.
11. Samir, C.; Stefan, M., *Angew. Chem. Int. Ed.,* **2012**, *51,* 5802-5808.
12. Patel, J.; Mujcinovic, S.; Jackson, W. R.; Robinson, A. J.; Serelis, A. K.; Such, C., *Green Chem.,* **2006**, *8,* 450-454.
13. D. W. Lemke, K. D. U., F. Amore, T. Abraham, Elevance Renewable Sciences Inc., Chicago (US), WO 020667, **2009**.
14. K. M. Wampler, S. A. C., G. E. Frater, L. Ondi, J. Varga, Elevance Renewable Sciences Inc., Woodridge (USA), US 0275595A1, **2014**.
15. Behr, A.; Krema, S.; Kamper, A., *RSC Adv.,* **2012**, *2,* 12775-12781.
16. Bosma, R. H. A.; Van den Aardweg, F.; Mol, J. C., *J. Chem. Soc. Chem. Commun.,* **1981**, 1132-1133.
17. Trnka, T. M.; Grubbs, R. H., *Acc. Chem. Res.,* **2001**, *34,* 18-29.
18. Mol, J. C., *J. Mol. Catal.,* **1994**, *90,* 185-199.
19. Mol, J. C.; Buffon, R., *J. Brazil. Chem. Soc.,* **1998**, *9,* 1-11.
20. Burdett, K. A.; Harris, L. D.; Margl, P.; Maughon, B. R.; Mokhtar-Zadeh, T.; Saucier, P. C.; Wasserman, E. P., *Organometallics,* **2004**, *23,* 2027-2047.
21. Forman, G. S.; McConnell, A. E.; Hanton, M. J.; Slawin, A. M. Z.; Tooze, R. P.; Van Rensburg, W. J.; Meyer, W. H.; Dwyer, C.; Kirk, M. M.; Serfontein, D. W., *Organometallics,* **2004**, *23,* 4824-4827.
22. Chatterjee, A. K.; Morgan, J. P.; Scholl, M.; Grubbs, R. H., *J. Am. Chem. Soc.,* **2000**, *122,* 3783-3784.
23. Van der Gryp, P.; Barnard, A.; Cronje, J.-P.; de Vlieger, D.; Marx, S.; Vosloo, H. C. M., *J. Membrane Sc.,* **2010**, *353,* 70-77.
24. O'Neal, E. J.; Jensen, K. F., *Chem. Cat. Chem.,* **2014**, *6,* 3004-3011.
25. Johns, A. M.; Ahmed, T. S.; Jackson, B. W.; Grubbs, R. H.; Pederson, R. L., *Org. lett.,* **2016**, *18,* 772-775.
26. Naoum, R.; Séguin, J. P.; Trant, J. F.; Frampton, M. B.; Hudlický, T.; Zelisko, P. M., *Tetrahedron,* **2016**, *72,* 4027-4031.
27. Öztürk, B. Ö.; Topoğlu, B.; Karabulut Şehitoğlu, S., *Eur. J. Lipid Sci. Tech.,* **2015**, *117,* 200-208.
28. Love, J. A.; Sanford, M. S.; Day, M. W.; Grubbs, R. H., *J. Am. Chem. Soc.,* **2003,** *125,* 10103-10109.

29. Antony, J., *Design of Experiments for Engeneers and Scientist*, 1st ed., Elsevier: London, **2003**.
30. Weissman, S. A.; Anderson, N. G., *Org. Process Res. Dev.,* **2014**, *19,* 1605-1633.
31. Minitab 17, *Getting Started Manual*.

Chapter 3 Fast initiating Ruthenium catalysts

3.1 Summary

The mechanism of activation of Grubbs 3rd generation pre-catalyst (GIII) (**262**) to form the metathesis active species (**263**, **264**, Scheme 3.1) has been studied using stopped-flow UV spectroscopy (SF-UV).

The initiation process was investigated by employing the commonly used irreversible reaction of the pre-catalyst (GIII) with ethyl vinyl ether (EVE) and by following the pre-catalyst (**262**) decay by UV.[1] After a careful instrument set-up development that ensured reproducible and reliable measurements under strictly anaerobic conditions, a series of kinetic data were collected. The model reaction was tested at different EVE concentrations and the effect of addition of 3-bromopyridine (3-BrPy) explored. Analysis and fitting of kinetic data obtained, suggested that a combination of both associative and dissociative pathways are operative in the initiation of Grubbs 3rd generation pre-catalyst (Scheme 3.1).

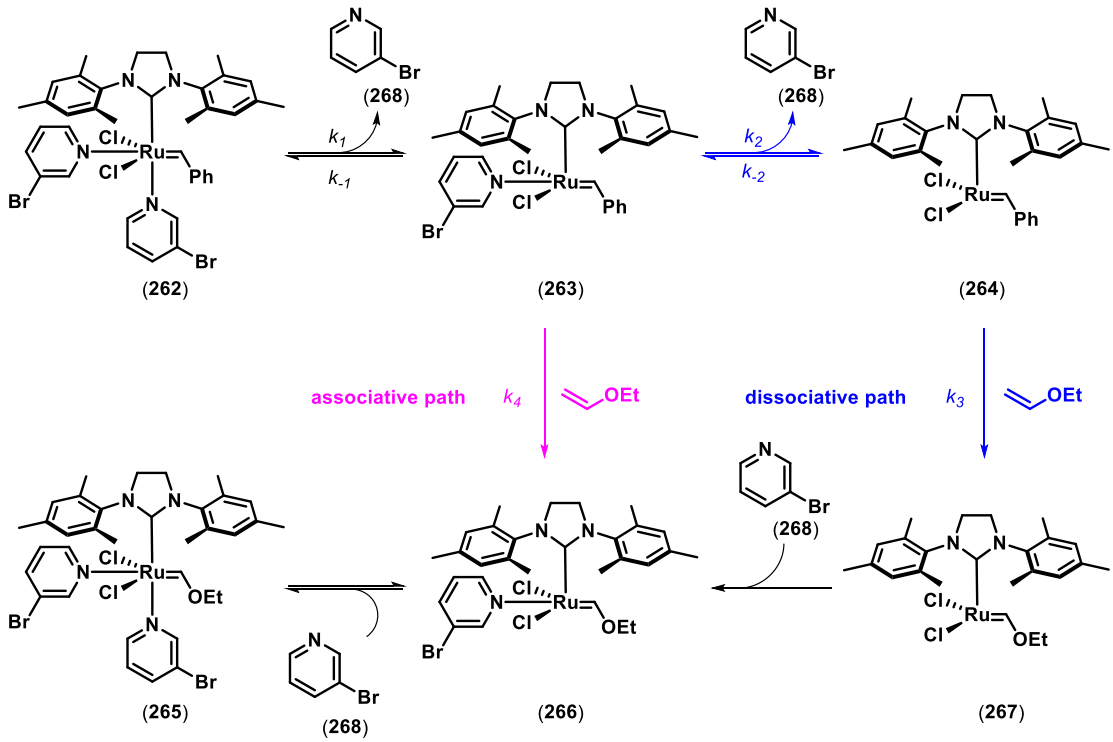

Scheme 3.1 Proposed initiation mechanism for Grubbs 3rd generation pre-catalyst (GIII)

3.2 Introduction

3.2.1 Mechanism of initiation of ruthenium metathesis catalysts

The mechanisms by which Grubbs and Hoveyda-Grubbs pre-catalysts generate their respective active catalyst species have been subject of numerous experimental and computational studies.[2] A detailed understanding of the initiation mechanism is crucial for the rational design of new pre-catalysts with improved activity, stability and selectivity and to exploit metathesis to its maximum potential.

Three different mechanisms have been proposed for Grubbs and Hoveyda-Grubbs pre-catalyst activation: associative, dissociative and interchange mechanisms (Scheme 3.2).[1] In the associative pathway (Scheme 3.2a), the olefin coordinates to the ruthenium pre-catalyst to form an 18-electron intermediate (**270**) which then loses a ligand (**L**) to give the active catalyst (**275**). The dissociative mechanism (Scheme 3.2b) involves first the loss of a ligand from the pre-catalyst (**272**) forming the 14-electron intermediate (**274**), which then coordinates to the olefin to yield the active catalyst (**275**). In the interchange initiation mechanism (Scheme 3.2c), the olefin coordination to the pre-catalyst metal centre and the loss of the ligand occur simultaneously.[1]

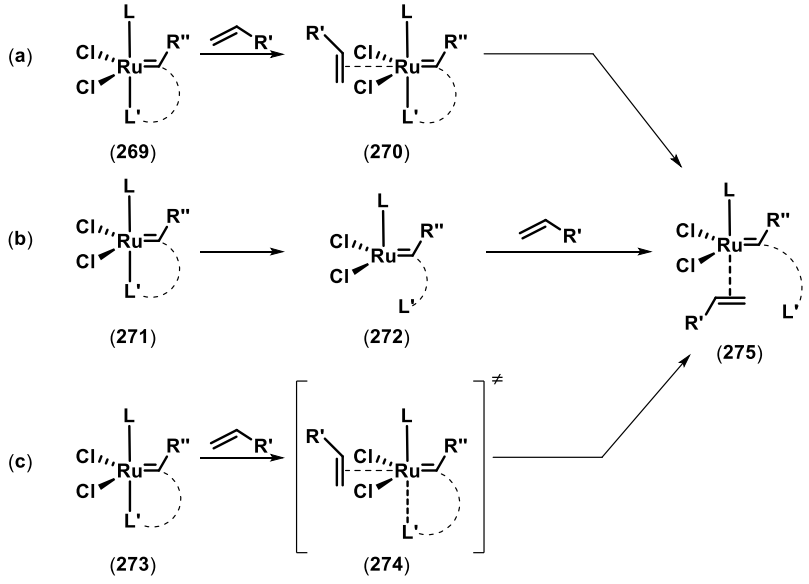

L = PR_3, NHC; **R'** = alkyl; **R''** = alryl; **L'** = PR_3, R'''O–§–

Scheme 3.2 Three possible initiation mechanisms for pre-catalyst activation (a) associative pathway, (b) dissociative pathway, (c) interchange pathway

Grubbs 1st (GI) and 2nd generation (GII) pre-catalysts (**276**, **277**, Figure 3.1) bearing phosphine ligands have been shown to initiate *via* a dissociative mechanism with the phosphine dissociation being the rate determining step.[2a]

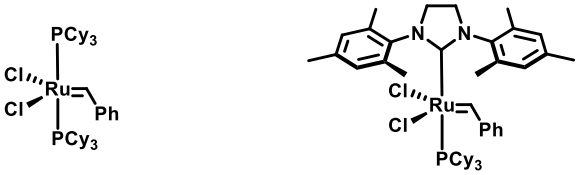

(**276**) (**277**)

Grubbs 1st generation **Grubbs 2nd generation**

Figure 3.1 Grubbs 1st (GI) and 2nd (GII) generation pre-catalyst

Hoveyda-Grubbs type pre-catalysts have been proposed to initiate through competing dissociative (Scheme 3.2b) and interchange (Scheme 3.2c) mechanisms depending on the steric and electronic properties of both the pre-catalyst and the olefin.[3] A more detailed study showed the associative interchange mechanism to have a late transition state;[3] this hypothesis takes into account the experimentally-determined first-order rate dependence on olefin concentration. Hoveyda-Grubbs complexes with electron-withdrawing substituents at the benzylidene ether group (Figure 3.2) have been reported to have faster dissociation and interchange mechanisms as the ruthenium centre is more electron-deficient.

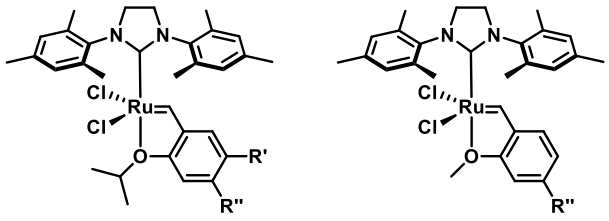

(**278 or 279**) (**280**)

Figure 3.2 Hoveyda-Grubbs type complexes
278: R' = H, R" = NEt_2, O*i*Pr, H, F, NO_2, OMe; **279**: R" = H, R' = NEt_2, O*i*Pr, H, F, NO_2, OMe; **280**: R" = H, NO_2

The associative interchange mechanism of sterically hindered complex (**280**, *i*PrO) was found to be slower than for less bulky complex (**278** or **279**, MeO) and it was reported to be preferred for electron-rich and sterically undemanding olefins (1-hexene and butyl vinyl ether). Less electron-rich and more bulky olefins (styrene and diethyl diallylmalonate (DEDAM)) showed a more important dissociative pathway with bulky pre-catalysts (**278**,

279). Interestingly DEDAM followed the preferentially associative interchange mechanism with less sterically hindered pre-catalyst (**280**) while styrene stays borderline between dissociative and associative interchange mechanisms.[3]

Effective pre-catalyst initiation would be achieved with the employment of an electron-deficient and sterically-accessible ruthenium pre-catalyst together with electron-rich and non-bulky olefins by promoting both interchange and dissociation pathways.

3.2.2 Grubbs 3rd generation pre-catalyst initiation

The initiation mechanism of the fast initiating Grubbs 3rd generation pre-catalyst (GIII) (**281**, Figure 3.3) has been the focus of a number of experimental and theoretical investigations in the last 20 years.[2b,4]

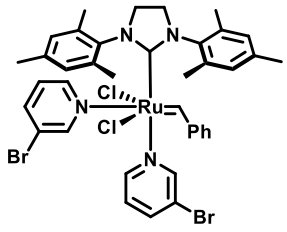

(**281**)

Figure 3.3 Grubbs 3rd generation pre-catalyst (GIII)

In 2002 Grubbs and co-workers estimated a lower limit for the GIII initiation rate ($k_{in} > 4\ s^{-1}$ at 5 °C) by UV experiments.[4a] Trzaskowski and Grela have recently investigated the GIII initiation mechanism by density functional theory (DFT) calculations[2b] taking into account three possible scenarios (Scheme 3.3). A one step dissociative mechanism was considered (Scheme 3.3a) where the two ligands both dissociate irreversibly to give a 14-electron complex (**285**). A two-step dissociative mechanism consisting of the reversible dissociation of one ligand followed by the detachment of the second ligand leading to the 14-electron complex (**285**, Scheme 3.3b). An associative pathway (Scheme 3.3c) which starts with the dissociation of one ligand to give a 16-electron complex (**284**), followed by olefin coordination and dissociation of the second ligand. Finally, an interchange mechanism (Scheme 3.3d) was considered where after the first ligand dissociation the olefin coordination and the second ligand dissociation occur simultaneously.

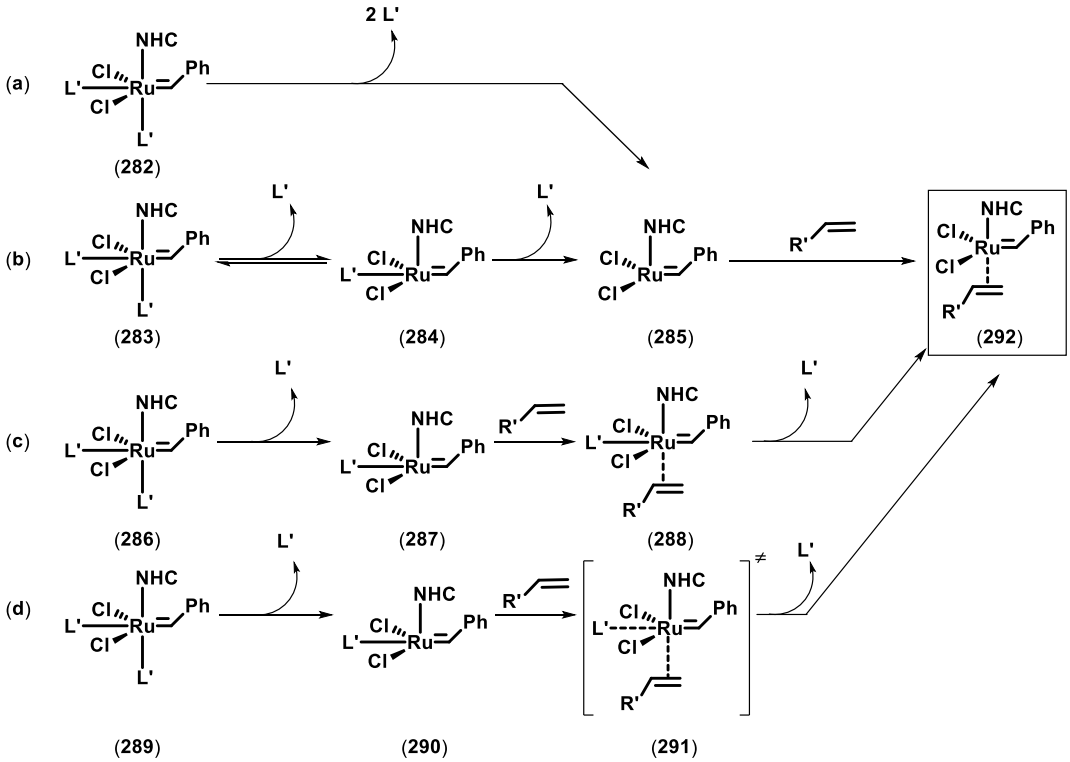

L' = 3-BrPy; **NHC** = N-heterocyclic carbene ligand; **R'** = alkyl

Scheme 3.3 Possible mechanistic scenarios for GIII initiation
(a) dissociative mechanism (one step), (b) dissociative mechanism (two-step),
(c) associative mechanism, (d) interchange mechanism

DFT calculations revealed that the dissociative path (Scheme 3.3a) is the most likely to happen in the initiation of GIII when 2-butene is used as a substrate; whereas an associative mechanism (Scheme 3.3c) is the most favoured in the presence of ethylene as an olefin. However, the DFT results showed a relatively small differences in energies between the two pathways which suggests the possibility of parallel simultaneous mechanisms for some systems.[2b]

Further studies by Walsh and co-workers on the mechanism of GIII initiation reported the formation of the mono-pyridine complex (**294**, Scheme 3.4) in solution from the six-coordinated solid complex (**293**, Scheme 3.4).[4b]

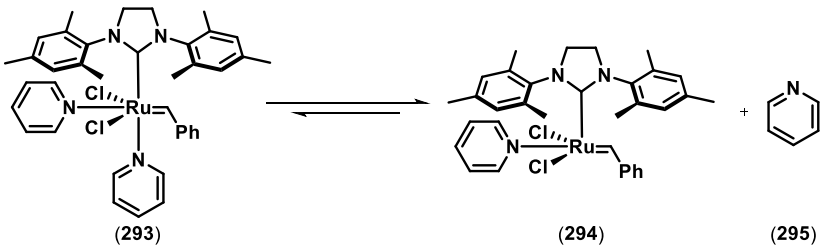

Scheme 3.4 Di-pyridine (**197**) and mono-pyridine (**198**) complexes equilibrium reaction

Moreover, it has been suggested that the non-coordinated pyridine complex (**285**, Scheme 3.3) is involved in the rate-determining step for ROMP of norbornene derivative **296** (Scheme 3.5). Indeed, the difference in polymerization rates between two pre-catalysts precursors (**299** and **300**, Scheme 3.5) corresponds to the difference in coordination strength between Py and 3-BrPy. This result implies that the same active ruthenium catalyst is formed in the polymerization turnover-limiting step from both catalyst precursors (**299** and **300**, Scheme 3.5).

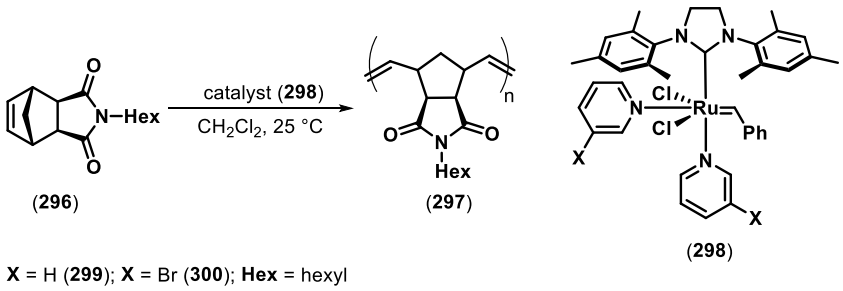

Scheme 3.5 Polymerization of *N*-hexyl-*exo*-norbornene-5, 6-dicarboximide via ring-closing metathesis

3.3 Project Objective

The catalyst screening performed for the ethenolysis of MO, detailed in Chapter 2, showed a significantly lower selectivity towards the ethenolysis products (**302** + **303**) with Grubbs 3rd generation pre-catalyst[5] (**306**, Scheme 3.6) compared to the slower-initiating Grubbs 1st generation pre-catalyst[2a] (**307**, Scheme 3.6). In order to further improve of the ethenolysis reaction, a deeper understanding of the mechanistic differences between these two pre-catalysts is required. To ascertain whether the two pre-catalysts are proceeding through the same active species, the initiation of GIII must first be investigated.

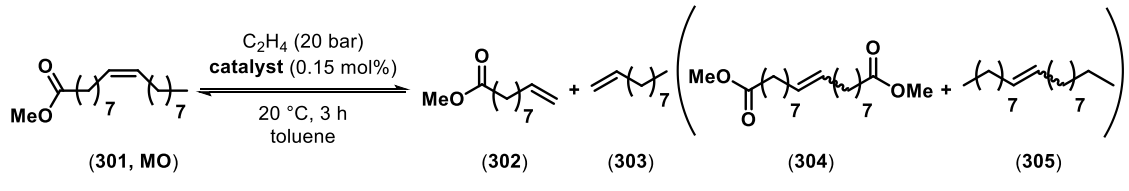

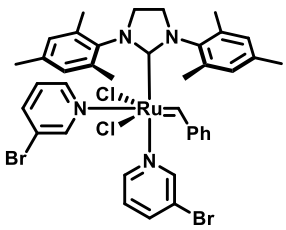

(**306**)

Grubbs 3rd generation
C = 63%, **S = 12%**,
TON = 420
k_{in} **> 4 s^{-1} (5 °C)**

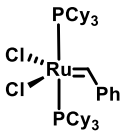

(**307**)

Grubbs 1st generation
C = 60%, **S = 99%**,
TON = 400
k_{in} **= 0.0018 s^{-1} (20 °C)**

Scheme 3.6 Ethenolysis of MO: GI and GIII compared results
C = conversion, S = selectivity, TON = turnover number, HGI = Hoveyda-Grubbs 1st generation pre-catalyst, constant pressure of ethylene

The aim of the project was to unravel the initiation mechanism of Grubbs 3rd generation pre-catalyst (Scheme 3.7) by employing stopped-flow UV spectroscopy (SF-UV).

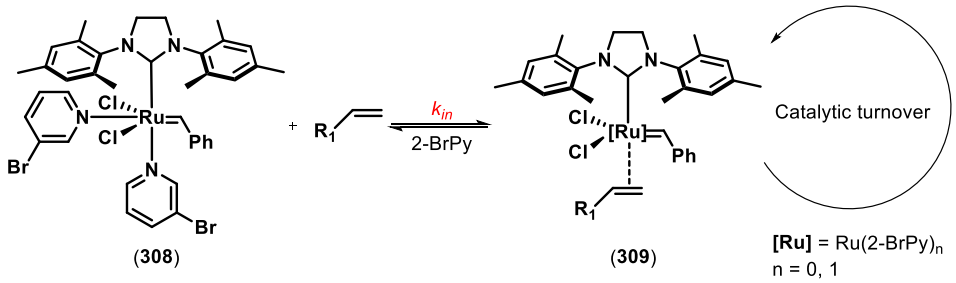

Scheme 3.7 Schematic metathesis mechanism for GIII, k_{in} = initiation rate

3.4 SF-UV studies

3.4.1 Grubbs 1st generation pre-catalyst initiation

In order to validate the use of SF-UV for the investigation of the GIII initiation mechanism, preliminary experiments were performed with Grubbs 1st generation pre-catalyst (GI). The initiation process for GI is proposed to follow a dissociative mechanism (Scheme 3.8),[2a] which involves reversible dissociation of one tricyclohexylphosphine ligand (PCy_3) from the pre-catalyst (**310**, Scheme 3.8) to form a 14-electron intermediate (**311**, Scheme 3.8). Subsequent binding of the olefin substrate leads to the active catalyst species (**312**) which can undergo productive metathesis.[2a]

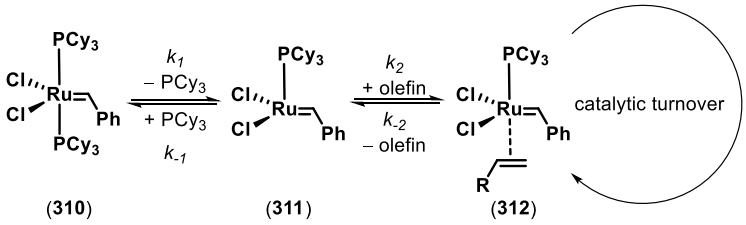

Scheme 3.8 Initiation mechanism for Grubbs 1st generation pre-catalyst (GI)[2a]

The catalytic activity of GI (**310**) has been shown to be related to both the PCy_3 dissociation rate (k_1) and the ratio of k_{-1} and k_2, which regulates whether the alkylidene species (**311**) is more prone to bind the olefin ($k_2 > k_{-1}$) or rebind the PCy_3 ($k_{-1} > k_2$). The proposed rate equation has been derived (Equation 3.1)[2a] by applying the steady-state approximation to the proposed intermediate (**311**) and assuming that the system is under pseudo-first order conditions, due to saturation in the olefin component.

$$rate = \frac{k_2\, k_1[\mathbf{310}][olefin]}{k_{-1}\ [PCy_3]+k_2\ [olefin]}$$

Equation 3.1. Proposed rate equation for Grubbs 1st generation pre-catalyst (GI)[2a]

Grubbs and co-workers[2a] have studied the initiation mechanism of GI (**313**), by using its reaction with ethyl vinyl ether (EVE) as a model (Scheme 3.9) for the initiation event due to irreversible formation of the Fisher carbene (**315**, Scheme 3.9). The product formation (**315**, Scheme 3.9) was followed by UV spectroscopy at different EVE concentrations carrying out the experiments in a standard cuvette with a rubber septum.[2a] The initiation process was found to reach saturation at high EVE concentrations giving $k_{obs} = k_1 = k_{in} = 0.018\ s^{-1}$.[2a]

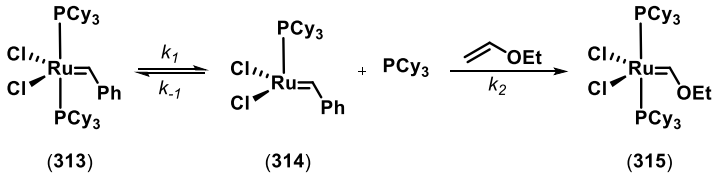

(**313**) (**314**) (**315**)

Scheme 3.9 Initiation rate measurement model reaction: pre-catalyst (GI) with EVE

To begin, the reported initiation process for GI was reproduced, by using a standard UV cuvette with a rubber septum, to ensure reliability and reproducibility of further data. The results obtained (Table 3.1), by measuring k_{obs} at different EVE concentrations (taking the average of the measured data) were in good accordance with the literature (k_{in} = 0.022 s^{-1} vs 0.018 s^{-1}[2a]).

[EVE] (M)	k_{obs}(s^{-1})
0.61	0.019
1.47	0.021
4.18	0.025

Table 3.1 k_{obs} at different [EVE]
Data measured by UV-vis in a standard cuvette with rubber septum

The GI initiation process (Scheme 3.9) was then used as a model experiment to test the suitability of the SF-UV system for further studies on Grubbs 3rd generation pre-catalyst (GIII). Separate stock solutions of GI and EVE in toluene were loaded in the SF-UV syringes (LS, Figure 3.4) from Schott reagent bottles (50 mL) capped with a four valve cap with threaded ports (B and picture on the right, Figure 3.4) *via* PEEK tubes (blue lines, Figure 3.4).

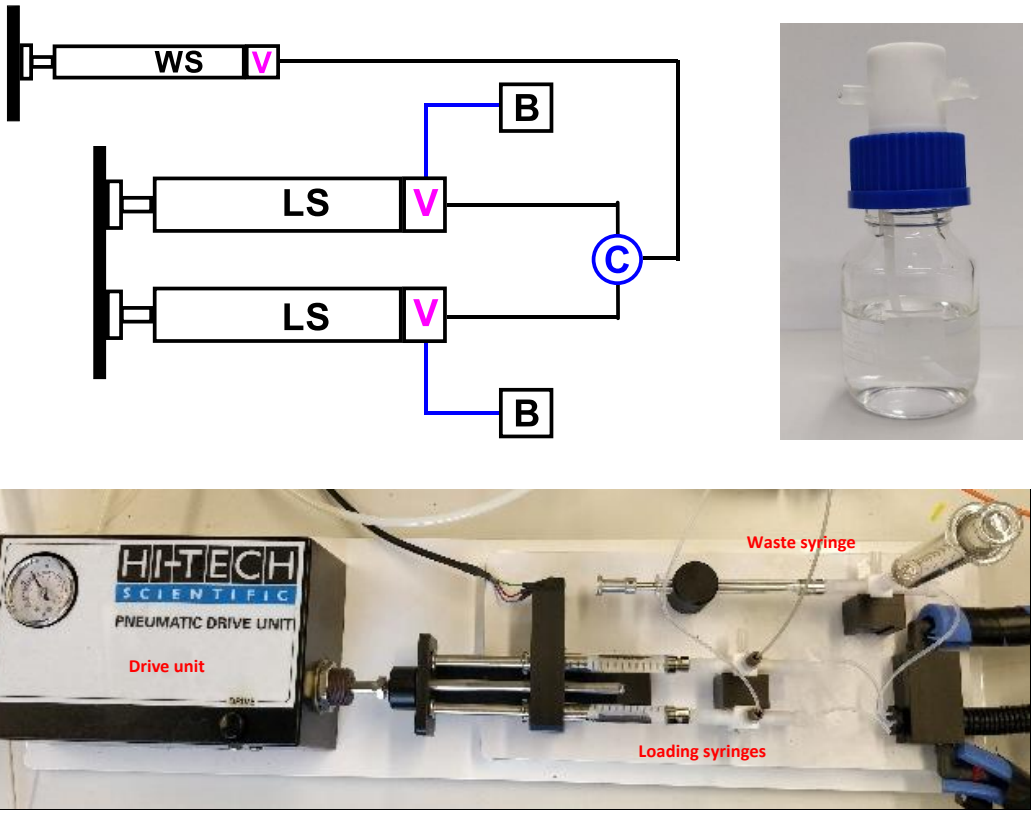

Figure 3.4 SF-UV standard set-up
B = Schott reagent bottles, V= three-ways valves, C = SF-UV cuvette, LS = loading syringes, WS = waste syringe

The UV spectra were collected over 5 half-lives (Figure 3.5A) and the formation of the Fisher carbene (**315**) at λ 484 nm was fitted to a first order exponential equation (Figure 3.5B).

(A) **(B)**

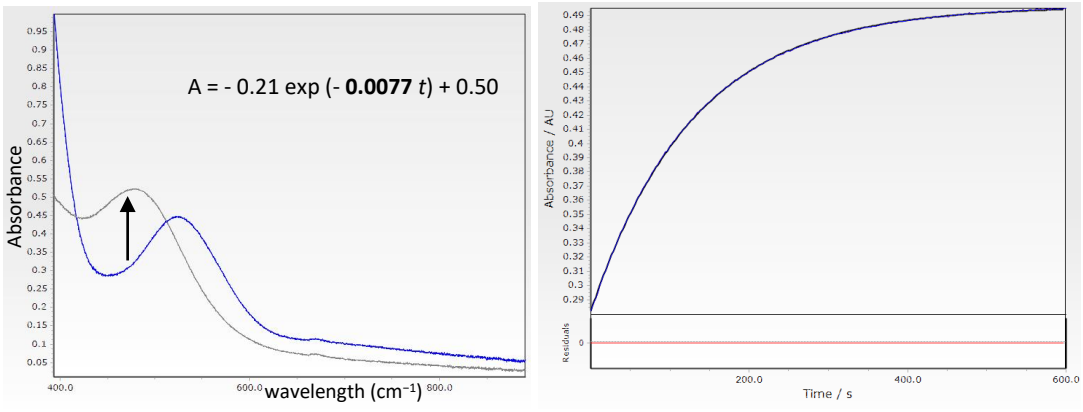

Figure 3.5 (A) UV spectra recorded for GI reaction with EVE spectrum at time zero (blue trace), spectrum at the end of the reaction (grey trace); **(B)** Representative first-order exponential fitting for GI reaction with EVE, A = absorbance, *t* = time, k_{obs} = 0.0077 s^{-1}; [GI] = 8.14 10^{-4} M, [EVE] = 0.198 M

The data collected *via* SF-UV at different EVE concentrations were fitted to equation 3.2 (Figure 3.6). Equation 3.2 was derived from equation 3.1 by taking into account that k_{obs} is proportional to the rate in pseudo-first order conditions and the phosphine (PCy_3) concentration is constant throughout the experiment.

$$k_{obs} = \frac{1}{\left(c\,\frac{1}{k_1[EVE]}\right)+\frac{1}{k_1}}$$

Equation 3.2. k_{obs} equation for Grubbs 1st generation pre-catalyst (GI)

c = constant = $\frac{k_{-1}}{k_2}\,PCy_3$

The initiation rate constant for GI was found to be 0.013 s^{-1} (Figure 3.6) under saturation conditions ([EVE] = 0.91 M, $k_{obs} = k_1 = k_{in}$), which is consistent with previously run experiment in the standard cuvette (k_{in} = 0.022 s^{-1}). The slightly higher value obtained by using the SF-UV technique could be related with its better air tightness in comparison with a standard cuvette.

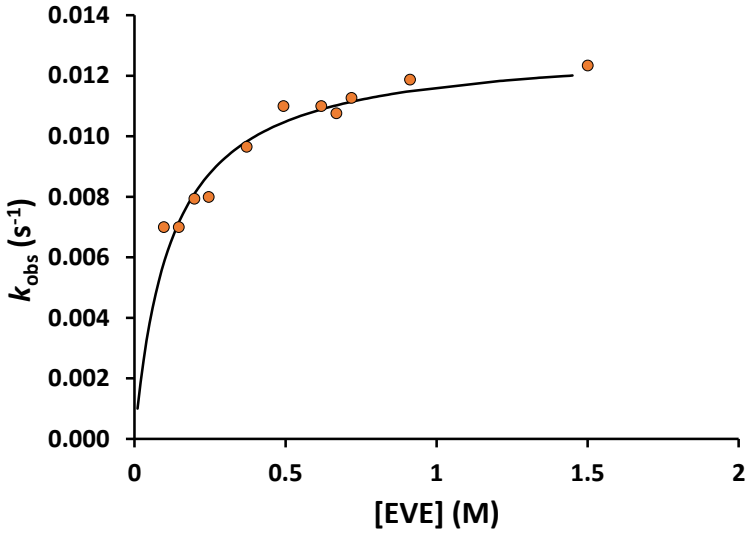

Figure 3.6 Grubbs 1st generation pre-catalyst saturation curve at different EVE concentrations (SF-UV). Experimental data (orange dots), simulated data (black line)

In conclusion, the SF-UV system with a standard set-up (Figure 3.4) was validated to be a suitable technique for the study of ruthenium catalysts by reproducing the reported initiation rate constant for GI, within experimental error.[2a]

3.5 Grubbs 3rd generation pre-catalyst initiation

3.5.1 SF-UV method development

After the SF-UV system was proven to be suitable for ruthenium pre-catalysts initiation studies, the Grubbs 3rd generation pre-catalyst initiation was investigated. Firstly, GIII (**317**) was synthesised from GII (**316**) following a reported procedure (Scheme 3.10).[4a]

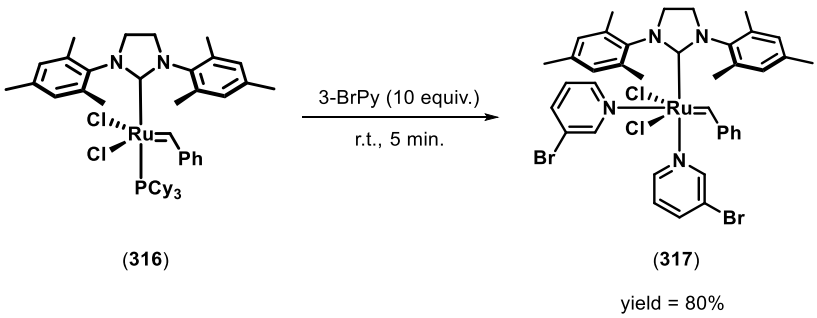

Scheme 3.10 Synthesis of Grubbs 3rd generation pre-catalyst[4a]

The reaction of GIII with EVE (Scheme 3.11)[5] was chosen as a model reaction for initiation rate measurement. The pre-catalyst (**318**, Scheme 3.11) decay was followed at λ 354 nm (Scheme 3.11) and it was fitted to a first-order exponential equation giving the observed rate constant value (k_{obs}).

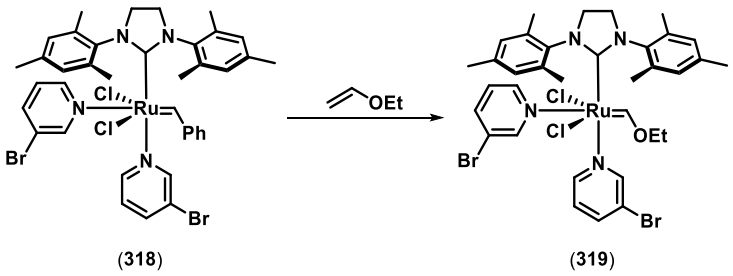

Scheme 3.11 Model reaction for the GIII initiation rate measurement

(A) **(B)**

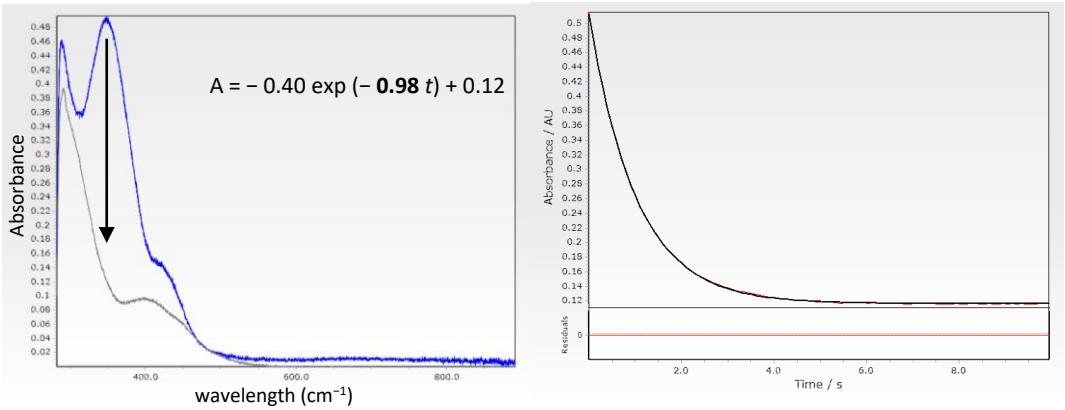

Figure 3.7 (A) UV spectra recorded for GIII reaction with EVE, spectrum at time zero (blue trace), spectrum at the end of the reaction (grey trace); **(B)** Representative first order exponential fitting for GI reaction with EVE
A = absorbance, *t* = time, k_{obs} = 0.98 s^{-1}; [GIII] = 4.6 10^{-5} M, [EVE] = 0.63 M

The experiments carried out with the standard SF-UV set-up gave inconsistent values of k_{obs} in sequential shots (Figure 3.8). The SF-UV set-up needed to be adapted to be suitable for performing experiments with GIII as the data reproducibility was found to be very poor with the standard set-up previously used with GI (Figure 3.4).

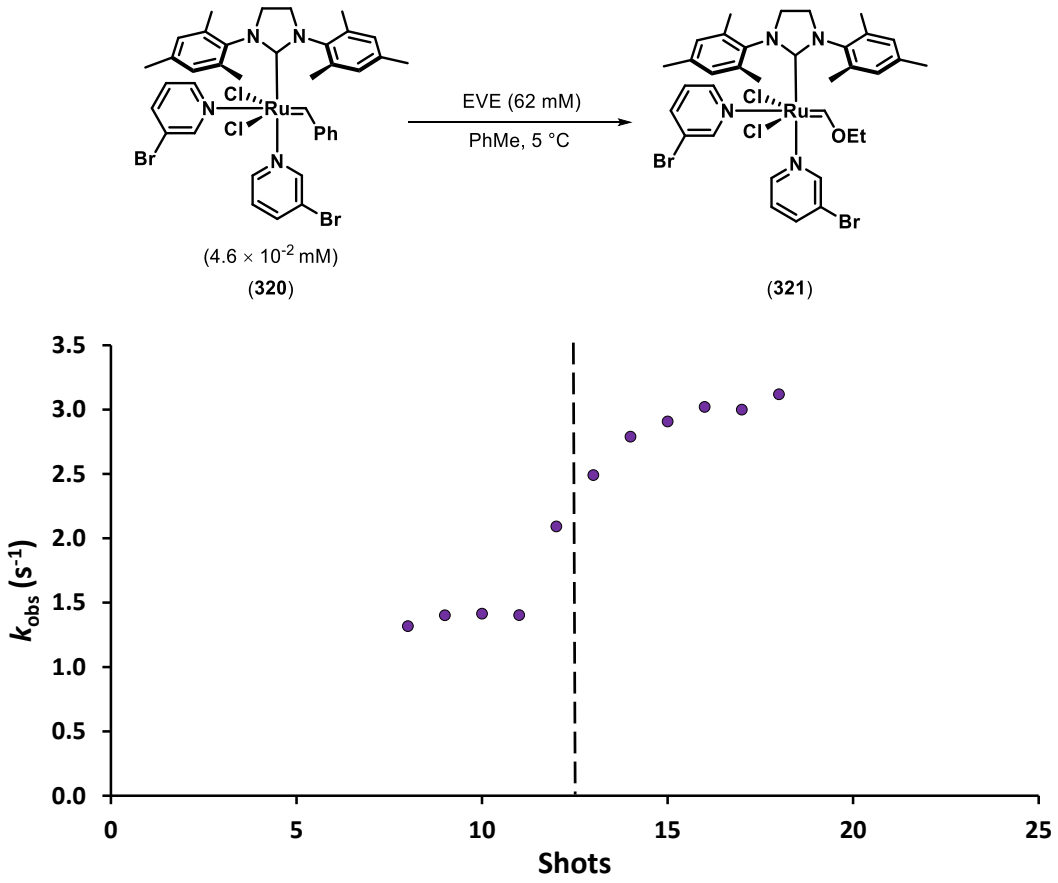

Figure 3.8 GIII data employing SF-UV standard set-up
Syringes loading point indicated with a dashed line

The temperature effects were firstly ruled out by thermally insulating the system leading to a temperature fluctuation of ± 0.2 °C during the experiment (measuring the temperature at the cuvette holder). The data measured employing the thermally insulated SF-UV (yellow dots, Figure 3.9) did not show significant difference compared to the data collected *via* the non-thermally insulated system (purple dots, Figure 3.9).

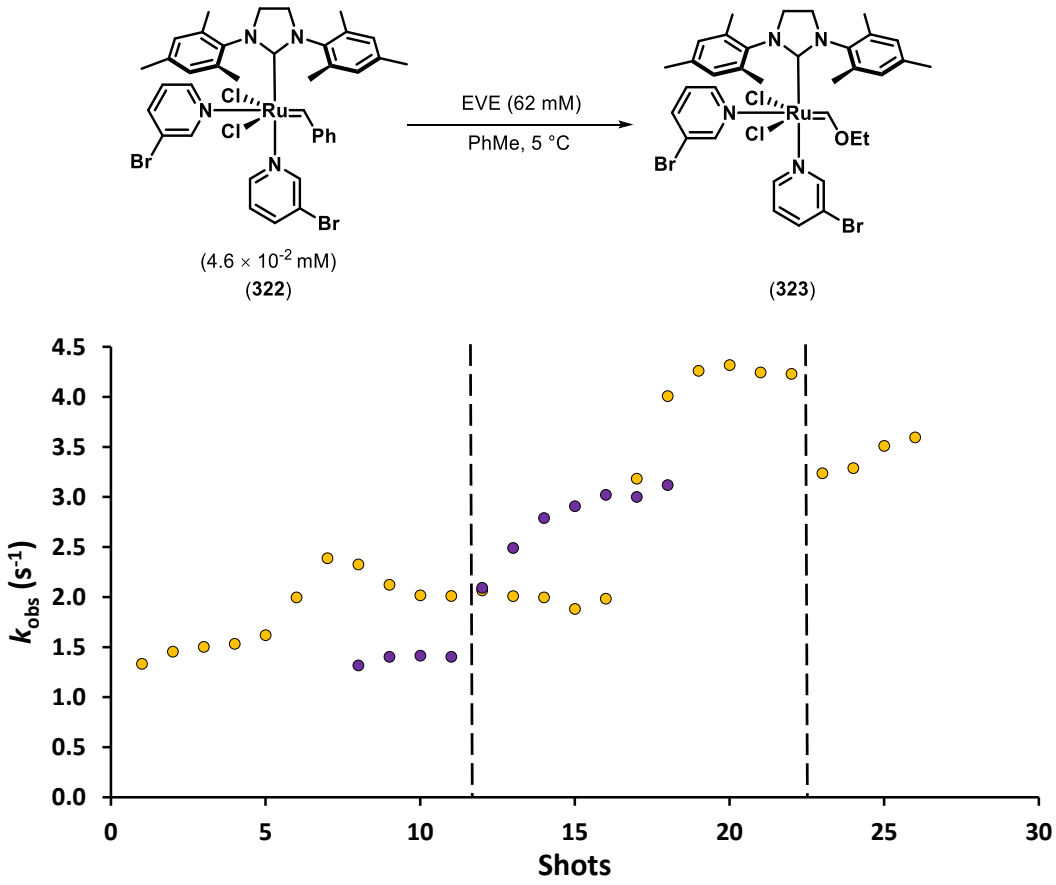

Figure 3.9 GIII data employing SF-UV thermally insulated standard set-up
Syringes loading point indicated with a dashed line;
non-insulated system (purple dots); insulated system (yellow dots)

The fluctuation seen in the measured k_{obs} could be related to oxidation of the free 3-BrPy ligand which would consequently accelerate the formation of the active catalyst (**325**, Scheme 3.12), due to change in the position of initial equilibrium (K_x, Scheme 3.12). Catalyst decomposition would then occur at the end of the experiment (Figure 3.9).

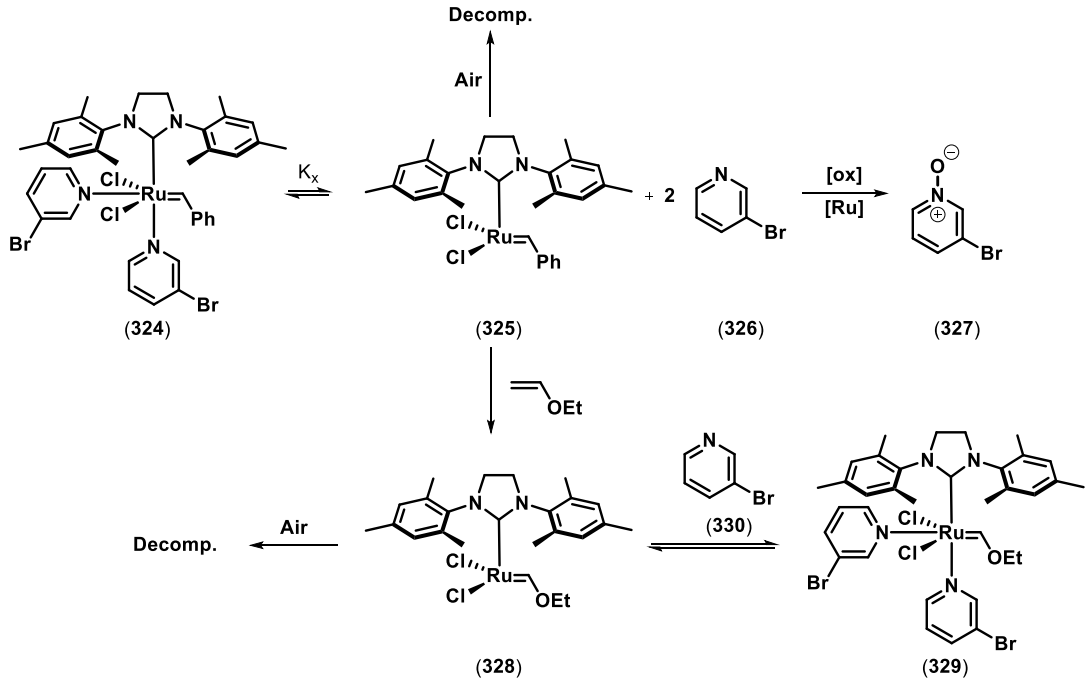

Scheme 3.12 Proposed acceleration of GIII initiation by 3-BrPy oxidation

The standard SF-UV set-up involves the stock solutions being drawn from the Schott reagent bottles into the SF-UV syringes (LS, Figure 3.10) which could have allowed air to be introduced to the stock solutions through the three-way valves (V, Figure 3.10). In order to test this hypothesis, external syringes were employed (E, Figure 3.10) to enable the stock solutions to be pushed into the SF-UV syringes (LS, Figure 3.10), ensuring over-pressure during the manipulations.

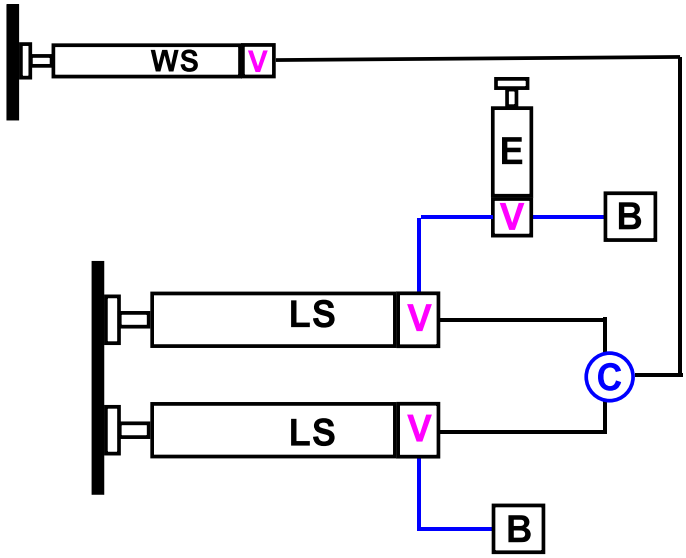

Figure 3.10 SF-UV standard set-up adapted with external syringe
B = Schott reagent bottles, V= three-ways valves, C = SF-UV cuvette, E = external syringe, LS = loading syringes, WS = waste syringe

The data obtained by following the initiation model reaction *via* the SF-UV with the adapted set-up (Figure 3.11) still gave fluctuations, which ruled out the possible air contamination of the system *via* the three-way valves (V, Figure 3.10), under pressure during the manipulations.

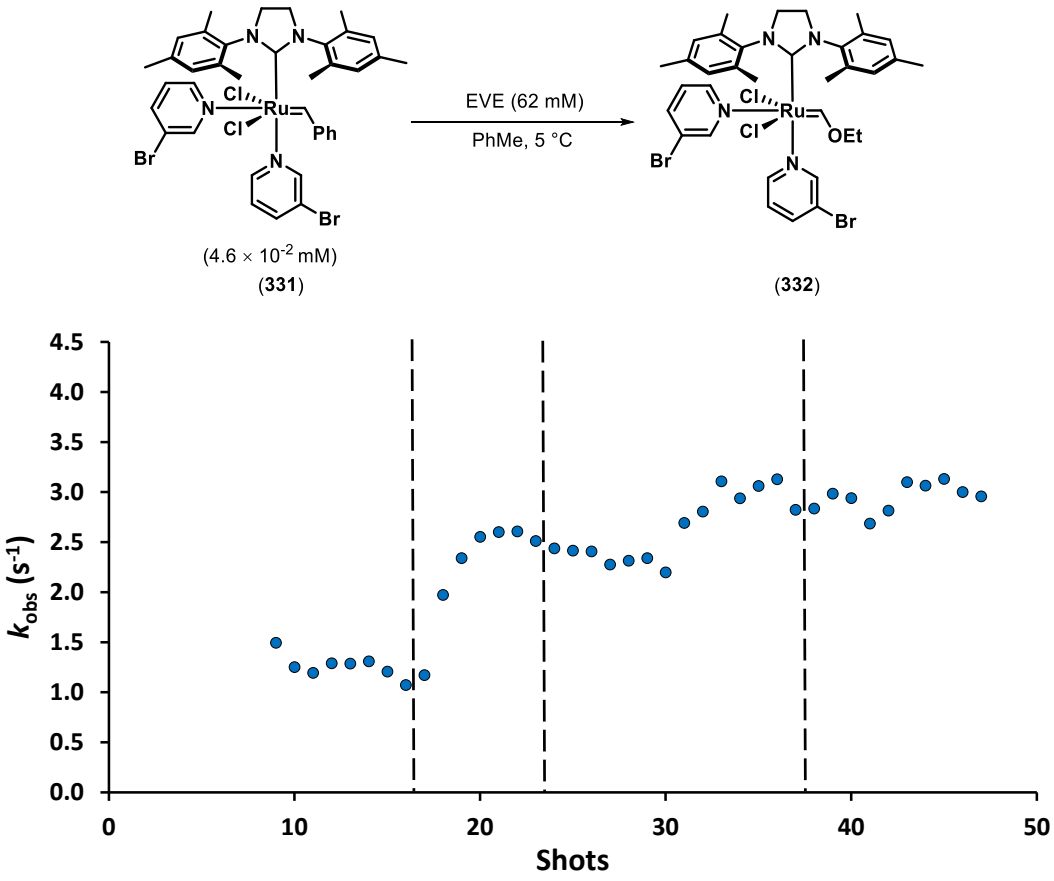

Figure 3.11 GIII data employing SF-UV standard set-up adapted with external syringe Syringes loading point indicated with a dashed line

The possibility that the air can permeate through the PEEK tubes (blue lines, Figure 3.10) was then investigated by surrounding them with an outer Nalgene 180 PVC tube to form a jacket of nitrogen (N_2) flow. The measured rate constants by using a nitrogen flow jacket for both the pre-catalyst stock solution (grey dots, Figure 3.12) and the EVE stock solution (blue dots, Figure 3.12) still showed fluctuations. A slight improvement was seen when the pre-catalyst stock solution was loaded into the SF-UV syringes *via* the external syringe and using the nitrogen jacket (pink dots, Figure 3.12).

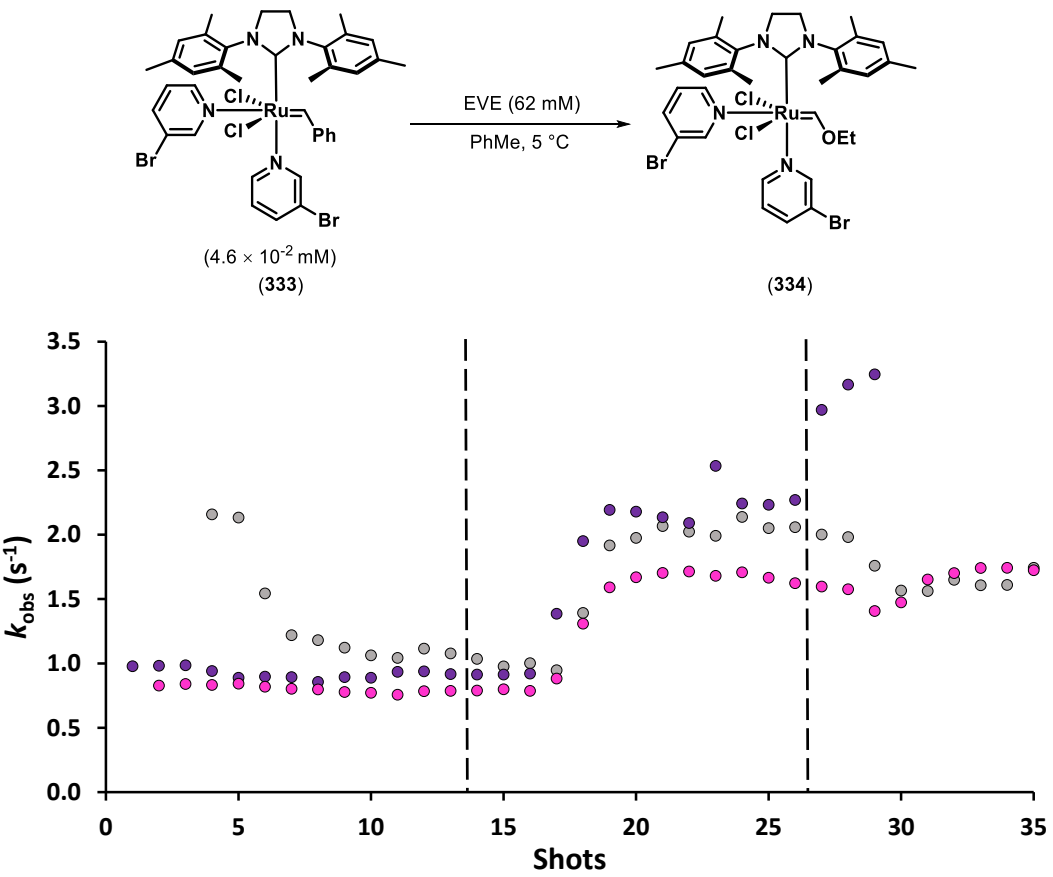

Figure 3.12 GIII data employing SF-UV standard set-up adapted with PEEK tubes in N_2 jacket
Syringes loading point indicated with a dashed line;
N_2 jacket for the pre-catalyst stock solution (grey dots),
N_2 jacket for the EVE stock solution (purple dots), N_2 jacket for the pre-catalyst stock solution + external syringe (pink dots)

In order to obtain consistent rate constant measurements for the reaction under study (Scheme 3.11) a different type of tube material was tested. Although PEEK tubes are known to be less oxygen permeable[6] than Tefzel tubes,[7] the latter were found to be beneficial in the system under investigation (green dots, Figure 3.13).

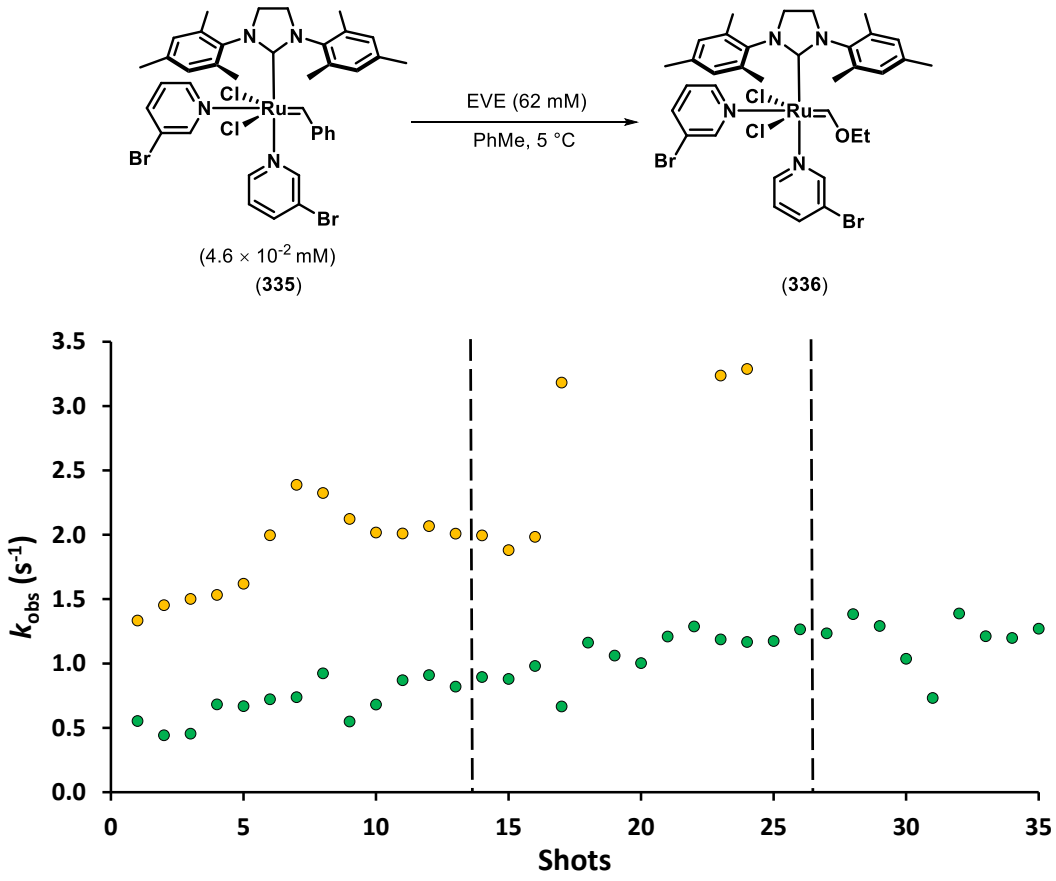

Figure 3.13 GIII data employing SF-UV standard set-up
Syringes loading point indicated with a dashed line; PEEK tubes (yellow dots), Tefzel tubes (green dots)

However the k_{obs} measurements obtained by employing the Tefzel tubes were still fluctuating. These results can be explained by taking into account that the solutions reaching the SF-UV cuvette have been in the tubes (between the loading syringes and the cuvette, Figure 3.10) and are not fresh solutions from the Schott reagent bottles. Indeed, when the system was flushed twice with the volume of two syringes loadings between consecutive SF-UV syringes loadings (orange dots, Figure 3.14) the results were more consistent than the previous experiment (green dots, Figure 3.14).

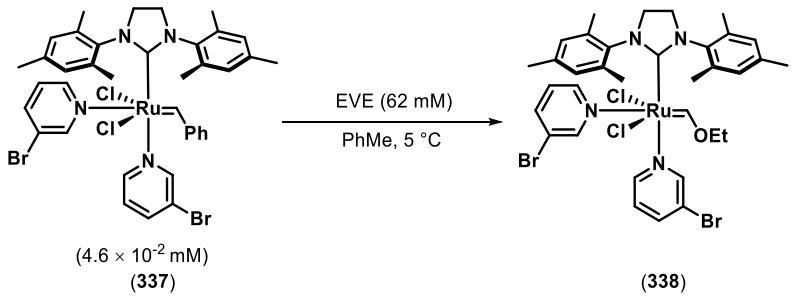

(4.6×10^{-2} mM)
(**337**)

(**338**)

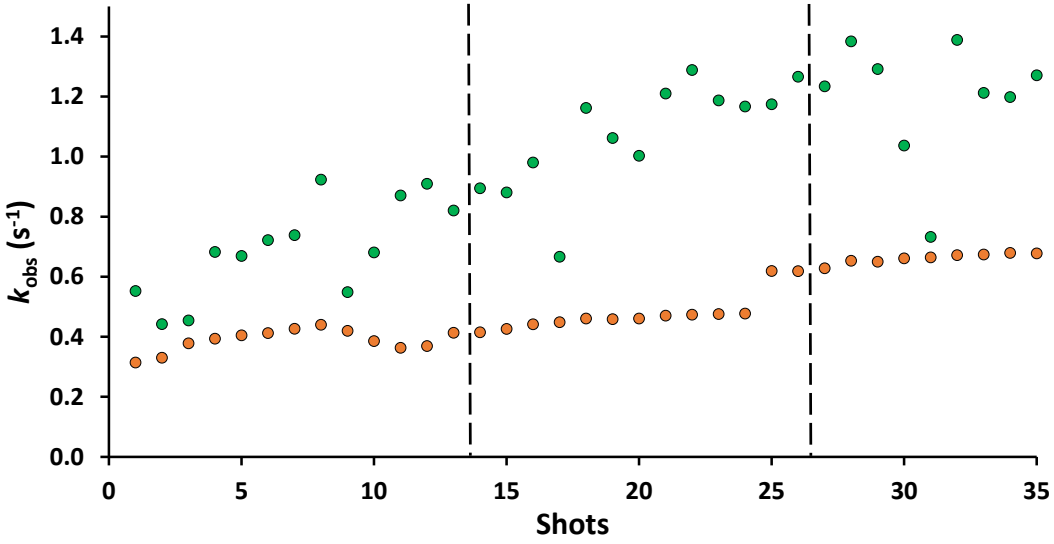

Figure 3.14 GIII data employing SF-UV standard set-up with Tefzel tubes
Syringes loading point indicated with a dashed line; without flushing stock solutions between loadings (green dots), flushing of stock solutions between loadings (orange dots)

Finally, an improved SF-UV set-up was built (Figure 3.15), taking into account the various tests done. Gas tight syringes – instead of Schott reagent bottles – were used to push the stock solutions (pre-catalyst and EVE in toluene) into the SF-UV syringes (LS, Figure 3.15); in addition, Tefzel tubes were employed to connect the gas tight syringes to the SF-UV system (blue lines, Figure 3.15). The experiments were also carried out by flushing the system twice with stock solutions between consecutive syringes loadings.

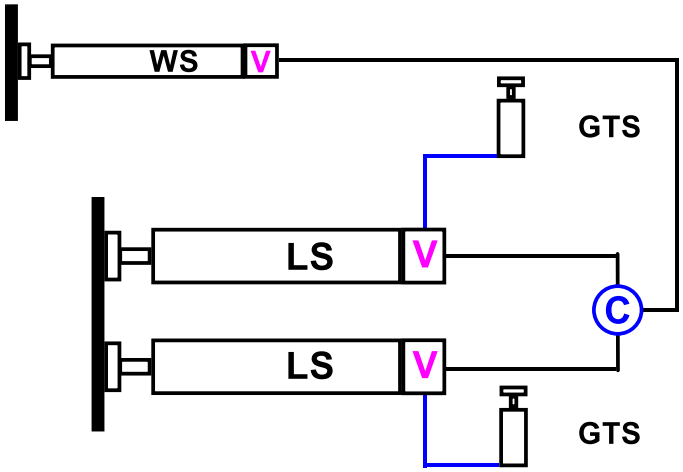

Figure 3.15 SF-UV improved set-up
V= three-ways valves, C = SF-UV cuvette, LS = loading syringes, WS = waste syringe, GTS = gas tight syringes

The k_{obs} measurements performed using the improved SF-UV set-up were found to be consistent throughout sequential syringes loadings (Figure 3.16).

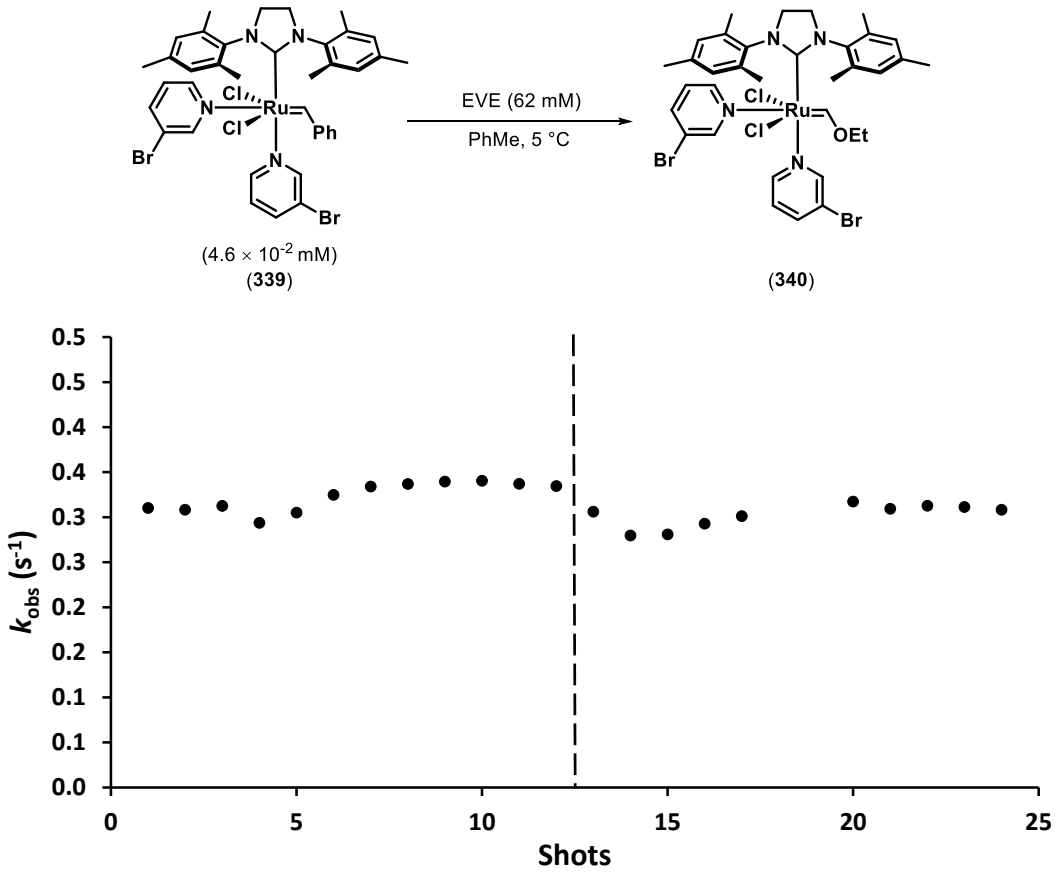

Figure 3.16 GIII data employing SF-UV improved set-up
Syringes loading point indicated with a dashed line

In conclusion, the use of Tefzel tubes – instead of PEEK tubes – to load the stock solutions in the SF-UV syringes was found to be beneficial to gain consistent measurements thought out subsequent syringes loadings of the same stock solutions. Moreover, the employment of gas tight syringes – instead of Schott reagent bottles – as reservoirs for the freshly prepared stock solutions (before loading in the SF-UV system) and filling the loading syringes under over-pressure, decreased the k_{obs} fluctuations during the same experiment (black dots, Figure 3.17).

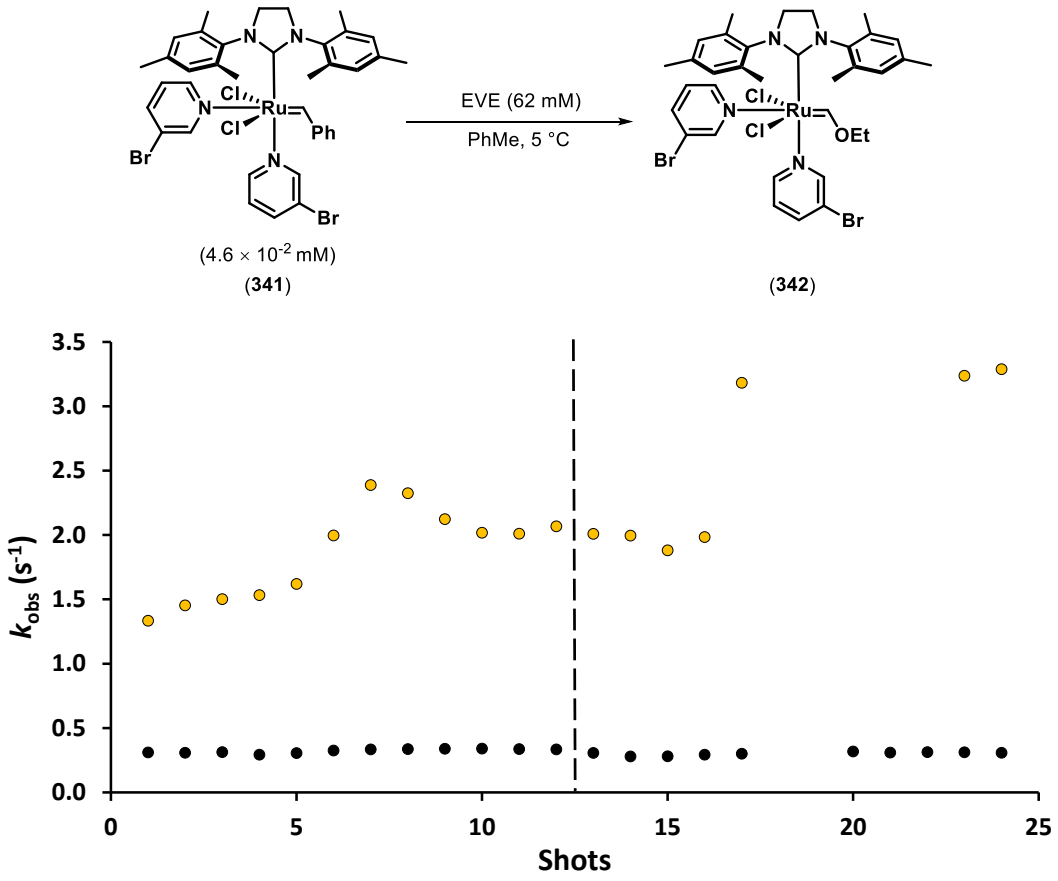

Figure 3.17 SF-UV measurements of k_{obs} for GIII
Syringes loading point indicated with a dashed line; SF-UV standard set-up (yellow dots) and SF-UV final set-up (black dots)

3.5.2 First model for Grubbs 3rd generation pre-catalyst initiation mechanism

With a reliable and reproducible SF-UV experimental procedure in hand, the kinetic impact of different reaction components was investigated. The experiments performed employing the improved SF-UV set-up (Figure 3.15) showed an increase in k_{obs} with EVE concentration (Figure 3.18) even at the highest olefin concentration investigated ([EVE] = 0.83 M), indicating that, in contrast to GI, the system does not reach saturation.

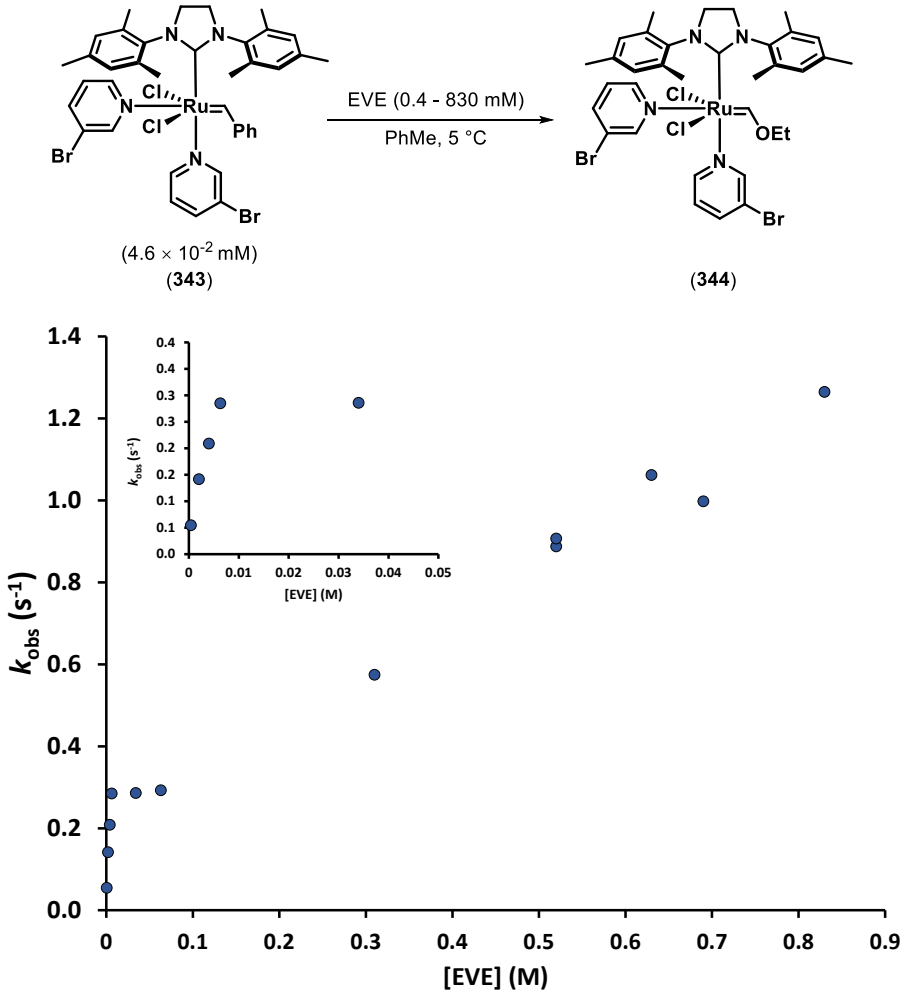

Figure 3.18 k_{obs} measurements for GIII at different [EVE]
Insert graph showing [EVE] range from 0 to 0.05 M

In order to rule out any effect of a change in medium at very high EVE concentrations, a SF-UV experiment was performed by replacing the majority of the olefin with diethyl ether (Et_2O) as a model. Specifically, the model reaction was performed at EVE concentration of 0.063 M and Et_2O was added to reach 0.83 M total concentration (EVE + Et_2O). The presence of a solvent effect would be shown by obtaining the same k_{obs} values for the latter experiment

and the experiment performed at EVE concentration of 0.83 M. The k_{obs} for the solvent effect test experiment with Et_2O was found to be 0.349 s^{-1}, which is in good accordance with the k_{obs} values obtained at EVE concentration of 0.063 M (0.274 s^{-1}) (Scheme 3.13). These results proved that no significant change in medium was occurring in the system under study.

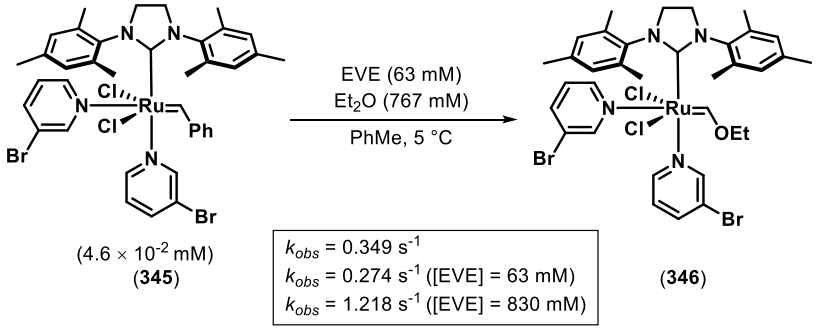

Scheme 3.13 GIII solvent effect test

In order to gain insight into the effect of the ligand on k_{in} of GIII, the effect of varying EVE concentration was studied with variable quantities of 3-BrPy added to the model reaction (Figure 3.19). The measured k_{obs} were found to decrease proportionally with increasing amounts of 3-BrPy added to the system (Figure 3.19).

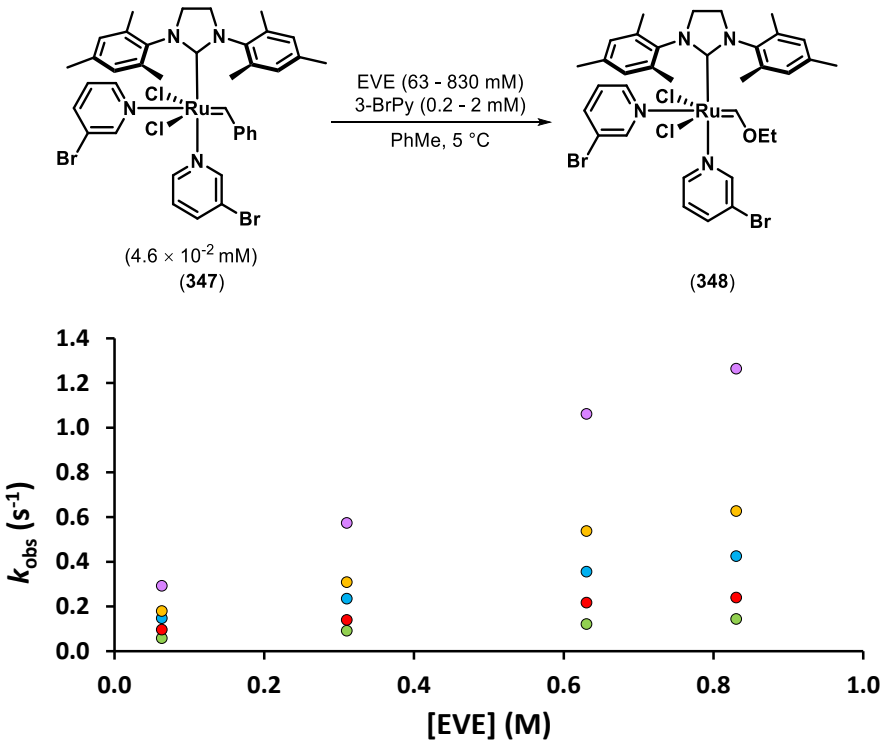

Figure 3.19 k_{obs} for GIII at different [EVE] and [3-BrPy]
[3-BrPy] = 0 M (pink dots), [3-BrPy] = 0.0002 M (yellow dots), [3-BrPy] = 0.0004 M (blue dots), [3-BrPy] = 0.001 M (red dots), [3-BrPy] = 0.002 M (green dots)

The kinetic model for the initiation of GIII was derived by firstly analysing the equilibrium for the first 3-BrPy detachment (Scheme 3.14)

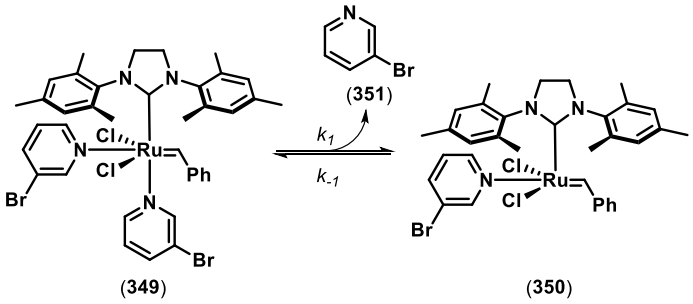

Scheme 3.14 Equilibrium between bibyridine and monopyridine complex

The equilibrium constant equation 3.3, where RuL_2 is the bipyridine complex (**349**), RuL the monopyridine complex (**350**), L is the bromopyridine ligand and L_A the added ligand, was solved by general quadratic equation for [RuL] and the ruthenium molar fraction (x_{RuL}) was calculated (Ru_T = total ruthenium)

$$K_1 = \frac{k_1}{k_{-1}} = \frac{[RuL][L+L_A]}{[RuL_2]} \quad \textbf{Equation 3.3}$$

$$x_{RuL} = \frac{[\boldsymbol{RuL}]}{[Ru_T]};\ [RuL] = x_{RuL}\,[Ru_T] \quad \textbf{Equation 3.4}$$

The possible reactions of the monopyridine complex (**353**) were considered (Scheme 3.15): a dissociative path where the monopyridine complex **353** loses the second ligand (**358**) and then it reacts with EVE and an associative path where the monopyridine complex **353** directly reacts with the olefin substrate (EVE).

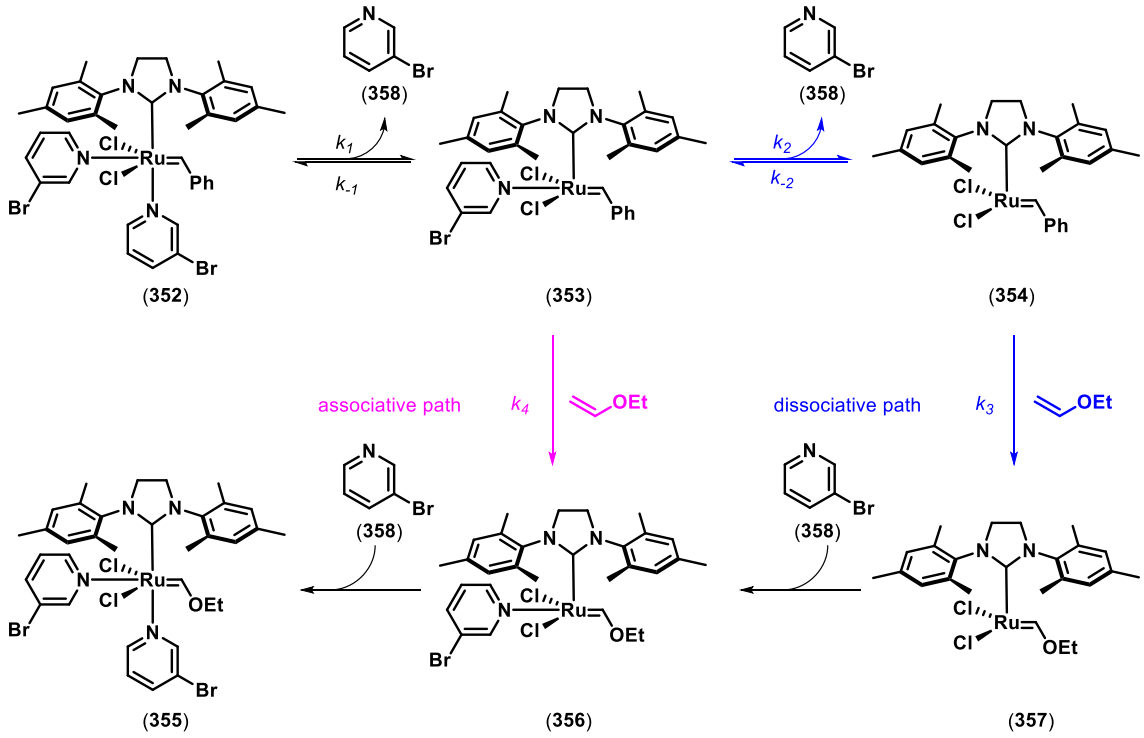

Scheme 3.15 Proposed initiation mechanism for GIII
k_2 = 0.32 s^{-1}, k_{-2} = 10 s^{-1}, k_3= 5 s^{-1}, k_4 = 1.32 s^{-1}

A steady-state approximation was then applied to the complex **354** and accordingly a kinetic equation was derived (Equation 3.5).

$$\boldsymbol{k_{obs} = x_{RuL}} \left(\frac{\boldsymbol{k_2}}{\dfrac{\boldsymbol{k_{-2}\,[L_t]}}{\boldsymbol{k_3\,[EVE]}} + \boldsymbol{1}} + \boldsymbol{k_4\,[EVE]} \right)$$

Equation 3.5. k_{obs} for GIII initiation mechanism model

This equation, which considers both a dissociative and an associative pathway to be involved in the initiation of GIII, gave the best fit of the experimental data collected by SF-UV (Figure 3.20C).

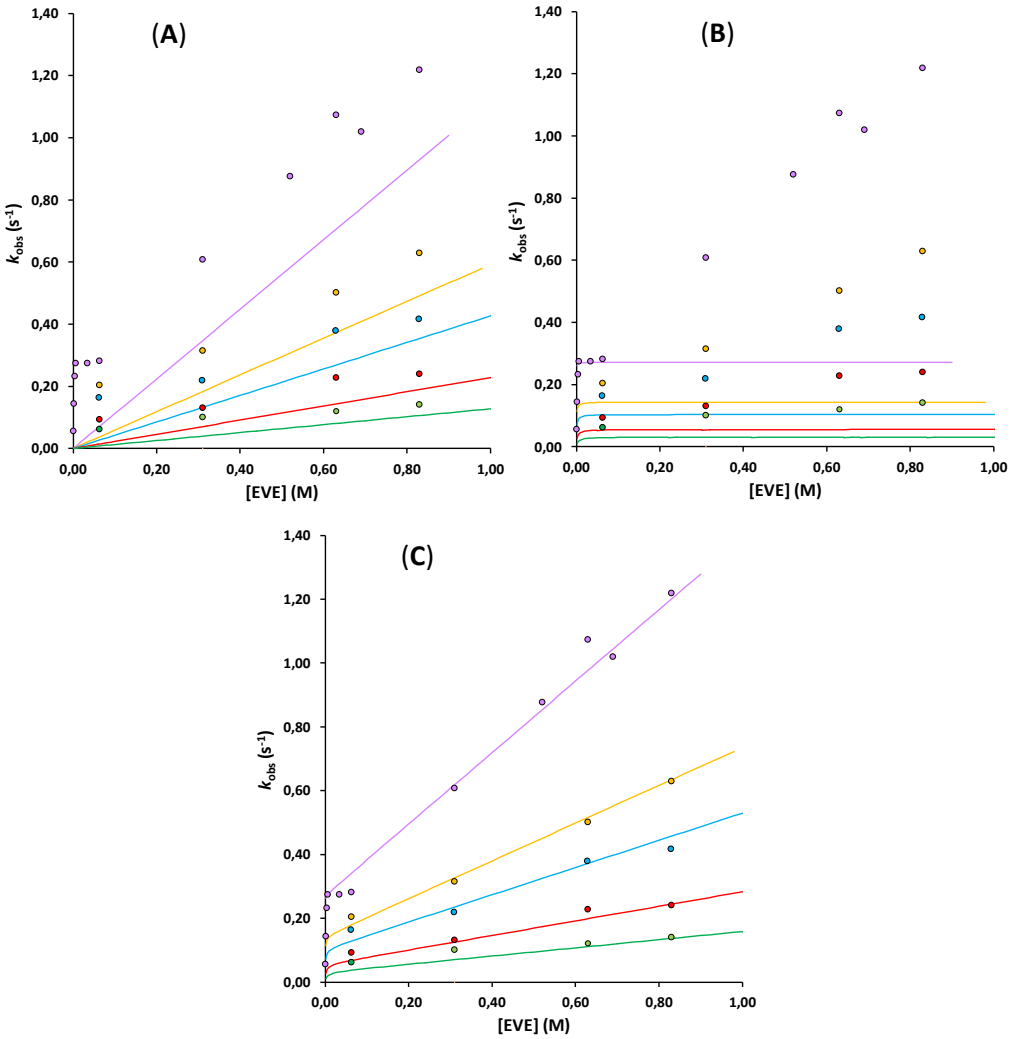

Figure 3.20 GIII data fitted to different pathways combination
A: associative pathway; B: dissociative pathway; C: combination of associative and dissociative pathways**,** [3-BrPy] = 0 M (pink dots), [3-BrPy] = 0.0002 M (yellow dots), [3-BrPy] = 0.0004 M (blue dots), [3-BrPy] = 0.001 M (red dots), [3-BrPy] = 0.002 M (green dots)

If a pure associative path was considered for GIII initiation (Scheme 3.16) the kinetic equation would be of the type of equation 3.6. The latter equation did not fit the experimental data as shown in Figure 3.20A.

$$k_{obs} = x_{RuL}\,(k_4\,[EVE]) \qquad \textbf{Equation 3.6}$$

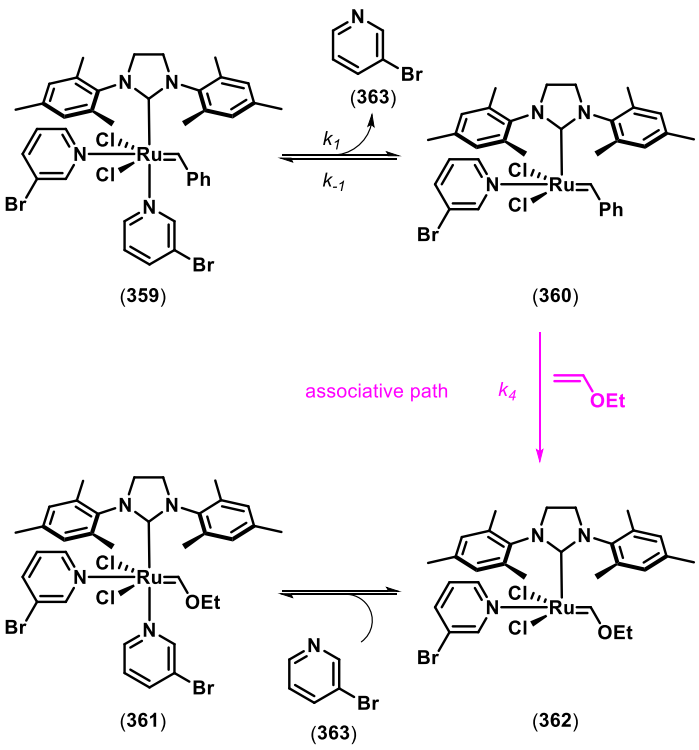

Scheme 3.16 GIII initiation mechanism: proposed associative pathway

The possibility of a pure dissociative pathway for the initiation mechanism of GIII was also considered (Scheme 3.17). The kinetic equation for a pure dissociative pathway (equation 3.7) would describe a saturation curve at high EVE concentrations as shown in Figure 3.20B.

$$k_{obs} = x_{RuL}\left(\frac{k_2}{\frac{k_{-2}\,[L_T]}{k_3\,[EVE]}+1}\right) \qquad \textbf{Equation 3.7}$$

The attempt to fit the experimental data to equation 3.7 failed (Figure 3.20B) as no saturation was reached even at the highest EVE (0.83 M) concentration investigated in the study.

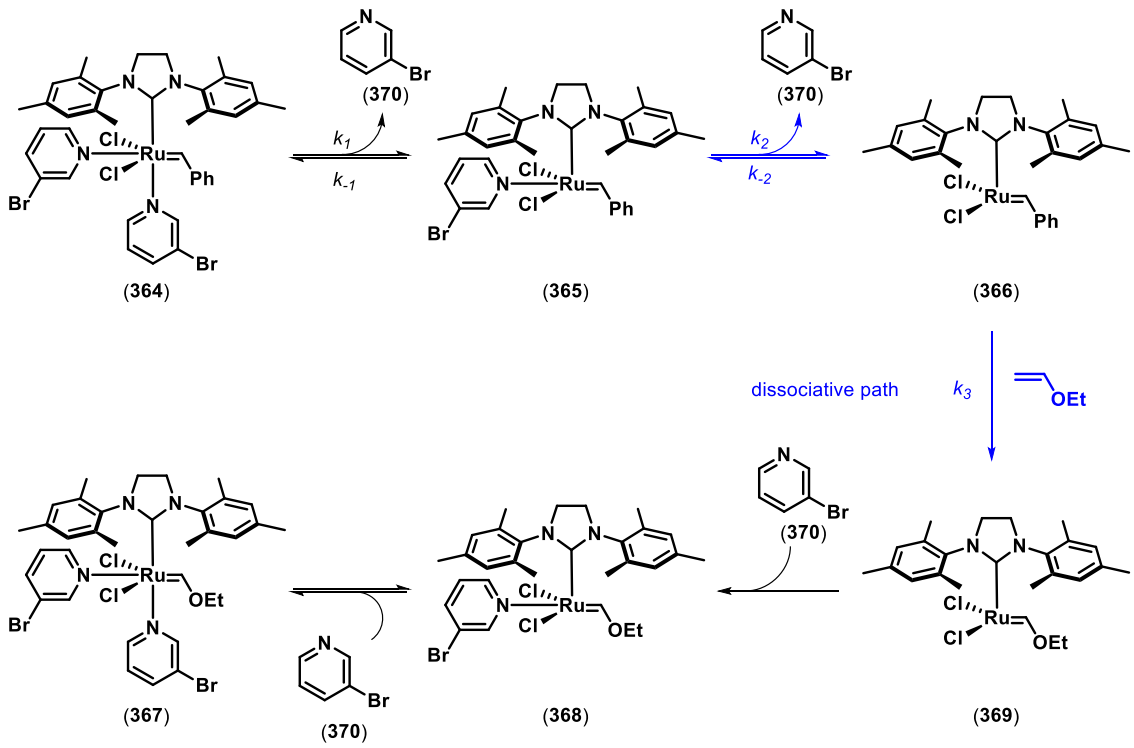

Scheme 3.17 GIII initiation mechanism: proposed dissociative pathway

Based on these results, a combined dissociative and associative mechanism was proposed for the initiation of GIII (Scheme 3.15). The proposed mechanism (Scheme 3.15) consists in the detachment of one of the 3-BrPy from the pre-catalyst (**352**) to form the mono-pyridine complex (**353**) which can undergo irreversible metathesis reaction with EVE to form the complex **356** (associative pathway). The latter can re coordinate with the free 3-BrPy giving the final product (**355**). Simultaneously the alkylidene complex (**353**) can lose the second 3-BrPy ligand leading to the active complex **354** which reacts with EVE to give the 14-electron complex (**357**) (dissociative pathway). The re coordination of the two 3-BrPy ligands to the complex **357** gives the final product **355**. The k_{obs} kinetic derivation for GIII initiation was derived by applying the steady-state approximation on the alkylidine species (**353**, Scheme 3.15) leading to Equation 3.5 (k_2 = 0.32 s^{-1}, k_{-2} = 10 $M^{-1}s^{-1}$, k_3= 5 s^{-1}, k_4 = 1.32 s^{-1}).

3.5.3 Second model for Grubbs 3rd generation pre-catalyst initiation mechanism

The proposed model is based on previous reported studies which measured the K_0 for the equilibrium in Scheme 3.18 to be mainly dominated by the mono-pyridine complex (**371**).[4b]

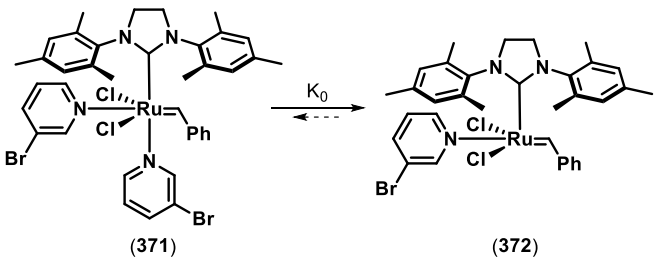

Scheme 3.18 Equilibrium between bipyridine and monopyridine complex

The possible reactions of the monopyridine complex (**374**) were investigated (Scheme 3.19): a dissociative path, an associative path and an interchange path.

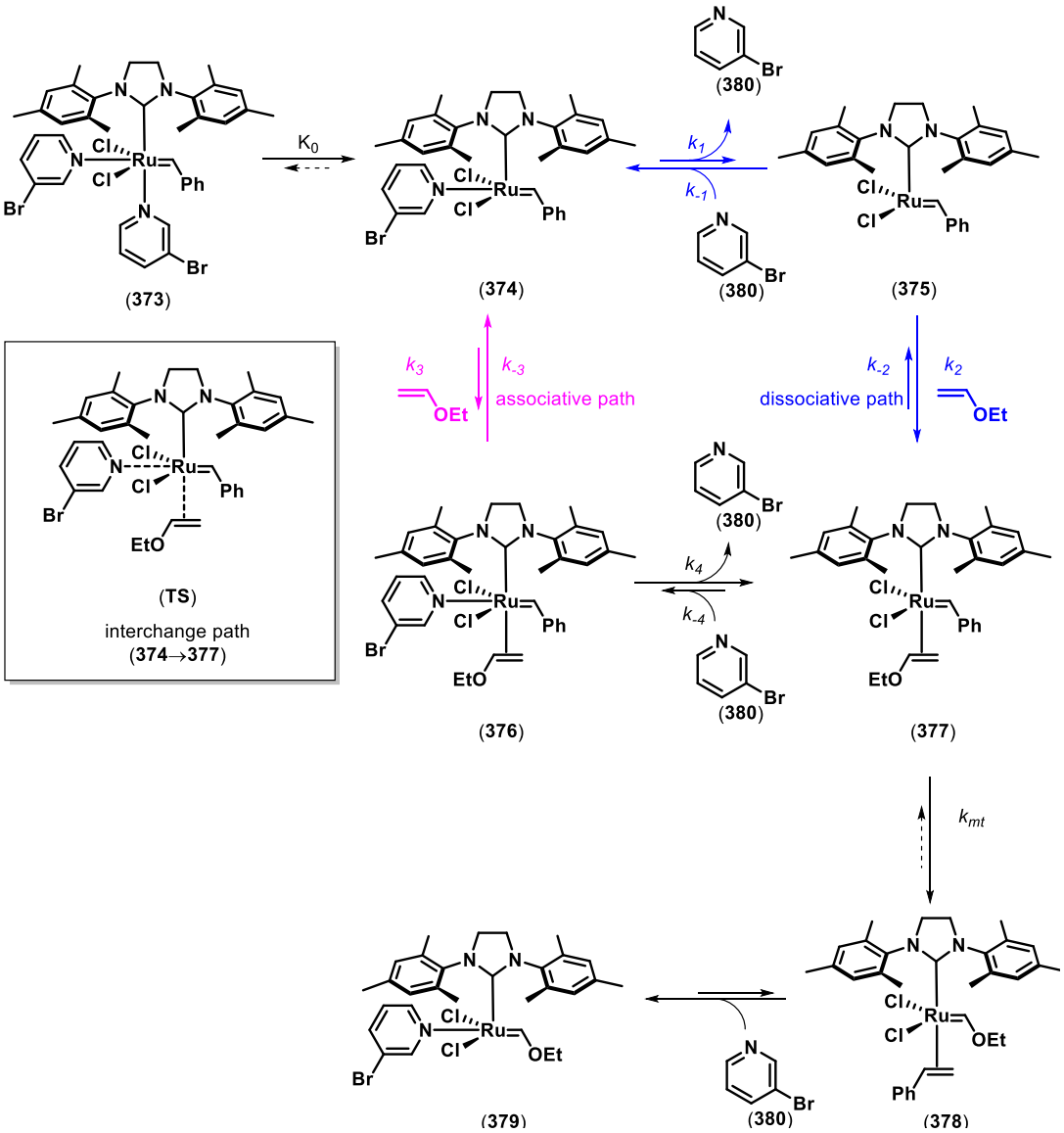

Scheme 3.19 GIII initiation mechanism: possible pathways
k_{mt} = kinetic constant for metathesis process

If a pure dissociative path was considered for GIII initiation (Scheme 3.20) the kinetic equation obtained (equation 3.8) by applying the steady-state approximation on **383** and **384** would eventually reach saturation at high EVE concentrations (Figure 3.21)

$$k_{obs} \approx \frac{1}{c\,[L]/[EVE] + 1/k_1}$$

Equation 3.8 kinetic equation for GIII initiation: pure dissociative path
EVE = ethyl vinyl ether, L = ligand, $c = 1/K_1K_2k_{mt} + 1/K_1k_2$

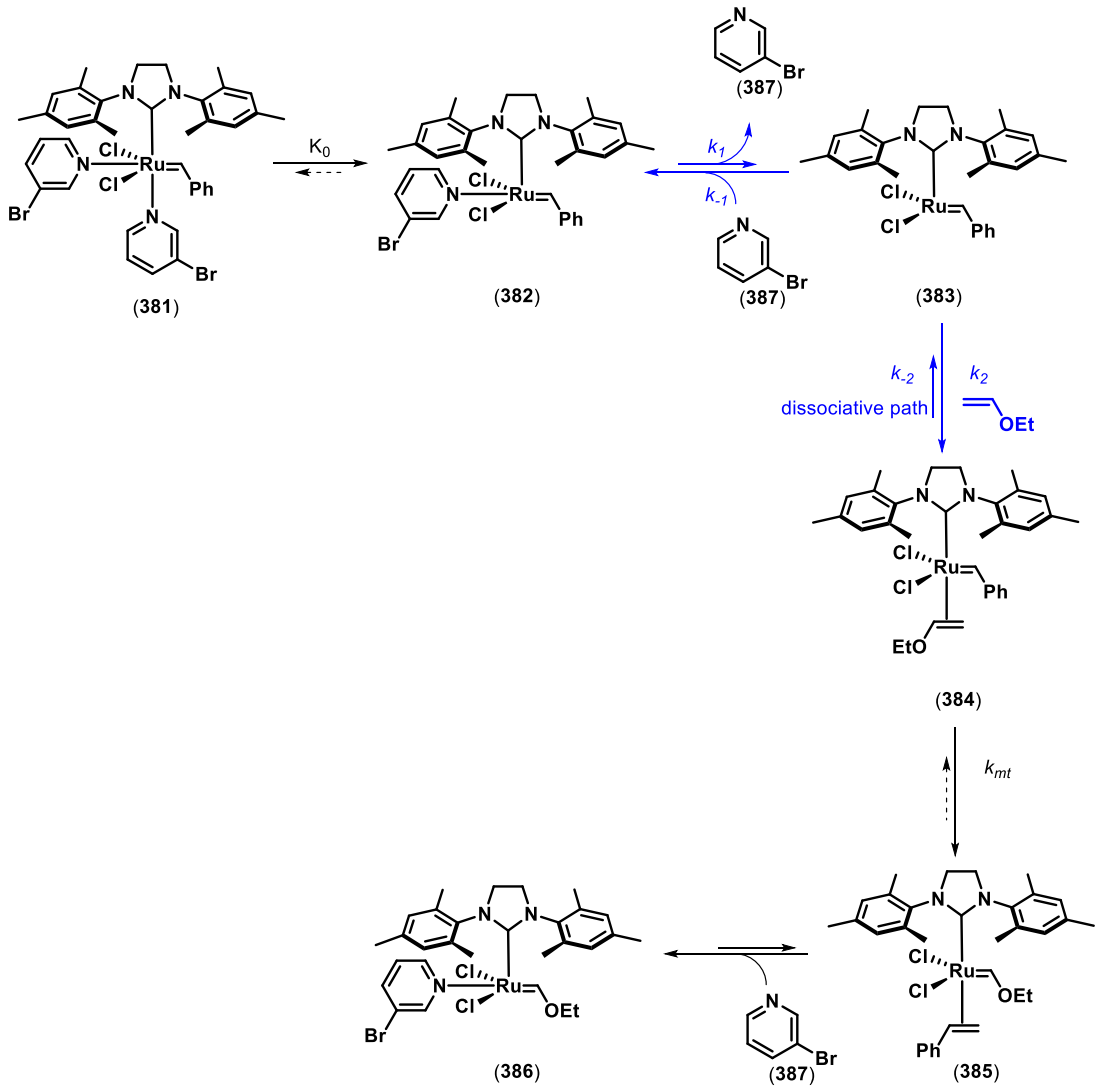

Scheme 3.20 GIII initiation mechanism: proposed dissociative pathway

The latter equation did not fit the experimental data as shown in Figure 3.21A.

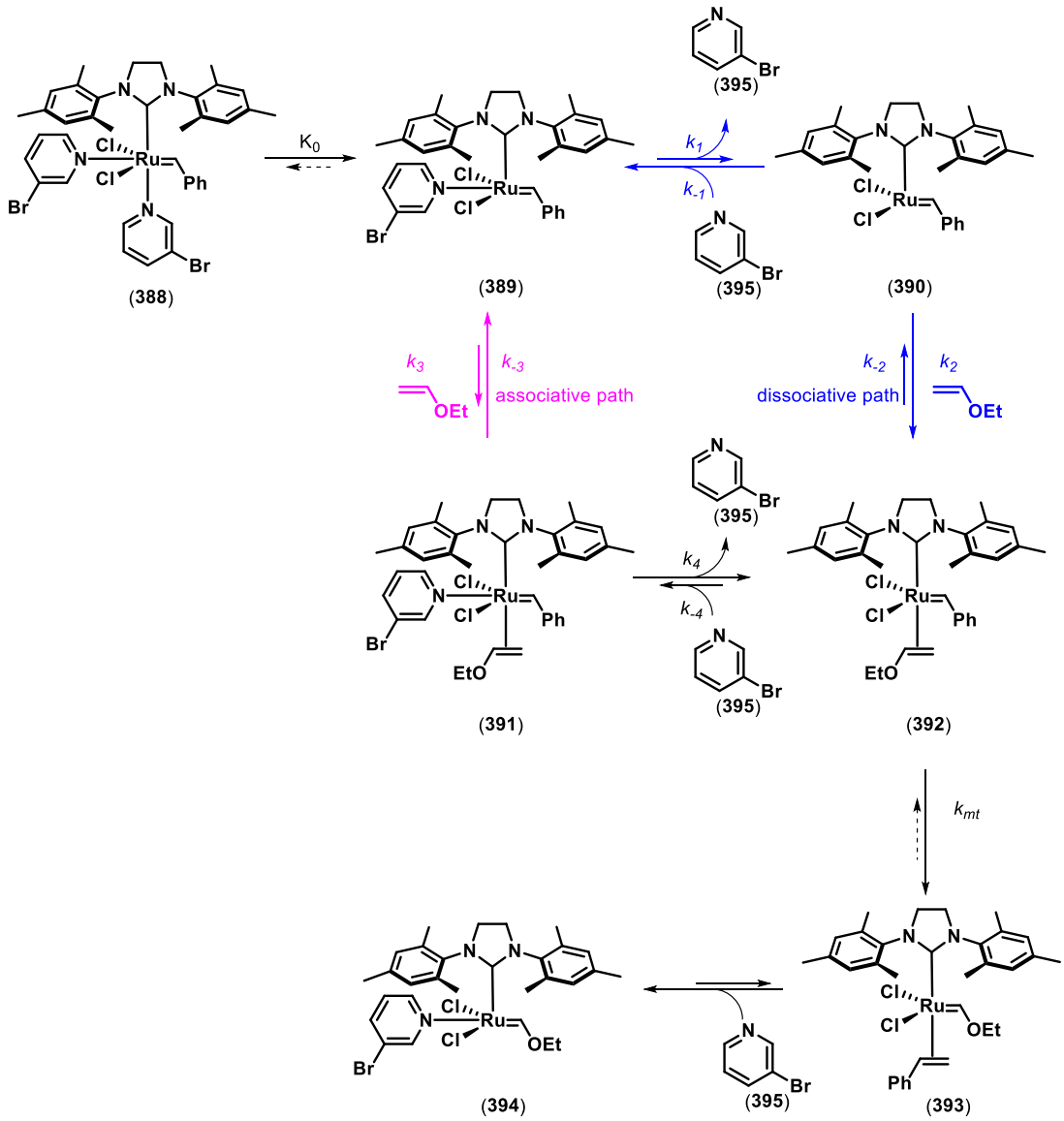

Scheme 3.21 GIII initiation mechanism: proposed divergent dissociative and associative pathway

The possibility of a divergent dissociative and associative pathway for the initiation mechanism of GIII was also investigated (Scheme 3.21). The kinetic equation would be of the type of equation 3.9, which is derived from application of the steady-state approximation on species **390**, **391** and **392**.

$$k_{obs} \approx \frac{1}{c\ [L]/[EVE]\ +\ 1/k_1} + \frac{[EVE]}{d[L]\ + e}$$

Equation 3.9 kinetic equation for GIII initiation: divergent dissociative and associative path
EVE = ethyl vinyl ether, L = ligand, c = $1/K_1K_2k_{mt}$ +$1/K_1k_2$, d = $1/K_3K_4k_{mt}$, e = $1/K_3k_4$+ $1/k_3$

The attempt to fit the experimental data to equation 3.9 failed (Figure 3.21B).

A convergent associative interchange and dissociative mechanism was proposed for the initiation of GIII (Scheme 3.22). The mechanism consists in the possibility for the monopyridine complex **397** to undergo ligand dissociation followed by the coordination of EVE (dissociative path) and concerted ligand dissociation and EVE coordination (interchange path).

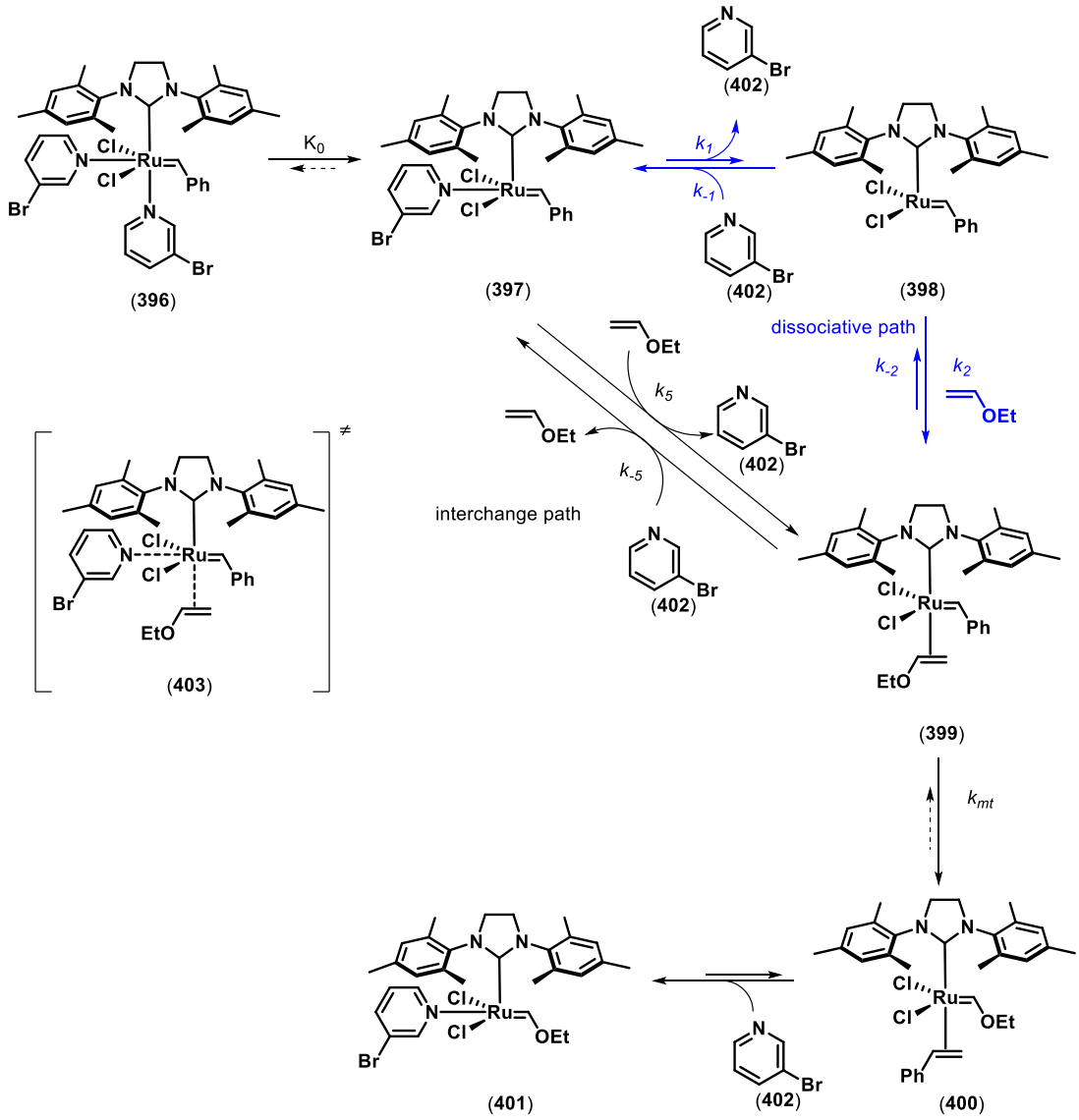

Scheme 3.22 Proposed initiation mechanism for GIII: convergent dissociative and associative interchange

The kinetic equation 3.10 was derived by applying the steady-state approximation on the species **398** and **399**.

$$k_{obs} \approx \frac{1 + f\,[L] + g\,[EVE]}{c\,[L]/[EVE] + 1/k_1 + h\,[L] + i\,[L]^2[EVE]}$$

Equation 3.10 kinetic equation for GIII initiation: convergent dissociative and associative path
EVE = ethyl vinyl ether, L = ligand, $c = 1/K_1K_2k_{mt} + 1/K_1k_2$, $h = k_5/K_1k_{mt}$, $i = k_{-5}/K_1k_2k_{mt}$

The equation which considers the convergent dissociative and associative interchange mechanism, did fit the best the experimental data collected by SF-UV, especially at low EVE concentrations (Figure 3.21C).

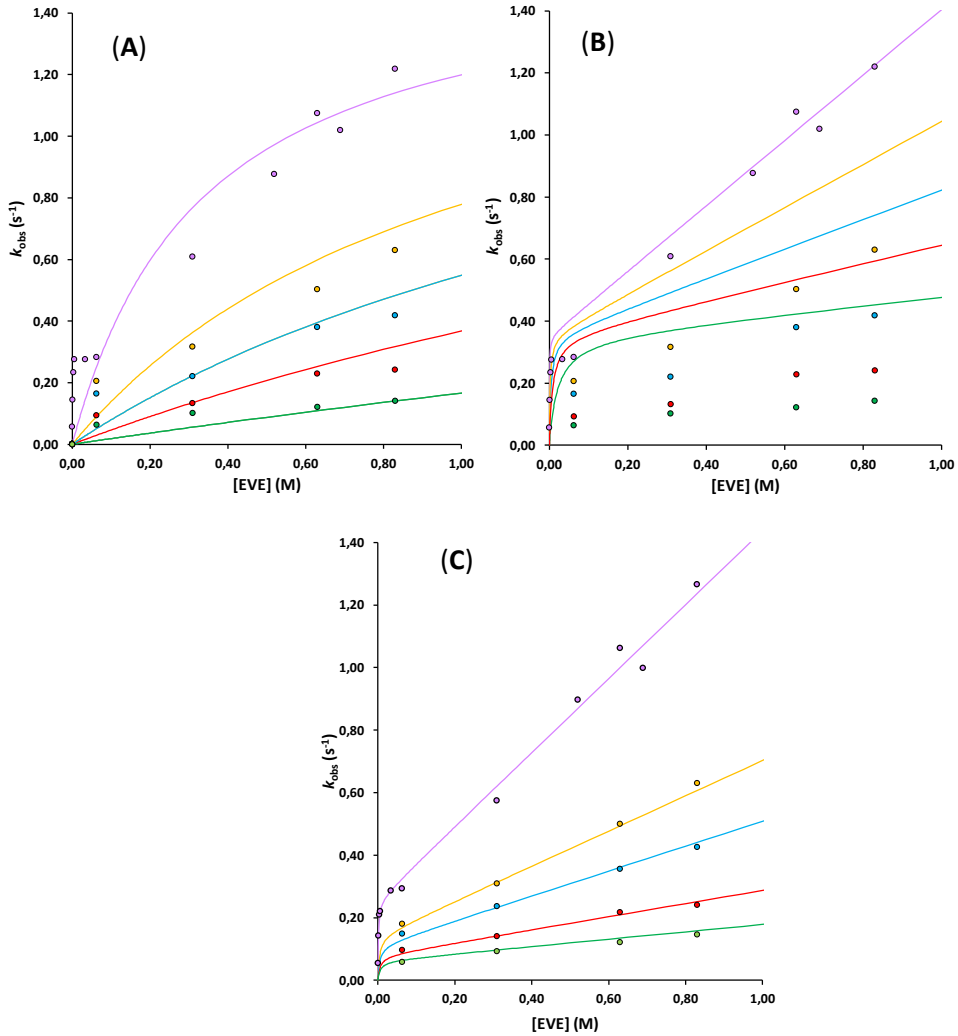

Figure 3.21 GIII fitting model with the experimental data
pathways**,** [3-BrPy] = 0 M (pink dots), [3-BrPy] = 0.0002 M (yellow dots), [3-BrPy] = 0.0004 M (blue dots), [3-BrPy] = 0.001 M (red dots), [3-BrPy] = 0.002 M (green dots)

The study performed on the initiation mechanism of GIII supports the reported conclusions[2b] that associative and dissociative pathways are kinetically relevant.

3.6 Conclusion and future work

The initiation mechanism of Grubbs 1st and 3rd generation pre-catalysts was investigated using SF-UV spectroscopy. The results obtained for GI (Scheme 3.23a) were found to be in good accordance with the literature.[2a] After the development of a reliable and reproducible SF-UV experimental procedure, the initiation mechanism of GIII was also studied. The model proposed for the initiation mechanism of GIII consists of convergent associative interchange and dissociative pathways (Scheme 3.23b) and the experimental data fits the proposed mechanistic model.

(a) Grubbs 1st generation catalyst initiation

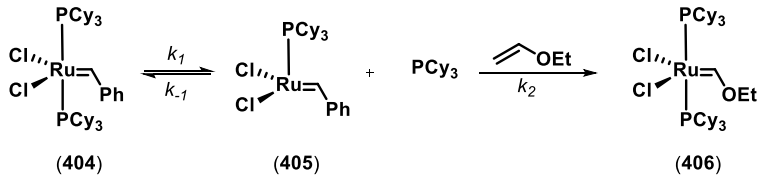

(404) (405) (406)

(b) Grubbs 3rd generation catalyst initiation

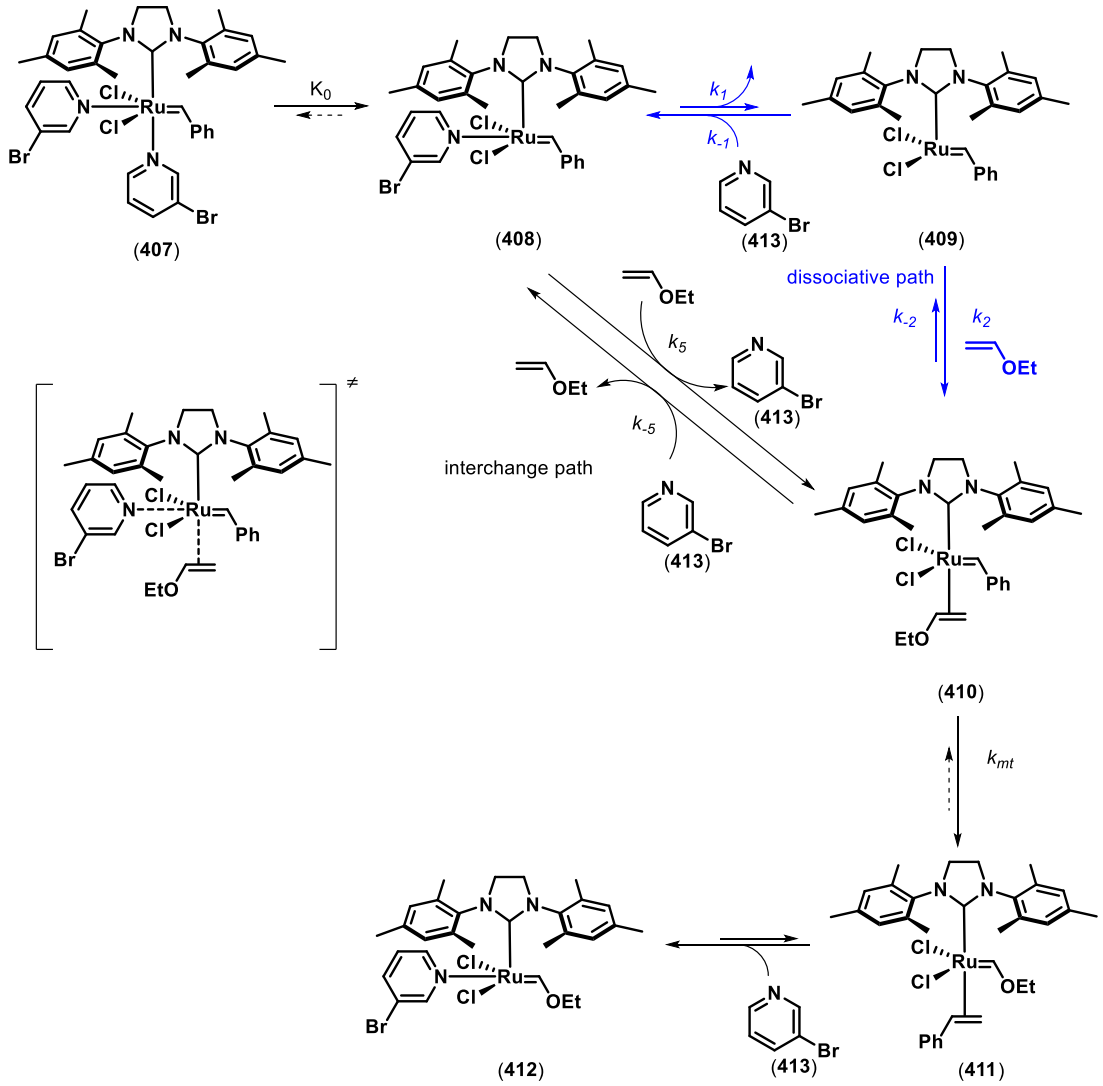

(407) (408) (413) (409) (410) (412) (413) (411)

Scheme 3.23 GI initiation mechanism and GIII proposed initiation mechanism
k_{obs} = observed rate constant, k_{in} = initiation rate constant

Calculated k_{obs} at 5 °C for GI from reported activation parameters[2a] highlighted that the dissociation of the first ligand from the pre-catalyst is 10^2 faster for GIII compared to GI (k_1 = 0.32 s^{-1} vs 1.3 x 10^{-3} s^{-1} at 5 °C), in accordance with GIII being a fast initiation metathesis

pre-catalyst. The proposed mechanism for the initiation of GIII involves the formation of two catalytically active species (**408**, **409**, Scheme 3.23), in contrast with the initiation of GII that leads to one alkylidene active species (**408**). The formation of different alkylidene active species in GII and GIII initiation, according to the mechanism proposed in this study, can affect the selectivity of the ethenolysis of MO (17 % for GII and 12 % for GIII).

Future work could include testing the GIII initiation at different pre-catalyst concentrations with fixed EVE and 3-BrPy concentration. Moreover, studying the effect of air on the system could unravel the reason for the increase in k_{obs} observed with the standard SF-UV set-up (Figure 3.8). Following by SF-UV and NMR the GIII reaction with air and the subsequent addition of EVE will give more information about the active species involved in the process.

3.7 References

1. Nelson, D. J.; Manzini, S.; Urbina-Blanco, C. A.; Nolan, S. P., *Chemical Communications* **2014**, *50,* 10355-10375.
2. (a) Sanford, M. S.; Ulman, M.; Grubbs, R. H., *J. Am. Chem. Soc.* **2001**, *123,* 749-750; (b) Trzaskowski, B.; Grela, K., *Organometallics* **2013**, *32,* 3625-3630.
3. Thiel, V.; Hendann, M.; Wannowius, K.-J.; Plenio, H., *J. Am. Chem. Soc.* **2012**, *134,* 1104-1114.
4. (a) Love, J. A.; Sanford, M. S.; Day, M. W.; Grubbs, R. H., *J. Am. Chem. Soc.* **2003**, *125,* 10103-10109; (b) Walsh, D. J.; Lau, S. H.; Hyatt, M. G.; Guironnet, D., *J. Am. Chem. Soc.* **2017**, *139,* 13644-13647.
5. Love., J. A.; Morgan, J. P.; Trnka, T. M.;Grubbs, R. H., *Angew. Chem. Int. Ed.* **2002**, *41,* 4035-4037.
6. RESTEK Inert PEEK tubing product details. http://www.restek.com/catalog/view/944/25068 (accessed 30 July).
7. bullettin,f.f.p. https://www.chemours.com/Teflon_Industrial/en_US/assets/downloads/tefzel-etfe-film-properties.pdf (accessed 30 July).

Chapter 4 Conclusion and future work

Ethenolysis of methyl oleate (**419**) was studied both from a synthetic and a mechanistic point of view. Synthetic efforts were aimed at optimising the reaction conditions for high conversion of methyl oleate (**419**) and high selectivity of the ethenolysis products (**414**, **418**) over self metathesis products (**421**, **422**, Figure 4.1). A detailed mechanistic study of the initiation of fast initiating Grubbs 3rd generation pre-catalyst (GIII) was subsequently carried out, utilizing SF-UV techniques. Modelling of the acquired kinetic data led to postulation of a combination of possible initiation pathways being operative.

Firstly, the ethenolysis of methyl oleate (**419**) was investigated, evaluating a range of commercially available metathesis pre-catalysts. After initial optimisation, design of experiments was applied on the best performing pre-catalyst (HGI), after which conditions were achieved giving excellent substrate conversion and selectivity towards the desired ethenolysis products (94 % conversion, 96 % selectivity, 187 TON, Figure 4.1). These optimised conditions represent a promising starting point for the employment of membrane separation technique to the system, in order to obtain higher selectivity and TON by separation of the products and recycling of the catalyst. Screening of commercially available membranes will be useful to identify the most suitable in terms of solvents compatibility, ethylene pressure and temperature resistance, catalyst and reactants compatibility and permeability.

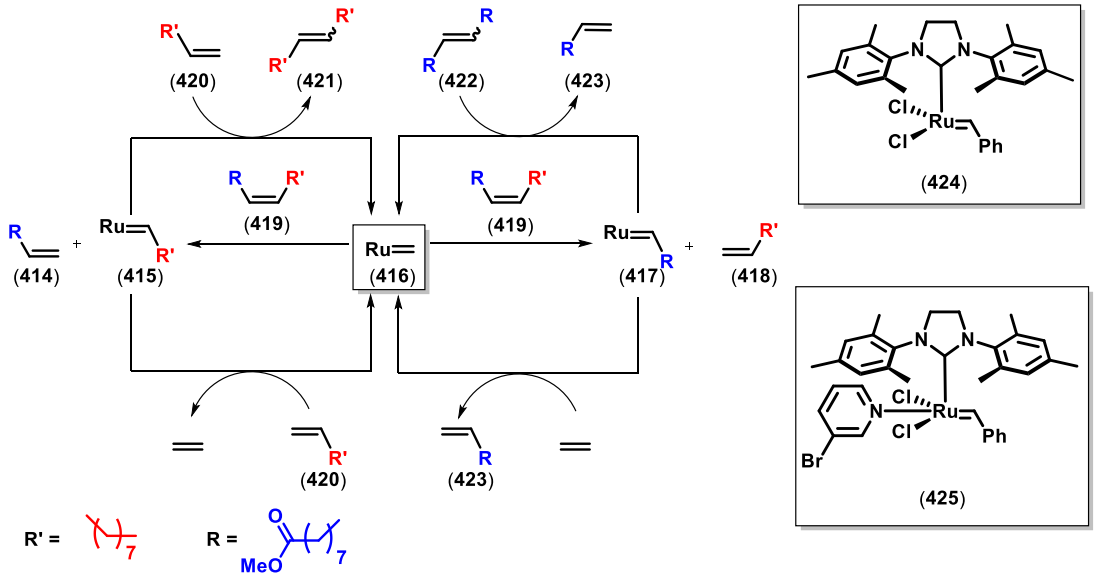

Figure 4.1 Ruthenium catalysed ethenolysis of methyl oleate (**419**) and side-reactions and possible alkylydene species

Interestingly, the catalyst screening highlighted the difference in selectivity for Grubbs 1st (GI), 2nd (GII) and 3rd generation (GIII) pre-catalysts. Grubbs 1st generation pre-catalyst was the most selective pre-catalyst of the three, which can be related to the formation of a different active catalyst species than GII and GIII. Grubbs 2nd (GII) and 3rd generation (GIII) pre-catalysts showed different selectivity values (17 % and 12 % respectively). The predicted active catalysts generated from GII and GIII would be the same (**424**, Figure 4.1) if a pure dissociative pathway was involved in the initiation of both of them. Investigations into the initiation mechanism of GIII were performed using SF-UV, following optimisation of instrumental setup, a reliable and reproducible reaction monitoring method was achieved. The effects of changing concentration of ethyl vinyl ether and the addition of 3-bromopyridine were evaluated. These studies allowed kinetic data to be modelled against two initiation pathways, associative and dissociative. From these studies it is proposed that a combination of associative and dissociative pathways is operative in the initiation of Grubbs 3rd generation pre-catalyst. Accordingly, the difference in selectivity between GIII and GII was proposed to be related with the formation from GIII pre-catalyst of two active catalysts (**424**, **425**, Figure 4.1), which can both react with an olefin substrate. This enhanced reactivity for GIII in comparison with GII could lead to undesired self metathesis of the substrate. In order to further investigate the selectivity of GIII in the ethenolysis of MO, competitive experiments (EVE *vs* MO) could be performed which would give insight on the favoured pathway (dissociative or associative) for MO. A deeper understanding of the initiation mechanism of GIII will also be crucial for the future development of new fast initiating metathesis pre-catalysts and SF-UV experiments varying the GIII concentration would be useful to improve the current mechanistic model.

Chapter 5 Experimental Details

5.1 General experimental details

5.1.1 Techniques

Unless otherwise stated, all reactions were performed in oven-dried glassware under a nitrogen atmosphere, using standard Schlenk-line techniques or in an N_2-filled glove-box.

5.1.2 Reagents and solvents

All commercial reagents were obtained from Sigma-Aldrich, with exception of CatMETiumRF2® and CatMETiumRF3® that were purchased from Evonik Industries AG. Methyl oleate and *n*-nonane were degassed by bubbling nitrogen gas before use. Ethylene gas research grade N3.2 was purchased from BOC Industrial gasses UK.

Anhydrous organic solvents were obtained from a solvent purification system (MBraun SPS 800) situated in the School of Chemistry, University of Edinburgh. These solvents were dispensed using gas-tight syringes under a positive pressure of nitrogen. Commercial grade solvents were used for extractions, TLC analysis and flash column chromatography.

5.1.3 Analysis

5.1.4 NMR spectroscopy

NMR spectra were recorded at 27 °C on Bruker Ascend 400 or Bruker Ascend 500 spectrometers. ^{1}H and ^{13}C $\{^{1}H\}$ spectra were referenced to residual solvent signals and solvent signals respectively, or to a TMS internal standard. Coupling constants, *J*, were calculated to the nearest 0.1 Hz using MestreNova (versions 9 and 10). The following abbreviations (and their combinations) are used to label the multiplicities: s (singlet), d (doublet), t (triplet), q (quartet), m (multiplet), app (apparent) and br (broad).

5.1.5 Gas-chromatography

Gas-chromatography (GC) was carried out using a Shimadzu GC-2010 instrument with FID detection and a 25 m x 0.2 mm capillary column (HP-Ultra 2 from Agilent) with H_2 as a carrier gas. As a routine, the following temperature programme was used: 50 °C (2 min), then heating to 300 °C (12 min), finally 300 °C (5 min).

5.1.6 UV-spectroscopy

UV spectra were recorded on an Ocean-Optics USB400 Miniature Fiber Optic Spectrometer fitted with a DH2000-BALUV lamp (deep-UV deuterium and tungsten halogen lamps), solarised resistant grade optical fibres.

Experiments were performed in a standard cuvette of Quarts SUPRASIL® with a 10 mm-light path purchased from Hellma Analystics.

SF-UV experiments were carried out with a Hi-Tech Scientific SFA-20 rapids kinetics stopped-flow accessory attached alongside a quartz 10 mm-path cuvette were used for the quick mixing. Reagents were loaded in two independent 2.5 mL syringes and mixed them with a pneumatic drive at constant air pressure (5 bar). UV-vis analysis were performed with a 284-890 nm spectral window. Data were analysed with 5.02 version kinetic studio software.

5.2 Synthetic procedures

5.2.1.1 Methyl 9-decenoate

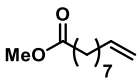

(**426**)

Prepared by following procedure of P. M. Zelisko and co-workers.[1]

In a 25 mL round bottomed flask 9-decenoic acid (1.2 g, 7.0 mmol) and *p*-toluene sulfonic acid (0.076 g, 0.4 mmol) were dissolved into 8 mL of methanol. The reaction mixture was left stirring and heated to reflux with molecular sieves (4 Å). After 4 hours the crude mixture was cooled down and methanol was removed using a rotary evaporator. The remaining crude mixture was extracted into 8 mL of diethyl ether, neutralized with 1.5 mL of $KHCO_3$ saturated aqueous solution and washed with 2 x 1.5 mL of brine, while the combined aqueous phases were extracted with 4 mL of diethyl ether. The combined ethereal fractions were washed with 2.5 mL of brine and dried over Na_2SO_4. The organic phase was then filtered through a medium porosity glass filter and the solvent was removed on the rotary evaporator. The product was obtained as a clear and colourless liquid (0.9 g, 76 % yield) matching reported spectral data:[1]

^{1}H NMR (500 MHz, $CDCl_3$): δ_H 5.84 (1H, m, C*H*=CH_2), 4.99 (2H, m, CH=C*H*$_2$), 3.68 (3H, s, OC*H*$_3$), 2.32 (2H, t, *J* = 7.4 Hz, $CH_3OCOCH2$), 2.05 (2H, m, C*H*$_2$CH=CH_2), 1.63 (2H, m, $CH_3OCOCH_2CH_2$), 1.33 (8H, m, $OCH_3CO(CH_2)_2(CH_2)_4(CH_2)_2CH=CH_2$); ^{13}C NMR (101 MHz, $CDCl_3$): δ_C 174.5, 139.2, 114.3, 51.5, 34.3, 33.9, 29.2, 25.1.

5.2.1.2 Grubbs 3rd generation pre-catalyst (GIII)

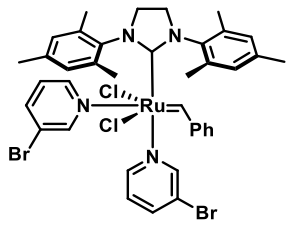

(**427**)

Prepared by following the procedure by Grubbs and co-workers.[2]

Grubbs 2nd generation pre-catalyst (0.5 g, 0.6 mmol) and 3-bromopyridine (1.1 mL, 11.0 mmol) were added to a 20 mL vial. The vial was capped and the reaction mixture was left stirring for 5 minutes while the color changed from red to bright green. Pentane (20 mL) was layered onto the green solution to start the green solid precipitation at room temperature. The vial was then capped and left at −20 °C overnight (freezer). The green precipitate was collected by vacuum-filtration and washed with 4 x 10.0 mL of room temperature pentane. After drying the precipitate under vacuum, the product (**427**) was obtained as a green powder (0.4 g, 80% yield) matching reported spectral data:[2]

^{1}H NMR (400 MHz, CD_2Cl_2): δ_H 19.07 (1H, s, C*H*Ph), 8.70 (2H, br. s, pyridine), 8.56 (2H, br. s, pyridine), 7.98 (2H, br. s, pyridine), 7.93 (2H, br. s, pyridine), 7.78 (2H, d, *ortho* C*H*, *J* = 7.3 Hz), 7.51 (1H, t, *para* C*H*, *J* = 7.3 Hz), 7.10 (2H, app t, meta C*H*, *J* = 7.7 Hz), 6.78 (4H, br. s, Mes C*H*), 4.05 (4H, br. s, NCH_2CH_2N), 2.59 (6H, br. s, Mes CH_3), 2.22 (12H, s, Mes CH_3).

^{13}C NMR (100 MHz, CD_2Cl_2): δ_C 314.7, 217.1, 157.3, 155.0, 152.4, 151.9, 151.6, 148.5, 139.2, 138.9, 130.6, 130.5, 129.9, 128.6, 128.6, 128.4, 125.3, 51.4, 21.4, 20.7.

5.3 Catalyst screening

In the glove box the solutions of methyl oleate (0.80 mL, 2.36 mmol) and *n*-nonane (0.40 mL, 2.24 mmol) as internal standard (IS) in 1 mL solvent (toluene or dichloromethane) and the desired catalyst (0.15 mol%) in 1 mL solvent (toluene or dichloromethane) were prepared. Both solutions were transferred into a 10 mL stainless steel autoclave under an inert atmosphere and then pressurised with ethylene at 20 bar. The autoclave was left stirring at 20 °C (oil bath) under a constant pressure of ethylene. After 3 hours the autoclave was cooled down and depressurised and the reaction mixture was quenched by adding 0.10 mL of EVE.

The quenched reaction mixture was passed through silica gel together with a mixture of *n*-hexane, EtOAc (1:5) and analysed by GC-FID.

5.4 Design of experiments

Minitab 17 software was used to perform the design of experiments.

5.4.1 Two-levels full factorial

The two-levels full factorial design was used to investigate the following factors: temperature, ethylene pressure, catalyst loading and reaction time. Maximum and minimum levels for each factor were chosen taking into account experimental restrictions: a maximum pressure of 60 bar and a maximum temperature of 50 °C for the commercially available membranes; a maximum pressure of 100 bar for the autoclave. Accordingly, the levels of factors were given as input to the software (Table 5.1).

Factor	Min level	Max level
Temperature (°C)	20	50
Ethylene pressure (bar)	20	40
Reaction time (min)	15	30
Catalyst loading (mol%)	0.15	0.40

Table 5.1 Input factors two-levels full factorial design

The series of experiments generated by the software were carried out (Table 5.2).

Run	Factor A: T (°C)	Factor B: time (min)	Factor C: Cat. load. (mol%)	Factor D: C_2H_4 pres. (bar)	Conv. (%)
1(+,−,−,+)	40	15	0.15	40	70
2(−,−,−,−)	20	15	0.15	20	67
3(+,−,+,−)	40	15	0.4	20	80
4(+,0, −,+)	40	30	0.15	40	74
5(+,0,+,+)	40	30	0.4	40	84
6(−,0, −,−)	20	30	0.15	20	74
7(−,−,+,+)	20	15	0.4	40	80
8(−,−,−,+)	20	15	0.15	40	68
9(−,0, −,+)	20	30	0.15	40	67
10(+,−,+,+)	40	15	0.4	40	82
11(+,0, −,−)	40	30	0.15	20	76
12(−,0,+,+)	20	30	0.4	40	86
13(+,−,−,−)	40	15	0.15	20	69
14(−,0,+, −)	20	30	0.4	20	87
15(−,−,+,−)	20	15	0.4	20	76
16(0,0,0,0)	30	22.5	0.275	30	82
17(+,0,+,−)	40	30	0.4	20	84

Table 5.2 Experiments for the two levels full-factorial design
T = temperature, time = reaction time, cat. load. = catalyst loading, pres. = pressure, conv. = conversion
(+) = maximum value, (−) = minimum value, (0) = centre point value of a variable
(−, −, +, −) = combination of minimum A, minimum B, maximum C, minimum D
Conditions: methyl oleate 2.36 mmol, catalyst loading, I.S (*n*-nonane) 2.24 mmol, ethylene pressure, 2 mL toluene, T, reaction time. Reaction mixture analysed by GC-FID.

The results obtained were processed and a normal plot of effect for conversion (Figure 5.1) and a main effects plot for conversion (Figure 5.2) were generated in order to identify the parameters effecting the most the system.

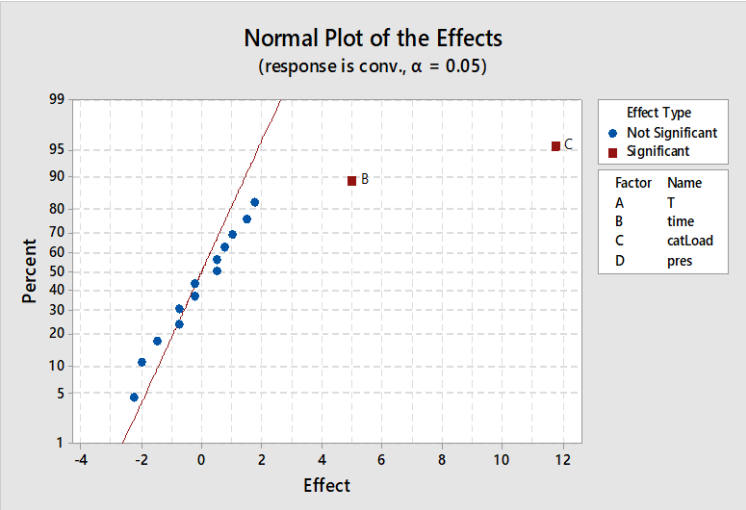

Figure 5.1 Normal plot of effects for the two-level full factorial design
factors: temperature (T = A), reaction time (time = B), catalyst loading (catLoad = C), C_2H_4 pressure (pres = D);
response = conversion (conv.); α = level of statistical significance (0.05 means good level of significance);
effects not affecting the reaction conversion (blue dots), effects affecting the reaction conversion (red squares)

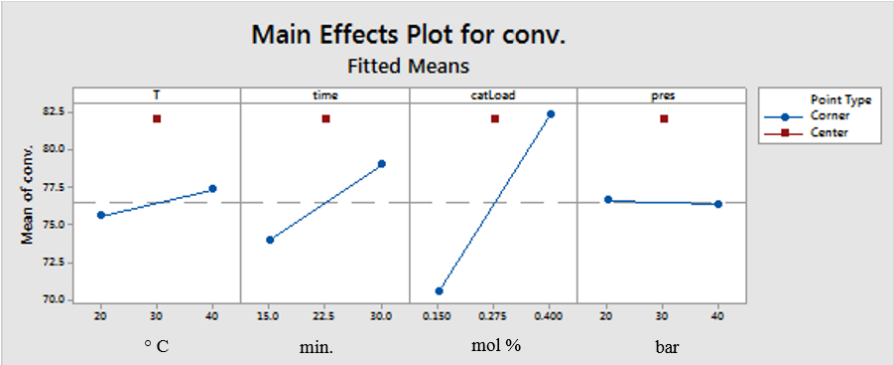

Figure 5.2 Main effects plot for the two-level full factorial design
factors: temperature (T), reaction time (time), catalyst loading (catLoad), C_2H_4 pressure (pres);
response = conversion (conv.);
corner type points (blue dots) = minimum and maximum level for each factor;
center type points (red squares) = measure process stability and variability

5.4.2 Central composite surface design

The parameters that were found to have a smaller effect on the conversion were kept at their best (ethylene pressure at 40 bar and temperature at 40 °C). Whereas the parameters which showed a great effect on the conversion were further optimised by a central composite response surface design. Maximum and minimum values for catalyst loading and reaction time were chosen, as done previously for the two-level full factorial design (Table 5.3).

Factor	Minimum level	Maximum level
Reaction time (min)	15	240
Catalyst loading (mol %)	0.01	1

Table 5.3 Input factors central composite design

The series of experiments generated by the software were carried out (Table 5.4).

Run	time (min)	Cat. load. (mol%)	Conv. (%)
1(1)	207	0.86	86
2(0)	128	0.51	88
3(0)	128	0.51	89
4(1)	48	0.86	90
5(0)	128	0.51	87
6(0)	128	0.51	86
7(−1)	15	0.51	83
8(1)	207	0.15	62
9(−1)	128	0.01	25
10(1)	48	0.15	65
11(−1)	240	0.51	86
12(−1)	128	1.00	90

Table 5.4 Experiments for the surface response design
T = temperature, time = reaction time, cat. load. = catalyst loading, pres. = pressure, conv. = conversion
(0) = central points; (1), (−1) = axial points
Conditions: Conditions: methyl oleate 2.36 mmol, catalyst loading, I.S (*n*-nonane) 2.24 mmol, ethylene 40 bar, 2 mL toluene, 40 °C, reaction time. Reaction mixture analysed by GC-FID.

5.5 UV-vis experiments

5.5.1 GI UV-vis measurements

Within a N_2 filled glovebox freshly prepared stock solutions of ethyl vinyl ether (in equivalents relative to GI) and GI (0.0139 M) in toluene were prepared in volumetric glassware. Then the EVE stock solution (1.6 mL) was transferred to a standard UV cuvette with a stirring magnet capped with a rubber septum and the GI stock solution was put in a 8 mL vial with a rubber septum.

Both stock solutions were transferred outside the glove-box. A solvent background spectrum was recorded. To the cuvette in the UV cuvette holder 100 µL of a 0.0139 M stock solution of GI in toluene was added through the rubber septum with a micro syringe loaded under inert atmosphere while stirring. The kinetics of the reaction were followed by monitoring the appearance of the product at 484 nm. 100 data points were recorded over a period of time of 200 s and the kinetic traces were fitted to a first order exponential. The observed pseudo first order rate constants (k_{obs}) are summarised in Table 5.5.

[EVE] (M)	EVE (equiv. to GI)	k_{obs}(s^{-1})
0.61	755	0.019
1.47	1880	0.021
4.18	5300	0.025

Table 5.5 GI k_{obs} at different [EVE]
Data measured by UV-vis in a standard cuvette with rubber septum

5.5.2 GI SF-UV measurements

Within a N_2 filled glovebox 10 mL stock solutions of GI (1.66×10^{-3} M) and EVE (in equivalents relative to GI) in toluene were prepared in volumetric glassware, then subsequently transferred to Schott reagent bottles and then capped with three valve caps with threaded ports (Diba Labware: Q-Series cap, GL32, 3 ports + valves). The sealed reagent bottles were removed from the glovebox and connected to a N_2-inlet and the syringe inlet line via standard HPLC adapters connected by PEEK tubes.

Prior to kinetic experiments the system was washed through with a toluene and a background spectrum was recorded. Equal quantities from each syringe (LS, Figure 5.3) were transferred to the cuvette leading to the final concentrations being half of that of the original stocks

The experiments were monitored by following the formation of the product at 484 nm and the spectra were processed by using a singular value decomposition (SVD) to filter the noise (Figure 5.4). A range from 100 to 300 data points were recorded over different periods of time (200 – 600 s).

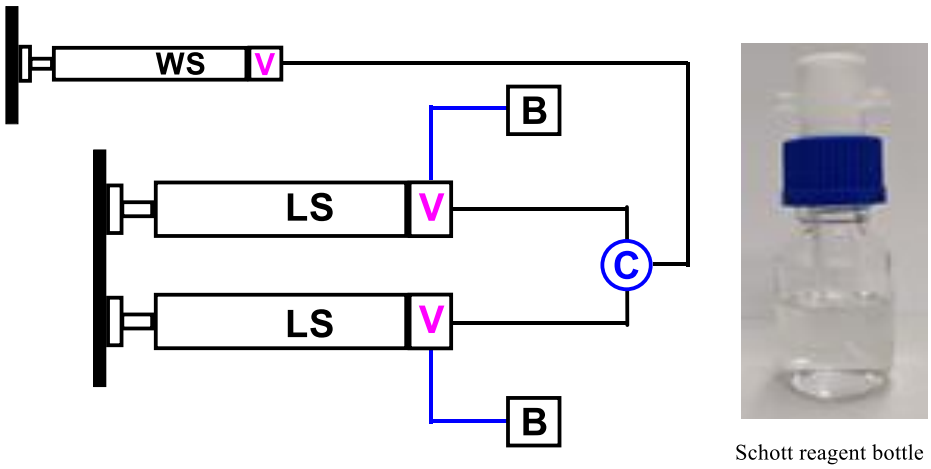

Figure 5.3 SF-UV standard set-up
B = Schott reagent bottles, V= three-ways valves, C = SF-UV cuvette, LS = loading syringes, WS = waste syringe

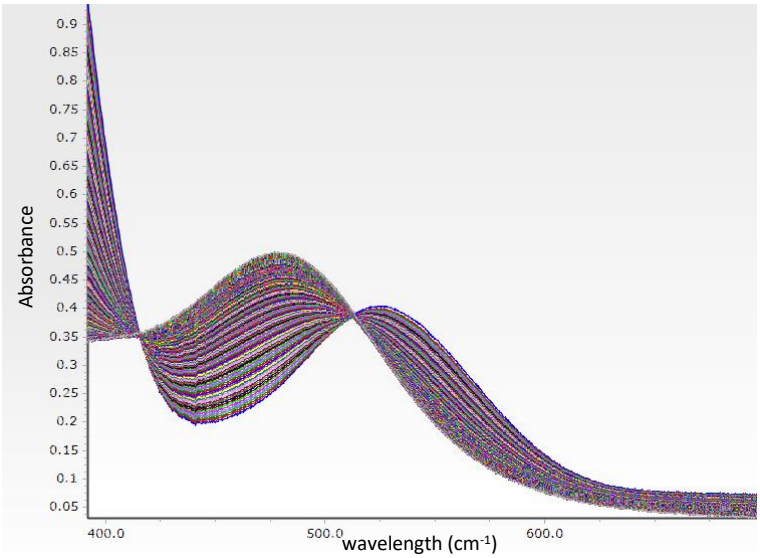

Figure 5.4 Representative UV spectrum for reaction of GI with EVE
[GI] = 8.14 10^{-4} M, [EVE] = 0.198 M

The kinetic traces were fitted to a first order exponential (Figure 5.5) and the observed pseudo first order rate constants are summarised in Table 5.6.

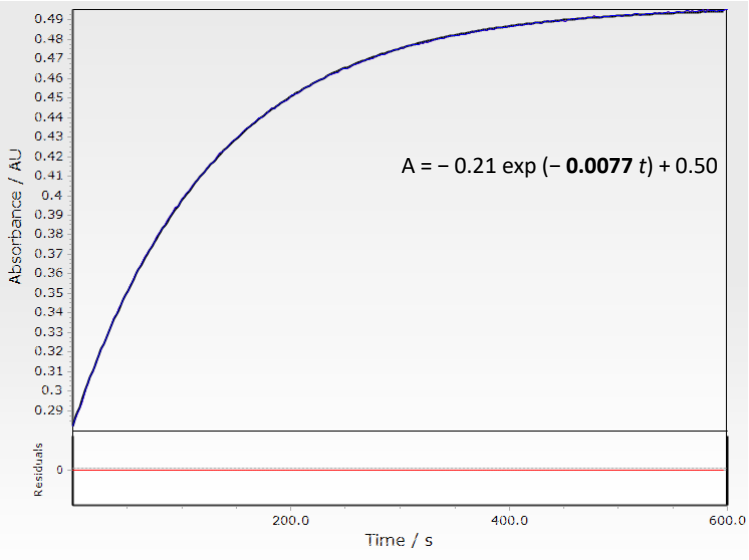

Figure 5.5 Representative first order exponential fitting for GI reaction with EVE
A = absorbance, t = time, k_{obs} = 0.0077 s^{-1}; [GI] = 8.14 10^{-4} M, [EVE] = 0.198 M

[EVE] (M)	k_{obs} (s^{-1})
0.096	0.0070
0.150	0.0070
0.200	0.0079
0.240	0.0080
0.370	0.0097
0.490	0.0110
0.620	0.0110
0.670	0.0108
0.720	0.0113
0.910	0.0119
1.500	0.0123

Table 5.6 GI initiation kinetic measurements by SF-UV
[GI] = 8.14 10^{-4} M, k_{obs} values averaged on minimum 3 measurements

The k_{obs} data were successfully fitted to the reported saturated equation (Figure 5.6).[3]

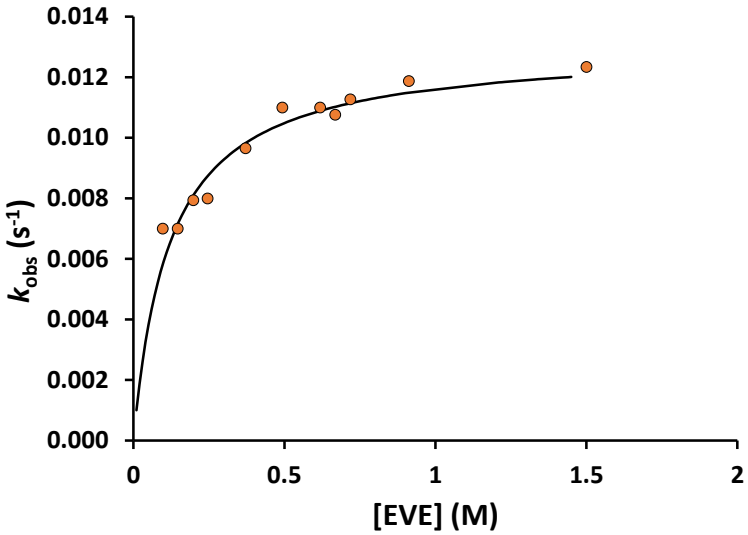

Figure 5.6 Grubbs 1st generation pre-catalyst saturation curve at different EVE concentrations (SF-UV)

5.5.3 GIII SF-UV measurements

Within a N_2 filled glovebox 10 or 50 mL stock solutions of GIII ($4.6\ 10^{-5}$ M) and EVE (in equivalents relative to GIII) with or without 3-BrPy (0.0008 – 0.002 M) in toluene were prepared in volumetric glassware, then subsequently transferred to 10 mL gas tight syringes (VWR). These were sealed with plugged flangeless nut, removed from the glovebox and attached to the SF-UV syringes *via* HPLC fittings. Prior to kinetic experiments the system was washed through with a toluene and a background spectrum was recorded. The system was flushed twice with both stock solutions to ensure non diluted stock solutions were mixed in the cuvette.

The experiments were monitored by following the decay of the pre-catalyst at 354 nm and the spectra were processed by using a singular value decomposition (SVD) to filter the noise (Figure 5.8). 200 data points were recorded over different periods of time (8 – 80 s).

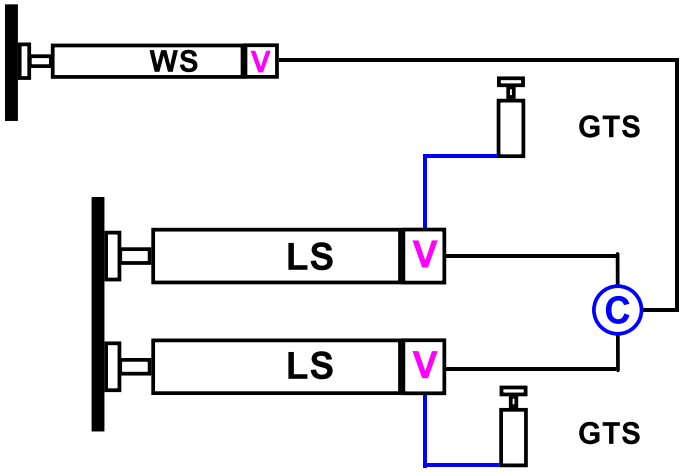

Figure 5.7 SF-UV improved set-up
V= three-ways valves, C = SF-UV cuvette, LS = loading syringes, WS = waste syringe

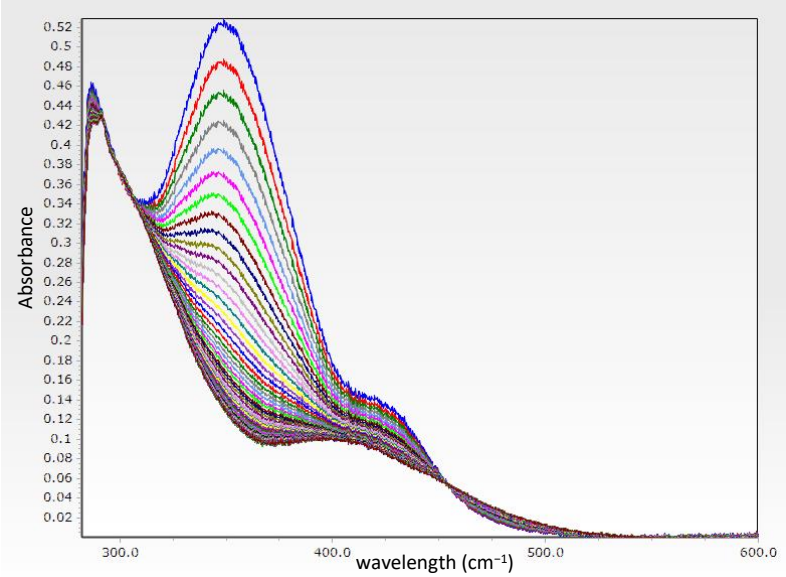

Figure 5.8 Representative UV spectrum for reaction of GIII with EVE
[GI] = 4.6 10^{-4} M, [EVE] = 0.63 M

The kinetic traces were fitted to a first order exponential (Figure 5.9) and the observed pseudo first order rate constants are summarised in Table 5.7.

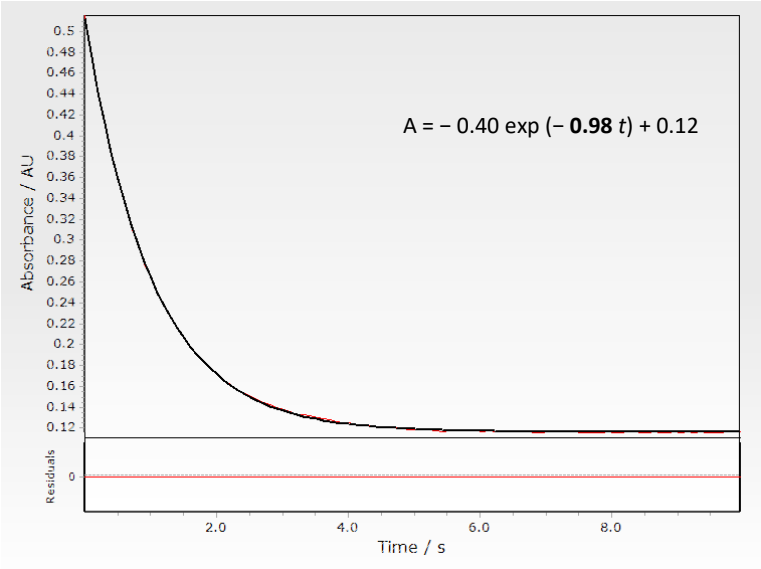

Figure 5.9 Representative first order exponential fitting for GI reaction with EVE
A = absorbance, *t* = time, k_{obs} = 0.98 s^{-1}; [GIII] = 4.6 10^{-5} M, [EVE] = 0.63 M

[EVE] (M)	3-BrPy	k_{obs} (s^{-1})
0.00040	0.0000	0.056
0.00200	0.0000	0.140
0.00400	0.0000	0.230
0.00630	0.0000	0.270
0.03400	0.0000	0.270
0.06300	0.0000	0.280
0.31000	0.0000	0.610
0.52000	0.0000	0.880
0.63000	0.0000	1.100
0.69000	0.0000	1.000
0.83000	0.0000	1.200
0.06300	0.0002	0.200
0.31000	0.0002	0.310
0.63000	0.0002	0.500
0.83000	0.0002	0.630
0.06300	0.0004	0.160
0.31000	0.0004	0.220
0.63000	0.0004	0.380
0.83000	0.0004	0.420
0.06300	0.0010	0.093
0.31000	0.0010	0.130
0.63000	0.0010	0.230
0.83000	0.0010	0.240
0.06300	0.0020	0.0620
0.31000	0.0020	0.100
0.63000	0.0020	0.120
0.83000	0.0020	0.141

Table 5.7 GIII initiation kinetic measurements by SF-UV
[GIII] = 4.6 10^{-5} M, k_{obs} values averaged on 20 measurements

5.5.3.1 First model k_{obs} kinetic derivation

The k_{obs} kinetic derivation for GIII initiation was carried out by applying the steady-state approximation on the alkylidine species (**430**) leading to equation 5.1.

$$k_{obs} = x_{RuL}\left(\frac{k_2}{\frac{k_{-2}\,[L_t]}{k_3\,[EVE]} + 1} + k_4\,[EVE]\right)$$

Equation 5.1 k_{obs} for GIII initiation mechanism model

In the GIII kinetic derivation for clarity the six-coordinated complex (**428**, Scheme 5.1) will be referred as RuL_2, the mono-pyridine complex (**429**, Scheme 5.1) will be RuL, the alkylidine species (**430**, Scheme 5.1) will be Ru and the free 3-bromopyridine (**434**, Scheme 5.1) will be L.

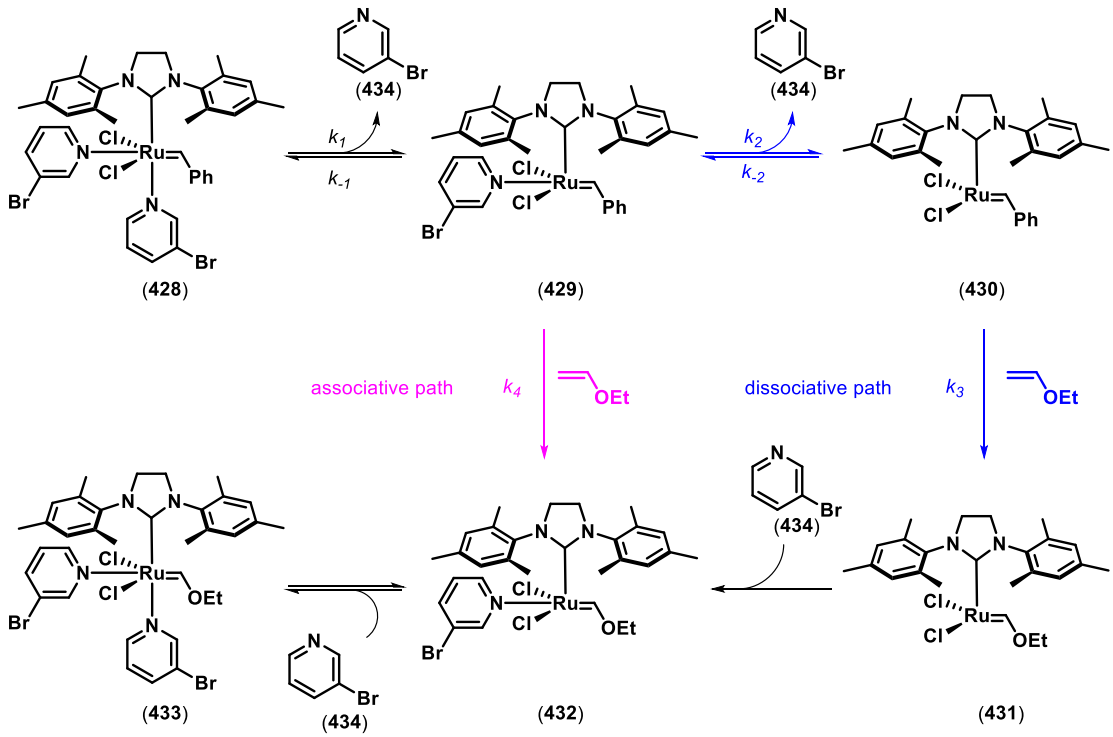

Scheme 5.1 Proposed initiation mechanism for GIII

Taking into account the first ligand dissociation process (Scheme 5.2) and the equilibrium constant for the process (K_1), the ruthenium molar fraction (x_{RuL}) can be calculated as followed. Referring to Ru_T as the total ruthenium amount, L_A as the added 3-bromopyridine and L_T as the total 3-bromopyridine amount.

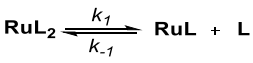

Scheme 5.2 Dissociation of the first ligand from GIII

$$K_1 = \frac{[RuL][L + L_A]}{[RuL_2]};$$

$$[RuL] = [L]; \quad [Ru_T] = [RuL] + [RuL_2], [RuL_2] = [Ru_T] - [RuL]$$

$$[RuL][RuL + L_A] = K_1\,([Ru_T] - [RuL])$$

$$[RuL]^2 + [RuL][L_A] = K_1\,[Ru_T] - K_1\,[RuL]$$

$$[RuL]^2 + [RuL]([L_A] + K_1) - K_1\,[Ru_T]\; = 0$$

Solving the quadratic equation for $[RuL]$:

$$[RuL] = \; -[L_A] - K_1 \; \pm \frac{\sqrt{[L_A]^2 + K_1\,(\,K_1 + 2\,[L_A] + [Ru_T])}}{2}$$

Considering the ruthenium molar fraction (x_{RuL}):

$$x_{RuL} = \frac{[RuL]}{[Ru_T]}; \;\; [RuL] = x_{RuL}\,[Ru_T]$$

Focusing on the possible reactions of the mono-pyridine complex (RL, Scheme 5.3 and **429**, Scheme 5.1) and applying the steady-state approximation on the alkylidene species (Ru, Scheme 5.3 and **430**, Scheme 5.2), the equation for [*Ru*] can be derived.

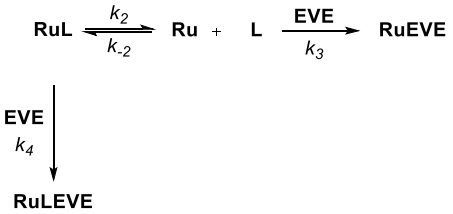

Scheme 5.3 Schematic mechanism for mono-pyridine reaction with EVE

$$[L_{TOT}] = [L_T] = [RuL] + [L_A]; [RuL] = [L]$$

$$[Ru] \ll [RuL] + [RuL_2]$$

$$rate = k_{obs}\,[Ru_T] = k_3\,[EVE][\boldsymbol{Ru}] + k_4\,[EVE][\boldsymbol{RuL}] \qquad \textbf{Equation 5.2}$$

$$\frac{d[Ru]}{dt} = 0 = k_2[RuL] - k_{-2}[Ru][L_T] - k_3[EVE][Ru]$$

$$[Ru](k_{-2}[L_T] + k_3[EVE]) = k_2[RuL]$$

$$[Ru] = \frac{k_2[RuL]}{k_{-2}[L_T]+k_3[EVE]} \qquad \textbf{Equation 5.3}$$

Inserting the equation for [*Ru*] (Equation 5.3) in the rate constant equation (Equation 5.2), the k_{obs} equation was obtained (Equation 5.4).

$$k_{obs}\,[Ru_T] = x_{RuL}\,[Ru_T]\,\frac{k_2\,k_3\,[EVE]}{k_{-2}\,[L_T] + k_3\,[EVE]} + x_{RuL}\,[RuL]k_4\,[EVE]$$

$$k_{obs} = x_{RuL}\left(\frac{k_2}{\frac{k_{-2}\,[L_T]}{k_3\,[EVE]}+1} + k_4\,[EVE]\right) \qquad \textbf{Equation 5.4}$$

The experimental data collected were fitted to Equation 5.4 (Figure 5.10) and the best fit found so far gave the following *k* values: k_2 = 0.32 s^{-1}, k_{-2} = 10 $M^{-1}s^{-1}$, k_3= 5 s^{-1}, k_4 = 1.32 s^{-1}.

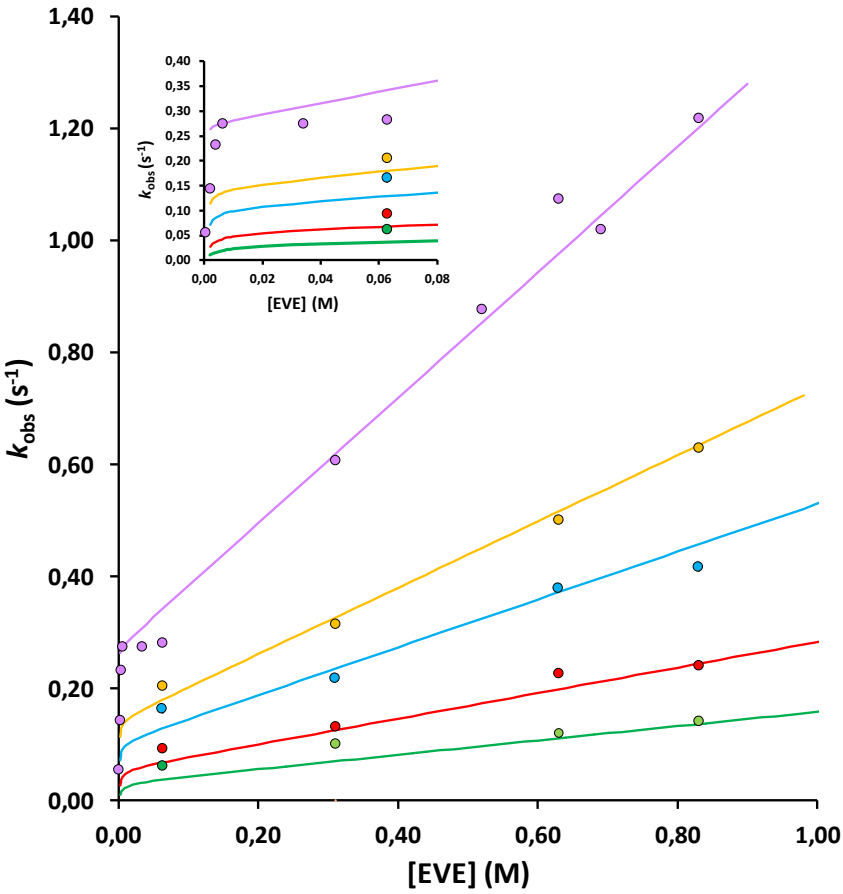

Figure 5.10 GIII fitting model with the experimental data
[3-BrPy] = 0 M (pink dots), [3-BrPy] = 0.0002 M (yellow dots), [3-BrPy] = 0.0004 M (blue dots),
[3-BrPy] = 0.001 M (red dots), [3-BrPy] = 0.002 M (green dots)
Insert graph showing [EVE] range from 0 to 0.08 M

5.5.3.2 Second model k_{obs} kinetic derivation

The k_{obs} kinetic derivation for GIII initiation as a convergent associative interchange and dissociative path was carried out by applying the steady-state approximation on the species (**437** and **438**) leading to equation 5.5.

$$k_{obs} \approx \frac{1 + f\,[L] + g\,[E]}{c\,[L]/[E] + 1/k_1 + h\,[L] + i\,[L]^2[E]}$$

Equation 5.5 kinetic equation for GIII initiation: convergent dissociative and associative path
EVE = ethyl vinyl ether, L = ligand, $c = 1/K_1K_2k_{mt} + 1/K_1k_2$, $h = k_5/K_1k_{mt}$, $i = k_{-5}/K_1k_2k_{mt}$

In the GIII kinetic derivation for clarity the six-coordinated complex (**435**, Scheme 5.4) will be referred as RuL_2, the mono-pyridine complex (**436**, Scheme 5.4) will be RuL, the alkylidine species (**437**, Scheme 5.4) will be Ru, the ruthenium complex coordinated to EVE (**438**, Scheme 5.4) will be RuEVE, final metathesis product (**440**, Scheme 5.4) will be Ru'L and the free 3-bromopyridine (**441**, Scheme 5.4) will be L.

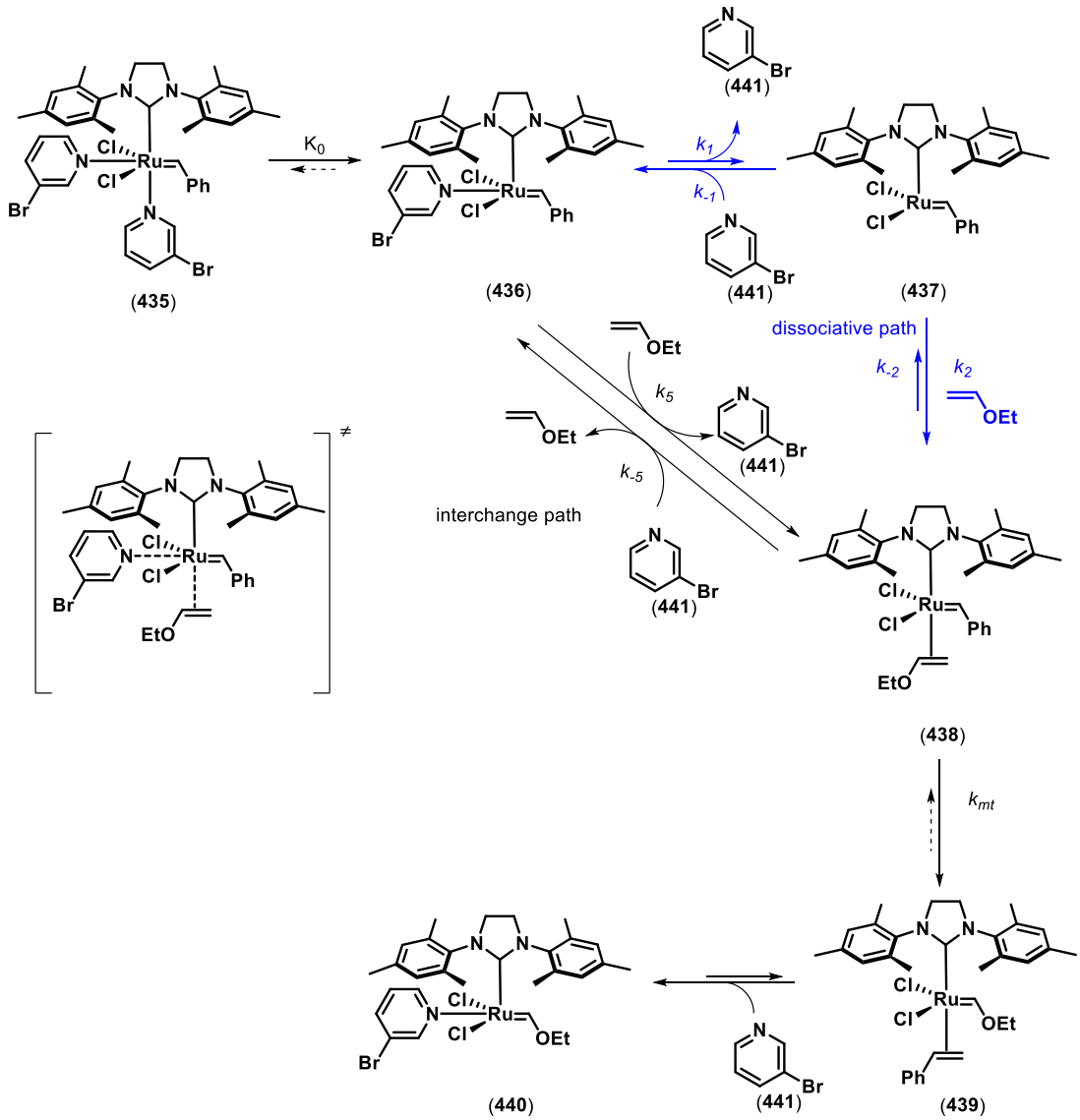

Scheme 5.4 Proposed initiation mechanism for GIII: convergent dissociative and associative interchange

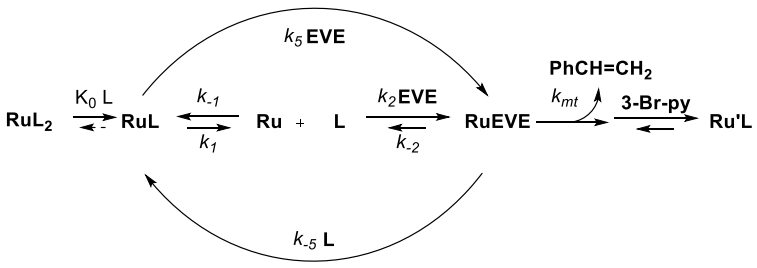

Scheme 5.5 Schematic mechanism for convergent dissociative and associative interchange path

Applying the steady-state approximation on RuEVE (Scheme 5.5):

$$\frac{d\,[RuEVE]}{dt} = 0$$
$$= k_5\,[RuL][EVE] + k_2\,[Ru][EVE] - k_{-5}\,[L][RuEVE] - k_{-2}\,[RuEVE] - k_{mt}\,[RuEVE]$$

$$k_5\,[RuL][EVE] + k_2\,[Ru][EVE] = k_{-5}\,[L][RuEVE] + k_{-2}\,[RuEVE] + k_{mt}\,[RuEVE]$$

Equation 5.6

Applying the steady-state approximation on Ru (Scheme 5.5):

$$\frac{d\,[Ru]}{dt} = 0 = k_1\,[RuL] + k_{-2}\,[RuEVE] - k_{-1}\,[Ru][L] - k_2\,[Ru][EVE]$$

$$k_1\,[RuL] + k_{-2}\,[RuEVE] = k_{-1}\,[Ru][L] + k_2\,[Ru][EVE]$$
$$[Ru]\,(k_{-1}\,[L] - k_2\,[EVE]) = k_1\,[RuL] + k_{-2}\,[RuEVE]$$

Solving for [Ru]:

$$[Ru] = \frac{k_1\,[RuL] + k_{-2}\,[RuEVE]}{k_{-1}\,[L] - k_2\,[EVE]} \qquad \textbf{Equation 5.7}$$

Substitution of [Ru] from equation 5.6 into equation 5.7

$$k_5\,[RuL][EVE] + \frac{k_1\,k_2[RuL][EVE] + k_{-2}\,k_2\,[RuEVE][EVE]}{k_{-1}\,[L] - k_2\,[EVE]}$$
$$= k_{-5}\,[L][RuEVE] + k_{-2}\,[RuEVE] + k_{mt}\,[RuEVE]$$

$$k_{-1}\,k_5\,[L][RuL][EVE] + k_2\,k_5\,[RuL][EVE]^2 + k_1\,k_2[RuL][EVE]$$
$$+ k_{-2}\,k_2\,[RuEVE][EVE]$$
$$= k_{-1}\,k_{-5}\,[L]^2[RuEVE] + k_2\,k_{-5}\,[L][RuEVE]\,[EVE]$$
$$+ k_{-1}\,k_{-2}\,[RuEVE][L] + k_{-2}\,k_2\,[RuEVE][EVE] + k_{-1}\,k_{mt}\,[RuEVE][L]$$
$$+ k_2\,k_{mt}\,[RuEVE][EVE]$$

Cancelling and rearranging:

$$[RuL]\,(k_{-1}\,k_5\,[L][EVE] + k_2\,k_5\,[EVE]^2 + k_1\,k_2[EVE])$$
$$= [RuEVE](k_{-1}\,k_{-5}\,[L]^2 + k_2\,k_{-5}\,[L]\,[EVE] + k_{-1}\,k_{-2}\,[L] + k_{-1}\,k_{mt}\,[L]$$
$$+ k_2\,k_{mt}\,[EVE])$$

$$\frac{[RuEVE]}{[RuL]}$$
$$= \frac{k_{-1}\,k_5\,[L][EVE] + k_2\,k_5\,[EVE]^2 + k_1\,k_2[EVE]}{k_{-1}\,k_{-5}\,[L]^2 + k_2\,k_{-5}\,[L]\,[EVE] + k_{-1}\,k_{-2}\,[L] + k_{-1}\,k_{mt}\,[L] + k_2\,k_{mt}\,[EVE]}$$

$$rate = k_{obs}\,[RuL] = k_{mt}\,[RuEVE]$$

$$k_{obs} = k_{mt}\,\frac{[RuEVE]}{[RuL]}$$

$$k_{obs} = \frac{k_{-1}\,k_5\,k_{mt}[L][EVE] + k_2\,k_5\,k_{mt}[EVE]^2 + k_1\,k_2k_{mt}[EVE]}{k_{-1}\,k_{-5}\,[L]^2 + k_2\,k_{-5}\,[L]\,[EVE] + k_{-1}\,k_{-2}\,[L] + k_{-1}\,k_{mt}\,[L] + k_2\,k_{mt}\,[EVE]}$$
$$= \frac{k_{-1}\,k_5\,k_{mt}[L][EVE] + k_2\,k_5\,k_{mt}[EVE]^2 + k_1\,k_2k_{mt}[EVE]}{(k_{-1}\,k_{-2} + k_{-1}\,k_{mt})[L] + k_{-1}\,k_{-5}\,[L]^2 + k_2\,k_{-5}\,[L]\,[EVE] + k_2\,k_{mt}\,[EVE]}$$

Dividing through by $k_1\ k_2\ k_{mt}[EVE]$

$$k_{obs} = \frac{1 + \frac{k_{-1}\,k_5\,[L]}{k_1\ k_2} + \frac{k_5\,[EVE]}{k_1}}{\frac{[L]}{[EVE]}\left(\frac{k_{-1}\,k_{-2}}{k_1\ k_2\,k_{mt}} + \frac{k_{-1}}{k_1\ k_2}\right) + \frac{k_{-1}\,k_{-5}\,[L]^2}{k_1\,k_2\,k_{mt}[EVE]} + \frac{k_{-5}\,[L]}{k_1\ k_{mt}} + \frac{1}{k_1}}$$

Leading to the following equation 6.7:

$$k_{obs} \approx \frac{1 + f\,[L] + g\,[E]}{c\,[L]/[E] + 1/k_1 + h\,[L] + i\,[L]^2[E]} \qquad \textbf{Equation 5.8}$$

With:

$$c = \frac{1}{K_1\,K_2\,k_{mt}} + \frac{1}{K_1\,k_2}$$

$$f = \frac{k_5}{K_1\, k_2\, k_{mt}}$$

$$g = \frac{k_5}{k_1}$$

$$h = \frac{k_{-5}}{K_1\, k_{mt}}$$

$$i = \frac{k_{-5}}{K_1\, k_2\, k_{mt}}$$

The equation 5.8 fitting the best the experimental data measured by SF-UV (Figure 5.11).

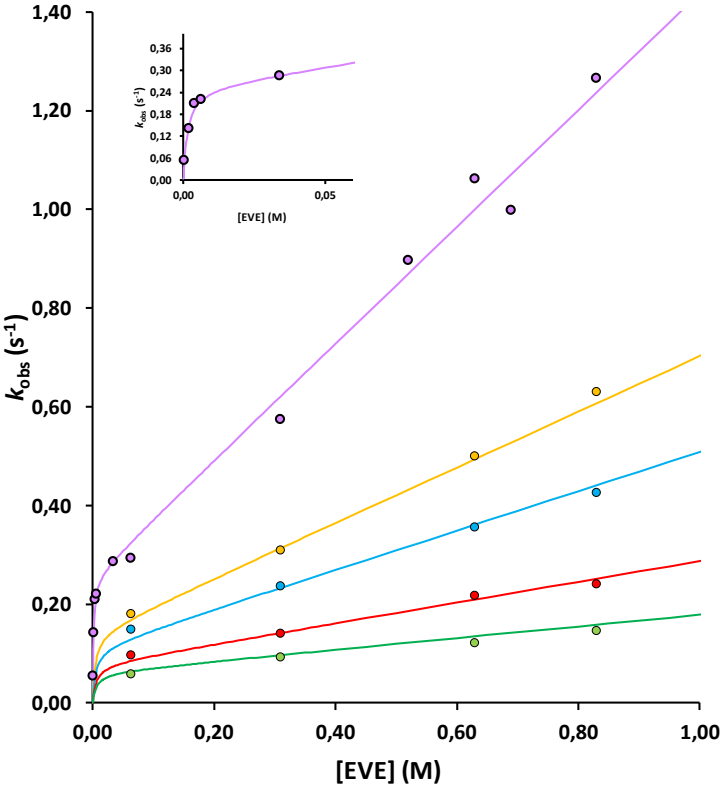

Figure 5.11 GIII fitting model with the experimental data
[3-BrPy] = 0 M (pink dots), [3-BrPy] = 0.0002 M (yellow dots), [3-BrPy] = 0.0004 M (blue dots), [3-BrPy] = 0.001 M (red dots), [3-BrPy] = 0.002 M (green dots)
Insert graph showing [EVE] range from 0 to 0.08 M

The k_{obs} kinetic derivation for GIII initiation as a purely dissociative path was carried out by applying the steady-state approximation on the alkylidine species (Ru and RuEVE, Scheme 5.6) leading to equation 5.9.

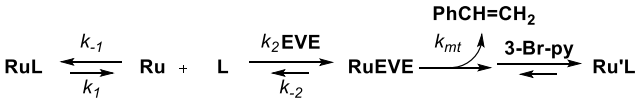

Scheme 5.6 Schematic mechanism for pure dissociative path

$$k_{obs} \approx \frac{1}{c\,[L]/[E] + 1/k_1} \qquad \textbf{Equation 5.9}$$

With:

$$c = \frac{1}{K_1 K_2 k_{mt}} + \frac{1}{K_1 k_2}$$

Applying the steady-state approximation on RuEVE:

$$\frac{d\,[RuEVE]}{dt} = 0 = k_2\,[Ru][EVE] - k_{-2}\,[RuEVE] - k_{mt}\,[RuEVE]$$

$$k_2\,[Ru][EVE] + k_2\,[Ru][EVE] = k_{-2}\,[RuEVE] + k_{mt}\,[RuEVE] \qquad \textbf{Equation 5.10}$$

Applying the steady-state approximation on Ru:

$$\frac{d\,[Ru]}{dt} = 0 = k_1\,[RuL] + k_{-2}\,[RuEVE] - k_{-1}\,[Ru][L] - k_2\,[Ru][EVE]$$

$$k_{-1}\,[Ru][L] + k_2\,[Ru][EVE] = k_1\,[RuL] + k_{-2}\,[RuEVE]$$

$$[Ru]\,(k_{-1}\,[L] + k_2\,[EVE]) = k_1\,[RuL] + k_{-2}\,[RuEVE]$$

$$[Ru] = \frac{k_1\,[RuL] + k_{-2}\,[RuEVE]}{k_{-1}\,[L] + k_2\,[EVE]}$$

Substituting the equation obtained for [Ru] in equation 5.10:

$$\frac{k_2\,[EVE]\,(k_1[RuL] + \,k_{-2}\,[RuEVE])}{k_{-1}\,[L] + \,k_2\,[EVE]} \;=\; k_{-2}\,[RuEVE] + \,k_{mt}\,[RuEVE]$$

Multiplying out:

$$k_1k_2\,[RuL][EVE] + k_2\,k_{-2}[RuEVE][EVE]$$
$$=\; k_{-1}k_{-2}\,[RuEVE][L] + \,k_{-1}k_{mt}\,[RuEVE][L] + \,k_2\,k_{-2}[RuEVE][EVE]$$
$$+\; k_2k_{mt}\,[RuEVE][EVE]$$

Rearranging and cancelling out:

$$k_1k_2\,[RuL][EVE] = [RuEVE]\,(k_{-1}k_{-2}\,[L] + \,k_{-1}k_{mt}\,[L] + \,k_2k_{mt}\,[EVE])$$

$$\frac{[RuEVE]}{[RuL]} \;=\; \frac{k_1k_2\,[EVE]}{[L]\,(k_{-1}k_{-2} \,+\, k_{-1}k_{mt}\,) \,+\, k_2k_{mt}\,[EVE]}$$

$$rate \;=\; k_{obs}\,[RuL] =\; k_{mt}\,[RuEVE]$$

$$k_{obs} \;=\; k_{mt}\,\frac{[RuEVE]}{[RuL]}$$

$$k_{obs} \;=\; \frac{k_1k_2\,k_{mt}[EVE]}{[L]\,(k_{-1}k_{-2} \,+\, k_{-1}k_{mt}\,) \,+\, k_2k_{mt}\,[EVE]}$$

Dividing by $k_1k_2\,k_{mt}[EVE]$

$$k_{obs} \;=\; \frac{1}{\frac{[L]}{[EVE]}\left(\frac{k_{-1}k_{-2}}{k_1k_2\,k_{mt}[EVE]} + \frac{k_{-1}k_{mt}}{k_1k_2\,k_{mt}[EVE]}\right) + \frac{k_2k_{mt}\,[EVE]}{k_1k_2\,k_{mt}[EVE]}}$$

$$k_{obs} \approx \frac{1}{c\;[L]/[E] \;+\; 1/k_1}$$

With:

$$c = \frac{1}{K_1 K_2 k_{mt}} + \frac{1}{K_1 k_2}$$

The k_{obs} kinetic derivation for GIII initiation as a purely associative interchange path was carried out by applying the steady-state approximation on the alkylidine species (RuEVE, Scheme 5.7) leading to equation 5.11.

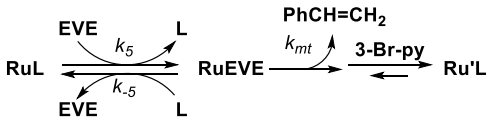

Scheme 5.7 Schematic mechanism for pure associative interchange path

$$k_{obs} \approx \frac{[EVE]}{d\,[L]+1/\,k_5} \qquad \textbf{Equation 5.11}$$

With:

$$d = \frac{1}{K_5 k_{mt}}$$

Applying the steady-state approximation on RuEVE:

$$\frac{d\,[RuEVE]}{dt} = 0 \; = k_5[RuL][EVE] - \; k_{-5}\,[RuEVE]\,[L] - \; k_{mt}\,[RuEVE]$$

$$k_{-5}\,[RuEVE]\,[L] + \; k_{mt}\,[RuEVE] \; = \; k_5[RuL][EVE]$$

$$[RuEVE]\,(k_{-5}\;[L] + \; k_{mt}\,) \; = \; k_5[RuL][EVE]$$

$$[RuEVE] = \frac{k_5[RuL][EVE]}{k_{-5}\;[L] + \; k_{mt}}$$

$$rate = \; k_{obs}\,[RuL] \; = \; k_{mt}\,[RuEVE]$$

$$k_{obs} = k_{mt} \frac{[RuEVE]}{[RuL]}$$

$$k_{obs} = k_{mt} \frac{k_5[RuL][EVE]}{[RuL]\,(k_{-5}\,[L] + k_{mt})}$$

Dividing for $k_5 k_{mt}$

$$k_{obs} = \frac{[EVE]}{\frac{k_{-5}\,[L]}{k_5\,k_{mt}} + \frac{k_{mt}}{k_5 k_{mt}}}$$

$$k_{obs} \approx \frac{[EVE]}{d\,[L] + 1/\,k_5}$$

With d:

$$d = \frac{1}{K_5 k_{mt}}$$

The k_{obs} kinetic derivation for GIII initiation as a purely associative step-wise path was carried out by applying the steady-state approximation on the alkylidine species (RuLEVE and RuEVE, Scheme 5.8) leading to equation 5.12.

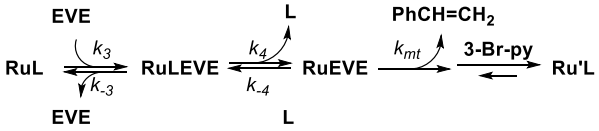

Scheme 5.8 Schematic mechanism for pure associative step-wise path

$$k_{obs} \approx \frac{[EVE]}{e + d\,[L]} \qquad \textbf{Equation 5.12}$$

With

$$d = \frac{1}{K_3 + K_4 + k_{mt}}$$

$$e = \frac{1}{K_3 + k_4} + \frac{1}{k_3}$$

Applying the steady-state approximation on RuEVE:

$$\frac{d\,[RuEVE]}{dt} = 0 = k_4[RuLEVE] - k_{-4}\,[RuEVE]\,[L] - k_{mt}\,[RuEVE]$$

$$k_4[RuLEVE] = k_{-4}\,[RuEVE]\,[L] + k_{mt}\,[RuEVE] \quad \text{Equation 5.13}$$

Applying the steady-state approximation on RuLEVE:

$$\frac{d\,[RuLEVE]}{dt} = 0$$
$$= k_3[RuL]\,[EVE] + k_{-4}\,[RuEVE][L] - k_4\,[RuLEVE] - k_{-3}\,[RuLEVE]$$

$$[RuLEVE]\,(k_4 + k_{-3}) = k_3[RuL]\,[EVE] + k_{-4}\,[RuEVE][L]$$
$$[RuLEVE] = \frac{k_3[RuL]\,[EVE] + k_{-4}\,[RuEVE][L]}{k_4 + k_{-3}} \quad \text{Equation 5.14}$$

Substituting equation 5.14 in equation 5.13:

$$\frac{k_3k_4[RuL]\,[EVE] + k_4k_{-4}\,[RuEVE][L]}{k_4 + k_{-3}} = k_{-4}\,[RuEVE]\,[L] + k_{mt}\,[RuEVE]$$

$$k_3k_4[RuL]\,[EVE] + k_4k_{-4}\,[RuEVE][L]$$
$$= (k_4 + k_{-3})\,(k_{-4}\,[RuEVE]\,[L] + k_{mt}\,[RuEVE])$$

$$k_3k_4[RuL]\,[EVE] + k_4k_{-4}\,[RuEVE][L]$$
$$= k_4k_{-4}\,[RuEVE]\,[L] + k_4k_{mt}\,[RuEVE] + k_{-3}k_{-4}\,[RuEVE]\,[L] + k_{-3}k_{mt}\,[RuEVE]$$

Cancelling and rearranging:

$$[RuEVE]\,(k_4k_{mt} + k_{-3}k_{-4}\,[L] + k_{-3}k_{mt}) = k_3k_4[RuL]\,[EVE]$$

$$\frac{[RuEVE]}{[RuL]} = \frac{k_3 k_4\,[EVE]}{k_4 k_{mt} + k_{-3} k_{-4}\,[L] + k_{-3} k_{mt}}$$

$$rate = k_{obs}\,[RuL] = k_{mt}\,[RuEVE]$$

$$k_{obs} = k_{mt}\,\frac{[RuEVE]}{[RuL]}$$

$$k_{obs} = \frac{k_{mt} k_3 k_4\,[EVE]}{k_4 k_{mt} + k_{-3} k_{-4}\,[L] + k_{-3} k_{mt}}$$

Dividing for $k_{mt} k_3 k_4$

$$k_{obs} = \frac{[EVE]}{\frac{k_4 k_{mt}}{k_{mt} k_3 k_4} + \frac{k_{-3} k_{-4}\,[L]}{k_{mt} k_3 k_4} + \frac{k_{-3} k_{mt}}{k_{mt} k_3 k_4}}$$

$$k_{obs} \approx \frac{[EVE]}{e + d\,[L]}$$

With

$$d = \frac{1}{K_3 + K_4 + k_{mt}}$$

$$e = \frac{1}{K_3 + k_4} + \frac{1}{k_3}$$

5.6 References

1. Naoum, R.; Séguin, J. P.; Trant, J. F.; Frampton, M. B.; Hudlický, T.; Zelisko, P. M., *Tetrahedron* **2016**, *72,* 4027-4031.
2. Love., J. A.; Morgan, J. P.; Trnka, T. M.;Grubbs, R. H., *Angew. Chem. Int. Ed.* **2002**, *41,* 4035-4037.
3. Sanford, M. S.; Ulman, M.; Grubbs, R. H., *J. Am. Chem. Soc.* **2001**, *123,* 749-750.